

Florida Institute of Technology

Scholarship Repository @ Florida Tech

Theses and Dissertations

12-2024

Using Nano-ITIES for Detection of Metal Ions in Complex Aqueous Solutions

Mohammed Muzammil Nishar Ahmed

Florida Institute of Technology, mnisharahmed2019@my.fit.edu

Follow this and additional works at: <https://repository.fit.edu/etd>



Part of the [Chemical Engineering Commons](#)

Recommended Citation

Nishar Ahmed, Mohammed Muzammil, "Using Nano-ITIES for Detection of Metal Ions in Complex Aqueous Solutions" (2024). *Theses and Dissertations*. 1475.

<https://repository.fit.edu/etd/1475>

This Dissertation is brought to you for free and open access by Scholarship Repository @ Florida Tech. It has been accepted for inclusion in Theses and Dissertations by an authorized administrator of Scholarship Repository @ Florida Tech. For more information, please contact kheifner@fit.edu.

Using Nano-ITIES for Detection of Metal Ions
in Complex Aqueous Solutions

by

Mohammed Muzammil Nishar Ahmed

A Dissertation submitted to the Department of Chemistry and Chemical
Engineering of
Florida Institute of Technology
in partial fulfillment of the requirements
for the degree of

Doctor of Philosophy
in
Chemical Engineering

Melbourne, Florida
December, 2024

We, the undersigned committee, hereby approve the attached dissertation,
“Using Nano-ITIES for Detection of Metal Ions
in Complex Aqueous Solutions.”

by

Mohammed Muzammil Nishar Ahmed

Pavithra Pathirathna, Ph.D.

Assistant Professor

Chemistry and Chemical Engineering

Major Advisor

Manolis M. Tomadakis, Ph.D.

Professor

Chemistry and Chemical Engineering

James R. Brenner, Ph.D.

Associate Professor

Chemistry and Chemical Engineering

Jessica Smeltz, Ph.D.

Associate Professor and Interim Department Head

Chemistry and Chemical Engineering

Abstract

Title: Using Nano-ITIES for Detection of Metal Ions in Complex Aqueous Solutions

Author: Mohammed Muzammil Nishar Ahmed

Advisor: Pavithra Pathirathna, Ph.D.

Recent urbanization has induced a rapid increase in heavy metal exposure to humans. The exploitation of heavy metals for economic gains coupled with poor and economically infeasible recycling methods have led to poor management of heavy metal wastes, which has opened up several pathways for heavy metals to enter the human body. Such heavy metals target many vital organs, but the early symptoms are common and difficult to diagnose. Severe symptoms appear in later stages and are very expensive to treat and the damage caused to the health are not typically reversible in such later stages. To counter this issue, it is pivotal to develop early detection systems for such heavy metal contamination. While it is essential to develop a reliable and robust heavy metal sensor, achieving it in a cost-effective manner will aid in widespread reach and adoption. While conventional methods have been well investigated and used, electrochemical methods for such analysis have gained growing interest in recent years due to their fast-processing times, ease of use, and cost-effectiveness. This dissertation presents a series of

studies aimed at achieving these goals using electrochemical detection. The research is divided into three projects, each building upon the findings of previous research. The first project introduces a novel nanopipette-based ion transfer between two immiscible electrolyte solutions (ITIES) sensors for the detection of Cd(II) ions. Utilizing 1,10-phenanthroline as an ionophore, the sensor demonstrates high sensitivity and selectivity in various complex matrices, including tris buffer and artificial seawater. The sensor successfully quantified the amount of Cd(II) in an environmental sample, which was validated using inductively coupled plasma mass spectrometry, which is the gold standard for detection of metals in aqueous solutions. The second project expands the sensor's capabilities to simultaneously detect multiple metal ions, specifically Cd(II) and Ca(II), in complex matrices such as artificial blood and urine. A simplified single-bore, single-ionophore configuration was studied to examine the practicality and ease of fabrication of the sensor. The performance of the sensor is used to evaluate the effectiveness of a common chelation agent used in chelation therapy during early stages of heavy metal exposure. The last project addresses the challenge of data interpretation in electrochemical sensing by integrating artificial intelligence (AI) with ITIES-based sensors. This unique approach integrates Artificial Neural Networks (ANN) and Convolutional Neural Networks (CNN) to analyze cyclic voltammograms (CVs). The CNN model is capable of differentiating Cd(II) from Cu(II) by using the shape of the CV alone and can identify faulty CVs from the good ones. The ANN model

is used to determine the analyte concentration. This integrated approach represents a significant advancement in electrochemical data analysis, making it more accessible to non-experts, thus aiding the widespread use of the sensor.

Table of Contents

Abstract	iii
Table of Contents	vi
List of Figures	ix
List of Tables.....	xiv
Acknowledgement.....	xv
Dedication	xvi
Chapter 1 Introduction	1
1.1 Global Impact of Heavy Metals	1
1.2 Heavy Metal Detection Methods	2
1.3 Electrochemical Methods of Heavy Metal Detection	4
1.4 Literature Gap	13
1.5 Research Objectives	15
1.6 Research Significance	17
Chapter 2 Electrochemical Detection of Cd(II) Ions in Complex Matrices with Nanopipets	19
Abstract	19
2.1. Introduction	20
2.2. Materials and Methodology	24
2.3. Results and Discussion.....	26
2.3.1 Cyclic voltammogram of Cd(II) at nano-ITIES.....	26
2.3.2 Calibration, stability, and selectivity.....	31

2.3.3 Cd(II)–ligand complexes.....	35
2.3.4 Analysis of an environmental sample	37
2.4. Conclusion	39
Chapter 3 Simplified Nano-ITIES System for Simultaneous Detection of Metal Ions in Aqueous Samples.....	40
Abstract	40
3.1. Introduction.....	41
3.2. Materials and Methodology	48
3.3. Results and Discussion.....	56
3.3.1 Testing in MP-AU.....	58
3.3.2 Testing in AB	60
3.3.3 Detection of Ca(II) in AB	63
3.3.4 Simultaneous detection of Cd(II) and Ca(II) in AB.....	64
3.3.5 EDTA calcium disodium as a binder for Cd(II).....	67
3.4. Conclusion	71
Chapter 4 Artificial Intelligence-Enhanced Differentiation and Quantification of Metal Ions Using ITIES-Based Electrochemical Sensors	73
Abstract	73
4.1. Introduction.....	75
4.2. Materials and Methodology	83
4.3. Results and Discussion.....	84
4.3.1 Electrochemical Detection of Heavy Metals.....	84
4.3.2 AI Architecture.....	92

4.4. Conclusion	107
Chapter 5 Conclusion and Future Work	109
5.1 Conclusion	109
5.2 Future Work	111
References	112
Appendix A	140
Appendix B	151
Appendix C	190
Appendix D	197
Appendix E	203
Appendix F.....	204

List of Figures

Figure 1 Yellowish-green trace is a representative CV of Cd(II) transfer and between water and DCE at 10 mV s^{-1} . Aqueous phase: $400 \mu\text{M}$ Cd(II) in 0.3 M KCl. Organic phase: 10 mM phen and 0.1 M TDDATFAB.....	28
Figure 2 Green trace is a representative CV of Cd(II) transfer between water and DCE at 10 mV s^{-1} . Aqueous phase: $400 \mu\text{M}$ Cd(II) in ASW buffer, Organic phase: 10 mM phen and 0.1 M TDDATFAB.....	30
Figure 3 Calibration curve in ASW for Cd(II) transfer. Aqueous phase: $x \text{ mM}$ Cd(II) in ASW buffer, where $x= 5, 10, 50, 100, 200$ and 400 . Organic phase: 10 mM phen and 0.1 M TDDATFAB.....	33
Figure 4 Left: representative CVs for different concentrations of Cd(II) transfer in ASW. Right: current vs. time ($i-t$) traces for each concentration.....	33
Figure 5 Representative CVs obtained for Cd(II) ion transfer in the absence (green) and in the presence of EDTA (light blue), DTPA (yellow), NTA (dark purple), and DMSA (light purple) in ASW at pH 7.0.	36
Figure 6 Plot between the concentration of Cd(II) ions added and the steady-state current. Inset shows where the graph meets the x-axis and thus, Cd(II) concentration in the analyte sample.	38
Figure 7 Representation of synthesis of artificial blood a) step by step mechanism of polymerization leading to PSt-OEDA seed b) Explore the graphical depiction of ABS formation and, Scanning Electron Microscopy (SEM) images, showcasing the emergence of Artificial Blood (AB) particles in sizes ranging from $1-2 \mu\text{m}$ to $7-8 \mu\text{m}$. (St - Styrene, OEDA - Di(ethylene glycol)diacrylate (75%), PVP - Polyvinylpyrrolidone (M=40,000), AIBN - 2,2'-Azobis(2-methyl-propionitrile) (98%).)	50
Figure 8 A representative CV of Cd(II) transfer between MP-AU and DCE at a scan rate of 20 mV/s . Aqueous phase: 0.4 mM Cd(II) in MP-AU. Organic phase: 10 mM phen and 0.1 M TDDATFAB in DCE.	58

Figure 9 Calibration curve in MP-AU for Cd(II) transfer. Each data point represents the average current \pm standard error of the mean. Aqueous phase: x mM Cd(II) in MP-AU, where x = 0.01, 0.05, 0.1, 0.2 and 0.4. Organic phase: 10 mM phen and 0.1 M TDDATFAB.	59
Figure 10 A representative CV of Cd(II) transfer between AB and DCE at a scan rate of 20 mV/s. Aqueous phase: 0.4 mM Cd(II) in AB. Organic phase: 10 mM phen and 0.1 M TDDATFAB in DCE.	62
Figure 11 Calibration curve in AB for Cd(II) transfer. Each data point represents the average current \pm standard error of the mean. Aqueous phase: x mM Cd(II) in AB, where x= 0.01, 0.05, 0.1, 0.2, and 0.4. Organic phase: 10 mM phen and 0.1 M TDDATFAB.	63
Figure 12 A representative CV of Ca(II) transfer between AB and DCE at a scan rate of 20 mV/s. Aqueous phase: 0.4 mM Ca(II) in AB. Organic phase: 10 mM phen and 0.1 M TDDATFAB in DCE.	64
Figure 13 Representative CVs obtained for the simultaneous detection of Cd(II) and Ca(II) in AB, at a scan rate of 20 mV/s. Aqueous phase: x mM Cd(II) in AB, where x = 0.1, 0.2, and 0.4, and 2.5 mM Ca(II) in each case. The green arrow indicates the plateau potential region of Ca(II).	65
Figure 14 CV of 0.2 mM Cd(II) in AB (green) and 0.2 mM Cd(II) in AB in the presence of EDTA in the solution (light blue), with a scan rate of 20 mV/s. Organic phase: Organic phase: 10 mM phen and 0.1 M TDDATFAB in DCE.	68
Figure 15 CV of 0.4 mM Cd(II) in AB (green) and 0.4 mM Cd(II) in AB in the presence of EDTA in the solution (light blue), with a scan rate of 20 mV/s. Organic phase: Organic phase: 10 mM phen and 0.1 M TDDATFAB in DCE.	70
Figure 16 Representative CVs of 0.4 mM Cd(II) ion transfer between 0.3 M KCl and 0.1 M TDDATFAB in DCE: a) good, b) adsorptive, c) cross, d) incomplete, and e) noisy.	87

Figure 17 Representative CVs of f 0.1 mM Cu(II) ion transfer between 0.3 M KCl and 0.1 M TDDATFAB in DCE: a) good, b) adsorptive, c) cross, d) incomplete, and e) noisy.	88
Figure 18 Representative good CVs of a) 0.4 mM Cd(II) and b) 0.2 mM Cu(II) ion transfer between 0.3 M KCl and 0.1 M TDDATFAB in DCE.	89
Figure 19 Representative CVs of not good classification from ion transfer of 0.2 mM Cd(II) between 0.3 M KCl and 0.1 M TDDATFAB in DCE: a) adsorptive, b) cross, c)incomplete, d) noisy.....	90
Figure 20 A representative CV depicting the points that are extracted using MATLAB. These points provide the most vital information that represents the entire CV.	91
Figure 21 Modified LeNet architecture for CV classification	94
Figure 22 Line plots of the training and validation accuracy and loss values over 20 training epochs.	96
Figure 23 Cd(II) Classification of Good vs. Not Good CV Types.	97
Figure 24 Cu(II) Classification of Good vs. Not Good CV Types.	98
Figure 25 Line plots of the training and validation accuracy and loss values over 20 training epochs.	98
Figure 26 Classification of Cd(II) vs Cu(II) CVs.	99
Figure 27 Line plots of the training and validation accuracy and loss values over 20 training epochs.	99
Figure 28 Cd(II) Classification of Not Good CV Types (Noisy, Incomplete, Adsorptive, Cross).	100
Figure 29 ANN architecture with the training parameters.....	103
Figure 30 Variance of the concentration predictions for Cu(II).	105
Figure 31 Variance of the concentration predictions for Cd(II).	106
Figure 32 Representative SEM image of the nanopipete.....	140

Figure 33 Brown trace is a representative CV of Cd(II) transfer and between water and DCE at 10 mV s^{-1} . Aqueous phase: $400 \text{ }\mu\text{M}$ Cd(II) in tris. Organic phase: 10 mM phen and 0.1 M TDDATFAB. Orange trace represents the background CV. 141

Figure 34 Dark blue trace is a representative CV of Cd(II) transfer and between water and DCE at 10 mV s^{-1} . Aqueous phase: $400 \text{ }\mu\text{M}$ Cd(II) in PBS. Organic phase: 10 mM phen and 0.1 M TDDATFAB. Orange trace represents the background CV.142

Figure 35 Calibration curve in KCl for Cd(II) transfer. Each data point represents the average current \pm standard error of the mean obtained for 4 nanopipets with at least 3 replicates for each pipet (at minimum 12 replicates in total) Aqueous phase: $x \text{ }\mu\text{M}$ Cd(II) in KCl, where $x = 5, 10, 50, 100, 200$ and $400 \text{ }\mu\text{M}$. Organic phase: 10 mM phen and 0.1 M TDDATFAB.....143

Figure 36 Calibration curve in TRIS buffer for Cd(II) transfer. Each data point represents the average current \pm standard error of the mean obtained for 4 nanopipets with at least 3 replicates for each pipet (at minimum 12 replicates in total) Aqueous phase: $x \text{ }\mu\text{M}$ Cd(II) in TRIS buffer, where $x = 5, 10, 50, 100, 200$ and $400 \text{ }\mu\text{M}$. Organic phase: 10 mM phen and 0.1 M TDDATFAB.....144

Figure 37 Representative CVs for the transfer of interfering metal ions between water and DCE at 10 mV s^{-1} . Aqueous phase: $400 \text{ }\mu\text{M}$ M(II/III) in KCl. Organic phase: 10 mM phen and 0.1 M TDDATFAB.145

Figure 38 Representative CVs of $[\text{Cd-ligand}]^n$ transfer and between water and DCE at 10 mV.s^{-1} (where $n = -1$ or 0) Aqueous phase: $400 \text{ }\mu\text{M}$ Cd(II) in ASW. Organic phase: 10 mM phen and 0.1 M TDDATFAB.....146

Figure 39 SEM image of nanopipet taken at a magnification of $45000\times$ and spot size of 35.147

Figure 40 Representative CVs for different concentrations of Cd(II) transfer in MP-AU on the left. Current vs. time ($i-t$) traces for each concentration, on the

right. Each $i-t$ curve was obtained for 50 s by applying a constant potential obtained from the plateau region of the CV.....	147
Figure 41 A representative CV of Cd(II) transfer between undiluted AB and DCE at a scan rate of 20 mV/s. Aqueous phase: 0.4 mM Cd(II) in undiluted AB. Organic phase: 10 mM phen and 0.1 M TDDATFAB in DCE.	148
Figure 42 CV (green), and extended CV (light green) of 0.2 mM Cd(II) in AB in the presence of EDTA in the solution with a scan rate of 20 mV/s. Organic phase: Organic phase: 10 mM phen and 0.1 M TDDATFAB in DCE.	149
Figure 43 CV (green), and full range CV (blue) of 0.2 mM Cd(II) in AB in the presence of EDTA in the solution with a scan rate of 20 mV/s. Organic phase: Organic phase: 10 mM phen and 0.1 M TDDATFAB in DCE.	150
Figure 44 3D model of multi-electrode holder.	193
Figure 45 3D model of single and dual electrode holder.	193
Figure 46 Images of the single electrode holder with rubber holding mechanism	194
Figure 47 Image of multi-electrode holder.	195
Figure 48 Images of the constructed Faraday cage.	196
Figure 49 Example of half coin cell rate progression study with a potential window of 0.005 – 3.0V.....	201

List of Tables

Table 1	Ingredients of Artificial Urine.....	49
Table 2	Accuracy for Different Categories of CNN Classification	96
Table 3	ANN Results with the Mean Absolute Error and Mean Squared Error...	104
Table 4	Test Results of ANN Prediction of Concentration for 10 Randomly Selected Cu(II) Values	104
Table 5	Test Results of ANN Prediction of Concentration for 10 Randomly Selected Cd(II) Values.	105
Table 6	Experimental Parameters Used for the Standard Addition Method.....	146
Table 7	Silanization Setup Operating Parameters.....	190
Table 8	P-2000 Laser Puller Operating Parameters.....	192

Acknowledgement

The journey I went through during my Ph.D. has taught me many valuable things that I will keep dear to my heart. Before starting this journey, I had very little experience to show, and I felt lost. During my Ph.D., I had the pleasure of working with many different projects and ideas that were ever inspiring, and I thank the almighty for giving me this blessed opportunity. I thank my parents and family who supported my decision to pursue this journey. I would like to thank my advisor for believing in me and envisioning the path that is being realized. Her support and understanding in difficult situations and her valuable guidance in overcoming many obstacles, both academically and in life, have greatly helped shape me into the person I am today. I would also like to thank my committee members, Dr. Manolis Tomadakis, Dr. James Brenner, Dr. Christopher Chouinard, and Dr. Jessica Smeltz, for their constant support and feedback in shaping the research that was performed during this journey. I had the pleasure of working with amazing individuals who helped me understand various concepts in various fields. I would like to thank them for their constant support and input that helped me gain valuable knowledge that I apply in my research every day. Finally, I would like to thank each and every single person who believed in me both before and during my journey.

Dedication

To my wife, Rukhsar, who was there for me in the most vital times and ensured that I had all the right means to succeed. You are the one that makes my day lighter and makes me smile even in the most difficult of days. You have given a new dimension to life that gets beautiful every day. I dedicate all my hard work and effort put into this dissertation to you.

Chapter 1

Introduction

1.1 Global Impact of Heavy Metals

Heavy metal contamination poses a serious global threat to human health and the environment. Anthropogenic activities such as rapid industrialization, urbanization, and advanced technology adoption in developing countries have led to a significant rise in heavy metal pollution¹. Industrial effluents, nickel-cadmium batteries, cigarettes, electroplating, and paints are major sources of toxic cadmium release into the environment¹. Despite increasing global cadmium usage, no efficient recycling methods exist, putting humans at high risk of exposure from multiple sources². Other hazardous heavy metals like lead, mercury, arsenic, and chromium are also widespread pollutants³. In the Weihe River Basin in China, average concentrations of arsenic, lead, zinc, nickel, chromium, mercury, copper, and cadmium in sediments were found to be 15.42, 27.27, 88.05, 31.05, 75, 0.13, 29.47, and 1.05 mg kg⁻¹ respectively⁴, with cadmium and mercury posing the highest ecological risks. In the USA, an estimated 1,300,000 sites are contaminated with heavy metals, impacting over 10 million people⁵. A study on heavy metal contamination in road dust across 71 cities worldwide found concerning levels, with average concentrations of 72.8 mg kg⁻¹ for copper, 397 mg kg⁻¹ for zinc, 115 mg kg⁻¹ for lead, and 53.5 mg kg⁻¹ for chromium⁶. In Latin America, severe heavy

metal pollution has been reported in rivers like the Magdalena River in Colombia and in the Riachuelo basin in Argentina⁷. Many governing agencies take several measures to contain the exposure of such contaminants by placing threshold concentration limits and the WHO Guidelines for Drinking-Water Quality recommend a threshold value of 3 µg/L for Cadmium⁸.

The detrimental health effects of heavy metals are well-documented. Cadmium accumulation in the human body damages vital organs like the kidneys, lungs, and liver, and is linked to cell proliferation, apoptosis, chromosomal mutations, and various cancers⁹. Lead exposure impairs neurological development in children, while mercury is a potent neurotoxin^{9,10}. Globally, 1.8 million deaths and 46.2 million disability-adjusted life years (DALYs) were attributed to unsafe water containing heavy metals and other contaminants¹⁰. In the USA, an estimated 450,000 children aged 1-5 have elevated blood lead levels¹¹. Altogether, heavy metal pollution inflicts staggering economic losses from heavy metal-induced food pollution¹². Urgent action is needed to mitigate this growing crisis and protect global public and environmental health.

1.2 Heavy Metal Detection Methods

Traditionally, heavy metal analysis has been performed using non-electrochemical techniques such as spectroscopy, chromatography, and colorimetry¹³⁻¹⁷. Mass spectrometry, in particular, has been widely used for sensitive and selective

detection of heavy metals^{18,19}. Peng *et al.*²⁰ developed a dual-cloud point extraction method coupled with inductively coupled plasma mass spectrometry (ICP-MS) for preconcentration and determination of twelve heavy metals in water samples. They achieved enhancement factors ranged from 9.85 to 35.98, with detection limits between 0.012 and 0.36 $\mu\text{g L}^{-1}$. Shih *et al.*²¹ employed a dipole-assisted solid-phase extraction microchip combined with ICP-MS for online determination of trace heavy metals in natural water. The on-chip dipole-ion interactions between C-Cl moieties and metal ions facilitated the extraction, achieving detection limits from 3.48 to 20.68 ng L^{-1} .

Colorimetric methods have also been explored for heavy metal detection. Quantum dots (QDs) have gained attention as promising nanomaterials for colorimetric sensing due to their unique optical properties. Abdelhamid *et al.*²² synthesized mercaptopropionic acid-modified CdS quantum dots (CdS@MPA) and applied them in laser soft desorption/ionization mass spectrometry (QELDI-MS) to detect labile metal-drug interactions. The CdS@MPA provided a large surface area and strong UV absorption, enabling soft ionization of metallodrugs without destroying the weak bonds. These non-electrochemical techniques have been conventionally used for heavy metal analysis. However, these methods have several limitations, including high instrument and operational costs, complex operations requiring advanced skills, large and bulky instrumentation unsuitable for on-site use, and the need for laborious sample pretreatment procedures^{15,18}. For example, ICP-MS and

AAS require expensive equipment and are difficult for non-experts to operate, making them inaccessible to many²³. Moreover, the pre-treatment steps involved, such as acid digestion and extraction, are time-consuming and can alter the original metal speciation, which is critical for accurately assessing toxicity²³. These drawbacks have motivated the development of alternative techniques like electrochemical sensors that overcome many of these limitations.

1.3 Electrochemical Methods of Heavy Metal Detection

There are many electrochemical methods developed for the detection of heavy metals in aqueous samples. In the past decade, electrochemical sensors have shown a great leap in development due to their versatile application, analysis at fast speeds, and enabling rapid, sensitive, selective, and real-time measurements with simpler and more affordable devices²⁴. The popular electrochemical techniques for heavy metal ion detection in aqueous samples are amperometry, anodic stripping voltammetry, voltammetry, and electrochemical impedance spectroscopy.

Amperometry is a technique in which the working electrode or the working probe is held at a constant potential, and the response of the sensor is measured in terms of current. The potential can be held for short durations or longer holding times, which can be implemented to study the change in current response with time (chronoamperometry). Florescu *et al.*²⁵ used amperometry with TCNQ-modified screen-printed electrodes to detect heavy metal ions (Ni(II), Cu(II), Cd(II)) in

aqueous solutions. The sensitivity was improved by using acetylcholinesterase (AChE) enzyme inhibition, with Cu(II) causing the most significant decrease in enzymatic activity. Using AChE, the sensitivity for Cu²⁺ detection was 18.02 $\mu\text{A mM}^{-1}$, compared to 0.53 $\mu\text{A mM}^{-1}$ without the enzyme. Gumpu *et al.*²⁶ developed an amperometric urease inhibition-based biosensor using a Pt/CeO₂/urease-modified electrode to detect Pb(II) and Hg(II) ions in water samples. The biosensor exhibited detection limits of $0.019 \pm 0.001 \mu\text{M}$ for Pb(II) with a sensitivity of $89.2 \times 10^{-3} \mu\text{A } \mu\text{M}^{-1}$, and $0.018 \pm 0.003 \mu\text{M}$ for Hg(II) with a sensitivity of $94.1 \times 10^{-3} \mu\text{A } \mu\text{M}^{-1}$, along with a fast response time (<1 s), good stability for 20 days, and satisfactory repeatability and reproducibility. The sensor was successfully applied to detect Pb(II) and Hg(II) in Cauvery River water samples, with results in good agreement with atomic absorption spectroscopy (AAS) data.

While this technique is widely adopted, it has certain limitations. The selectivity of the sensor is difficult to control, and the current response from the sensor is solely attributed to the target analyte. In case of unexpected interference from the system, the signal may be enhanced or suppressed, and it is difficult to detect those changes from the sensor's response alone. To avoid such undesired events, extensive surface modification is required to ensure the sensor produces a response from the target analyte alone. Such surface modification can be cumbersome and expensive.

Another electrochemical technique is anodic stripping voltammetry. In this technique, the surface of the electrode is preconcentrated with the target analyte

during a deposition step, and a stripping anodic potential is applied to oxidize the deposited metal back into the solution. The potential and the current are recorded as responses and are used to study the analyte. The characteristics of the response help identify useful information about the analyte and examine any undesired reaction if present. Therefore, this technique provides more information than amperometry.

Guo *et al.*²⁷ synthesized a novel sulfur-bridged thiacalixarene-based metal-organic framework (Co-TIC4R-I) and used it to modify a glassy carbon electrode for the simultaneous electrochemical detection multiple metal ions using square wave anodic stripping voltammetry (SWASV). The Co-TIC4R-I modified electrode exhibited wide linear ranges (0.10-17.00, 0.05-16.00, 0.05-10.00, and 0.80-15.00 μM for Cd(II), Pb(II), Cu(II), and Hg(II), respectively), low detection limits (0.0067, 0.0027, 0.0064, and 0.0037 μM), good selectivity, reproducibility, and stability. Rajawat *et al.*²⁸ developed a carbon paste electrode modified with nanocellulosic fibers (NCF-MCPE) for the ultra-trace determination of Cd(II) and Pb(II) in aqueous solution using differential pulse anodic stripping voltammetry (DPASV). Under optimized conditions of acetate buffer pH 5 as the accumulating solvent, 0.1 M HCl as the stripping medium, and a scan rate of 50 mV s^{-1} , linear calibration ranges of 150-650 $\mu\text{g L}^{-1}$ for Cd(II) and 80-300 $\mu\text{g L}^{-1}$ for Pb(II) were obtained with detection limits of 88 $\mu\text{g L}^{-1}$ and 33 $\mu\text{g L}^{-1}$, respectively, after a 10 min accumulation time. Keramari *et al.*²⁹ used square wave anodic stripping voltammetry (SWASV) with a bismuth film-modified glassy carbon electrode and

a dsDNA-modified electrode to simultaneously determine multiple metal ions in soil samples. The bismuth film electrode achieved method quantification limits of 0.91, 0.88, 1.1, and 0.88 mg/kg for Zn(II), Cd(II), Cu(II), and Pb(II) respectively, with precisions ranging from 8.2 to 10.4%, while the dsDNA-modified electrode allowed Cu(II)/Cu(I) speciation with a recovery of 91.7% Cu(I) and RSD of 8.7% in a certified reference soil. Jongte *et al.*³⁰ developed a novel electrochemical sensor for simultaneous detection of Cd(II) and Pb(II) using differential pulse anodic stripping voltammetry with a glassy carbon electrode modified by Ag nanoparticle decorated silane-grafted bentonite. The sensor achieved detection limits of 0.79 $\mu\text{g L}^{-1}$ for Cd(II) and 0.88 $\mu\text{g L}^{-1}$ for Pb(II), with recoveries of 93-108% for Cd(II) and 99-113% for Pb(II) in real water samples.

Although anodic stripping voltammetry is widely adopted, it also has certain limitations. Like amperometry, this technique also needs extensive surface modification for successful operation, which makes electrode fabrication difficult and expensive. There may be some undesired interferences from the system of the analyte that may be hard to detect, which affects the accuracy of the results.

Another popular electrochemical technique is voltammetry. It is further sub-classified into cyclic voltammetry, square wave voltammetry, and differential pulse voltammetry, which all perform very similar functions, only differing in the way the potential is ramped. In this technique, a potential ramp is applied to go from a starting potential to a final potential, and a reverse scan is applied to go back to the

initial potential. The rate at which the potential is changed is called the scan rate. The Faradaic current response, derived from the redox reaction in the system, is recorded as a function of potential. The results provide three vital pieces of information that can be used to study the analyte: the peak potential (or half-wave potential), the current intensity, and the shape of the cyclic voltammogram (CV). The shape of the CV can provide information on the reversibility of the redox reaction and the diffusion/adsorption behavior of the analyte. Therefore, this technique has been very effective for the detection of various analytes in aqueous samples. Lu *et al.*³¹ developed a nickel oxide nanoparticle-decorated carbonized eggshell membrane (NiO/c-ESM) electrode for the electrochemical detection of urea using square wave voltammetry (SWV). The 3D porous NiO/c-ESM nanocomposite provided abundant active sites and efficient electron transport, enabling sensitive urea sensing with a linear range of 0.05-2.5 mM, a sensitivity of $0.462 \mu\text{A mM}^{-1} \text{cm}^{-2}$, and a low detection limit of $\sim 20 \mu\text{M}$. Sibit *et al.*³² developed a glassy carbon electrode modified with electropolymerized L-tyrosinamide for the electrochemical determination of Hg(II) ions using differential pulse anodic stripping voltammetry (DPASV). The poly(L-tyrosinamide) modified electrode exhibited a wide linear range from 0.5 to 1800 pM and a low limit of detection of 0.16 pM for Hg(II) detection. The sensor was successfully applied to measure Hg(II) in real river water and soil samples with recoveries between 99.2 and 105.2%. These voltammetry-based sensors show great

potential; however, there are certain limitations to this technique. This technique is limited to analytes that are electroactive species, which means that the analyte must undergo complex redox reactions in order to be detected. However, many analytes do not undergo redox reactions readily. Therefore, stringent electrode fabrications may be required to ensure that the analyte undergoes such redox reactions in the host environment. This makes the electrode fabrication process cumbersome and expensive.

Another electrochemical technique is electrochemical impedance spectroscopy. While all the above-discussed methods use direct current to detect the target analyte, EIS uses a sinusoidal alternating potential to probe the impedance of an electrochemical system over a range of frequencies. In such a system, the ions in the aqueous solution create an effect that is equivalent to combinations of resistors and capacitors, which induce impedance at zero phase shift and non-zero phase shift into the system. The impedance is measured as a complex quantity with real (resistive) and imaginary (capacitive) components, often represented as a Nyquist plot. The underlying principle of EIS is more advanced than the traditional electrochemical methods that use direct current and can provide more insights and information occurring at the electrode-electrolyte interface such as charge transfer, diffusion, and adsorption. Avuthu *et al.*³³ developed a fully screen printed three electrode electrochemical sensor on a flexible PET substrate for the detection of toxic heavy metal ions. Using electrochemical impedance spectroscopy (EIS), they

demonstrated highly sensitive detection of Pb(II) and Cd(II) ions, achieving a low detection limit of 1 nM for both analytes, which is several orders of magnitude below the FDA limit. The sensor showed an 18% and 52% change in impedance for 1 nM and 1 μ M concentrations of Pb(NO₃)₂ respectively, compared to DI water. Wei *et al.*³⁴ reported an electrochemical impedance spectroscopy method for the ultrasensitive and ultraspecific detection of Cr(VI) using a self-assembled monolayer of azacrown on gold electrodes. By exploiting the high affinity and specific binding of the azacrown to HCrO₄⁻ at pH 5.0, which hinders electron transfer, they achieved a detection limit of 0.0014 ppb Cr(VI) with a sensitivity of 4575.28 k Ω [log c (ppb)]⁻¹ over the linear range of 1–100 ppb. The azacrown modified electrode showed good selectivity for Cr(VI) with low interferences. Although EIS is an advanced electrochemical technique, it involves complex reactions and is an expensive instrument with which to perform accurate measurements. It also provides a lot more information than just the qualitative and quantitative analysis of the analyte and thus is not ideal for making a cost-effective, easy-to-use sensor.

The electrochemical techniques mentioned above require the target analyte to undergo complex redox reactions, thus limiting the application to electroactive species. In this light, electrochemistry at the liquid-liquid interface has emerged as an attractive branch of electrochemistry. One such technique is called ion transfer

at the interface between two immiscible electrolyte solutions. The principle of this technique is that a potential can be applied to two immiscible electrolyte solutions and the potential difference will drive the ion transfer from one phase to the other phase. In most cases, the metal ions are in the aqueous phase, while an ionophore is added to the organic phase to facilitate the ion transfer from the aqueous phase at a lower potential by lowering the energy barrier for the ion transfer, which is dictated by the Gibbs free energy. This technique was first developed by Koryta *et al.*³⁵ and was initially used to study the transfer of biological molecules across the immiscible interface. Later, this technique was employed for kinetic studies of many other analytes, including metals³⁶⁻⁴⁰. Bingol³⁷ *et al.* investigated the assisted transfer of heavy metal ions, particularly Cd(II), across the water/1,2-dichloroethane interface using cyclic voltammetry and 4'-morpholinoacetophenone-4-phenyl-3-thiosemicarbazone (MAPPT) as the ligand. They determined that the assisted transfer of Cd(II) occurs via a quasi-reversible process following the transfer by interfacial complexation (TIC) mechanism, with a 1:3 (metal:ligand) stoichiometry and an association constant of $\log \beta = 15.46 \pm 0.11$. The authors also examined the assisted transfer of other heavy metal ions like Pb(II), Hg(II), Cu(II), and Zn(II), observing varying degrees of reversibility and transfer characteristics. Benvidi *et al.*³⁸ investigated the facilitated transfer of Cd(II) across a water/1,2-dichloroethane microinterface using cyclic voltammetry at a 25 μm diameter micropipette electrode, with 1,10-phenanthroline (phen) as the complexing agent.

They determined that Cd(II) forms a 1:3 complex with phen, with a formation constant of 3.9×10^{29} . The authors calculated diffusion coefficients for Cd(II) in water ($6.5 \times 10^{-6} \text{ cm}^2 \text{ s}^{-1}$), phen in DCE ($5.8 \times 10^{-6} \text{ cm}^2 \text{ s}^{-1}$), and the Cd-phen complex in DCE ($5.1 \times 10^{-6} \text{ cm}^2 \text{ s}^{-1}$) using voltammetric data.

While these studies used larger interfaces (in the μm range), Rodgers *et al.*⁴¹ performed various kinetic studies on ion transfer at liquid-liquid interface and concluded that a macropipet (internal diameter in the μm range) produces a linear diffusion whereas a nanopipet (internal diameter in the nm range) produces a hemispherical diffusion. Linear diffusion is when the influx of fluid flow follows a linear profile with some negligible end effects, while a hemispherical diffusion is when the end effects are so large that the influx of fluid follows a hemispherical pattern. Hemispherical diffusion provides a high mass transfer rate, which produces a sigmoidal response that is essential for fast kinetic measurements. Sigmoidal response avoids the effect of ohmic resistance and capacitive currents, which helps it overcome the significant interference from the matrix in which the target analyte is present.

Chen *et al.*⁴² synthesized a novel tris(crown ether) ionophore, TCEI, and investigated its performance for the electrochemical detection of potassium ions using nanointerfaces between two immiscible electrolyte solutions (nanoITIES). The researchers employed cyclic voltammetry and differential pulse stripping voltammetry at nanopipette electrodes with radii of approximately 100 nm to study

the facilitated ion transfer of K^+ across the water-1,2-dichloroethane interface. They demonstrated that TCEI exhibited superior selectivity for K^+ over Na^+ compared to conventional crown ether ionophores, achieving a detection limit of $0.8 \mu M$ for K^+ and a linear response range from 1 to $100 \mu M$, showcasing the potential of this novel ionophore for potassium sensing applications.

The fact that ITIES does not require the target analyte to undergo complex redox reactions and that this method detects the analyte using a simple ion transfer principle makes the electrode fabrication and instrumentation cost effective. The hemispherical diffusion ensures that the matrix effect is minimized, making this technique ideal for developing field electrodes. Furthermore, this technique does not require extensive sample pretreatment steps, which can alter the speciation of the metal, which is a crucial parameter in determining the toxicity of the metal. This technique is capable of delivering accurate information on metal speciation and involves a relatively simple and cost effective electrode fabrication step. Therefore, this study is dedicated to increasing our understanding of ITIES and expanding the realms of ITIES for the detection of heavy metal ions in aqueous samples.

1.4 Literature Gap

Many studies have reported the use of ITIES as an effective tool for the detection of a variety of analytes, including heavy metal ions. However, the reported studies

at micro-ITIES and nano-ITIES were performed in simple matrices where the metal of interest exists primarily in the unbound state. To the best of our knowledge, no studies have reported using ITIES to detect metals in the bound state. This is of great interest because metals are found in numerous bound forms with naturally present complexing agents in biological and environmental samples. Studying the response of an ITIES sensor toward heavy metals in a bound state will provide valuable information on the feasibility of the electrochemical technique in developing a fast and reliable sensor.

Furthermore, many studies designed for metal ion detection face significant challenges in mitigating the interfering effects of other ions that are predominantly present in the aqueous sample of interest. This is of significance as there are many potentially interfering ions that are abundant in environmental and biological samples, which may affect the performance of the sensor. Studying the effect of such ions in excess during the detection of a target analyte will provide insights into the robustness of the sensor for practical applications. Furthermore, many electrochemical studies develop multi-bore working electrodes to detect multiple analytes. While this method is broadly used, the fabrication of a double-bore electrode involves great difficulty and includes significant cross-talk or interaction between the two channels, which may reduce the accuracy of the sensor. Therefore, a simple single-bore configuration that is easy to fabricate must be developed and

studied to mitigate the challenges faced during multi-analyte detection.

There have been many electrochemical sensors that represent their result in the form of a CV. Although the peak potential and peak intensity can be quantified, there is no scientific method to quantify the shape of the CV. Due to sensor drift and other factors, it is challenging to differentiate the electrochemical response emerging from different metal ions that have small separations in their half-wave potential. Thus, the shape of the CV is a valuable characteristic feature for identifying the analyte and differentiating it from other analytes. Although these CVs can be easily analyzed by experts in the field, it is challenging for a nonexpert to look at and analyze these plots. Therefore, developing a smart method to analyze them will greatly improve the user-friendliness of such sensors.

1.5 Research Objectives

Based on the literature gap and extensive literature review, this dissertation was designed with three primary research objectives.

- i. Investigation of the performance of an ITIES sensor in various complex matrices*

For this objective, the ITIES sensor will be characterized in various complex matrices like artificial seawater, tris buffer solution, and phosphate buffer solution for the detection of Cd(II) ions. Then, the performance of the sensor will be

examined when Cd(II) is initially bound with chelating agents such as ethylenediaminetetraacetic acid (EDTA), 2,3-dimercaptosuccinic acid (DMSA), diethylenetriaminepentaacetic acid, (DTPA), and nitrilotriacetic acid (NTA). The sensor will then be used to detect dissolved Cd(II) ions in environmental water samples, and the result will be compared to the one reported using ICP-MS, which is the gold standard for the detection of metal ions in aqueous samples.

- ii. Develop a simplified ITIES configuration for the simultaneous detection of metal ions in aqueous system*

In this objective, we will examine a unique single bore single ionophore configuration for simultaneous detection of Cd(II) and Ca(II) ions in artificial blood and artificial urine. This study will incorporate preparing artificial urine using a comprehensive recipe to emulate a real human environment and preparing artificial blood by synthesizing artificial red blood cells (RBCs) and platelets. The concentration of Ca(II) will be in excess (at least 6.25 times) compared to that of Cd(II) ions, and the concentration of Ca(II) will represent the physiological concentration (2.5 mM). The ITIES sensor will then be used to examine the effect of a well-known chelating agent, EDTA disodium, on the detection of Cd(II) ions.

- iii. Develop AI architectures to study the electrochemical response of ITIES sensors for the detection of Cd(II) and Cu(II) ions*

In this objective, we will develop AI architectures like convolution neural network (CNN) and artificial neural network (ANN) to analyze the characteristic response from the ITIES sensor. CNN will be used to differentiate the good CVs from the not-good CVs, and then it will be employed to identify Cd(II) apart from Cu(II). CNN will also be used to differentiate between different imperfections in CVs, such as noisy, cross, adsorptive, etc. The ANN will then be used to quantify the concentration of both the analytes.

1.6 Research Significance

The study of ITIES in complex matrices in the first objective will evaluate the technology readiness level (TRL) of ITIES for heavy metal detection in complex and environmental samples. This is the first-time heavy metal detection has been performed on both complex and environmental samples using ITIES. The study of the electrochemical response of the sensor in the presence of strong ligands will increase our understanding of the strength of our sensor in detecting heavy metal ions in a bound state. Further, the comparison of the analysis of environmental samples with ITIES against the gold standard, ICP-MS, will be a huge step forward in increasing the reputation of ITIES as a powerful electroanalytical tool for environmental sample analysis. This objective seeks to widen the possibilities and the reach of electrochemistry at the liquid-liquid interface in developing analytical tools for real-world applications.

The development of a simplified configuration with ITIES to detect both target and

prominent interfering ions will give us valuable insights into the practical applicability of the sensor in real-world situations. It will expand our knowledge and understanding of the performance of the sensor in complex media with *in situ* interfering ions (Ca(II)). This objective will help us understand the response of ITIES sensor to a combination of metal ions and examine if the presence of one ion has an impact on another. It will also give us clarity on how the electrochemical signal will be affected and if the response of the primary analyte will be affected by the presence of interfering ions in excess. This study will shed light on the effect of chelation therapy as a viable medical remedy for early-stage Cd(II) poisoning.

The development of AI models to further study and evaluate the CVs from an ITIES experiment will help us make the sensor more user-friendly. It will vastly help untrained individuals operate the sensor without needing to have an electrochemical background to make informed decisions. This is the first study to develop CNN models to understand various imperfections in a CV and identify the imperfect CVs from the good ones. The CNN model can also differentiate between Cd(II) and Cu(II) CVs, using the shape of the CV alone, and it is the first time a scientific method has been developed to exploit the unique shape associated with each analyte for their identification. The ANN model will then be employed to predict the concentration of each analyte based on the electrochemical signal. The ANN model, with proper training, can be effective in handling baseline shifts and plateau potential current alignments, thus providing accurate results. Overall, the

integration of ITIES with AI will enable us to make the sensors more user-friendly and deployable for on-field applications in the hands of non-experts.

Chapter 2

Electrochemical Detection of Cd(II) Ions in Complex Matrices with Nanopipets

This dissertation chapter content covers research objective i. It was published in the journal of Royal Chemical Society Advances. Authors: Muzammil M. N. Ahmed, Faieza S. Bodowara, Wendy Zhou, Juliana F. Penteadó, Jessica L. Smeltz and Pavithra Pathirathna*

*Corresponding Author: Pavithra Pathirathna (ppathirathna@fit.edu); 150 W. University Blvd, Melbourne, FL 32904

Abstract

Heavy metal contamination and its detrimental health effects are a growing concern globally. Several metal mitigation systems and regulatory approaches have been implemented to minimize the negative impacts on human health. However, none of these function at maximum efficiency, mainly due to the lack of accurate information about metal speciation. Therefore, there is a critical need to develop novel, cheap, efficient, and robust metal detecting sensors. In this study, we describe the application of a nanopipet based electrochemical sensor to detect aqueous Cd(II) ions. The inner radius of our nanopipets is ~300 nm, and the

fundamental mechanism behind our sensor's response is ion transfer between two immiscible electrolyte solutions (ITIES). The absence of redox behavior makes ITIES an excellent, attractive electrochemical tool to study various ions in aqueous solutions. In this study, we used 1,10-phenanthroline as our ionophore in the organic phase (dichloroethane) to facilitate the transfer of Cd(II) ions from the polar aqueous phase to the less polar organic phase. Unlike previous studies, we characterized our nanopipet in complicated matrices, including, but not limited to, tris buffer and artificial seawater. We performed quantitative assessments to determine our sensor's limit of detection, stability, sensitivity, and selectivity. We further show that our nanosensor can detect free Cd(II) ions in the presence of strong complexing agents such as ethylenediaminetetraacetic acid, 2,3-dimercaptosuccinic acid, etc. We quantified the concentration of free Cd(II) ions in a water sample collected from a local lagoon. Thus, we showcased the power of our nanopipets to act as a robust, accurate, and efficient speciation sensor to detect Cd(II) ions in environmental samples.

2.1. Introduction

Exposure to heavy metals is a global health concern that results in various deleterious and harmful effects. Thus, regulation agencies such as the World Health Organization and Environmental Protection Agency⁴³ have determined permissible levels of heavy metals in drinking water, food, paint, and other sources, to ensure regulation in the environment, therefore minimizing human exposure. Among

different toxic metal ions, Cd(II) is a highly poisonous heavy metal largely present in industrial effluents. Anthropogenic Cd(II) sources include nickel-cadmium batteries, cigarettes, electroplating, and paints. Despite the rapid increase of Cd(II) usage across the globe, there is no efficient recycling method for Cd-containing compounds; thus, humans are at a high risk of exposure to Cd(II) via multiple sources. Accumulation of Cd(II) in the human body can cause a variety of detrimental health hazards, such as cell proliferation, apoptosis, chromosomal mutations, and damage to vital organs, including the kidneys, lungs, and liver^{44,45}.

Traditionally, metal analysis has been primarily performed with non-electrochemical techniques such as spectroscopy^{13,14} chromatography^{15,16} and colorimetry¹⁷. Although these tools are compelling, they are not well-suited for on-site measurements due to the sophisticated, physically large instruments, extensive labor, and analysis time. In contrast, electrochemical techniques offer an excellent platform for real time *in situ* metal analysis. These utilize small, robust, cheap electrodes that non-experts can easily handle, in addition to having faster response times. Chen *et al.* designed a novel electrochemical sensor by depositing BiSn nanoparticles on a glassy carbon electrode (GCE) to detect Cd(II) using differential pulse stripping voltammetry⁴⁶. Because the authors increased the surface area by integrating nanoparticles onto the carbon surface, they achieved an excellent limit of detection (LOD). Abdallah and colleagues recently developed another GCE-based electrode by depositing ion-imprinted polymer⁴⁷. Using anodic stripping

voltammetry, the authors detected Cd(II) in biological samples. However, conventional electrochemical techniques such as cyclic voltammetry, anodic stripping voltammetry, and linear sweep voltammetry require the target analyte to easily undergo the oxidation-reduction process. Furthermore, they often need complicated fabrication processes, thus limiting the versatility of these applications.

In this respect, electrochemistry at the liquid-liquid interface has emerged in recent decades as an active branch of electroanalytical chemistry. An ionophore is typically added to the organic phase to facilitate the ion transfer across the water-organic interface in the presence of an applied external voltage. While most researchers take advantage of ion transfer at the interface between two immiscible electrolyte solutions (ITIES) to study more complicated biological molecules such as proteins, few have reported studies with simple yet toxic metal ions⁴⁰. Wilke and Wang reported a thermodynamic study of Cd(II), Cu(II), and Pb(II) ion transfer across a water/nitrobenzene interface using ETH1062 as the ionophore with microITIES³⁶. Benvidi *et al.* characterized Cd(II) transfer across water/1,2-dichloroethane (DCE) using a different microITIES geometry in the presence of 1,10-phenanthroline (phen)³⁸. In contrast to microITIES, Bingol and Atalay studied the transfer mechanism of Cd(II) ions across an interfacial area of 0.27 cm² in the presence of a neutral ionophore 40-morpholinoacetophenone-4-phenyl-3-thiosemicarbazone³⁷. Lee *et al.* described a detailed study on Cu(II) ion transfer across water/1,2-DCE with picolinamide-phenylenevinylene³⁹. These studies

employed an interface of ~20–30 mm or above between the aqueous and organic phases, revealing exciting findings. Nano-ITIES show superior electrochemical performances over micro-ITIES, leading to enhanced mass transport and low ohmic drop. More recently, Chen *et al.* introduced a new tris(crown ether) ionophore for the assisted ion transfer of metal ions at nano-ITIES⁴². These reported studies at micro-ITIES and nano-ITIES were performed in simple matrices where the metal of interest exists primarily in the unbound state.

More precisely, metals are found in numerous bound forms with naturally present complexing agents in biological and environmental samples. In this work, we utilized a nano-ITIES-based electrochemical sensor to detect free Cd(II) ions in intricate matrices where Cd(II) is initially bound with strong chelating agents including, but not limited to, ethylenediaminetetraacetic acid (EDTA), 2,3-dimercaptosuccinic acid (DMSA), and diethylenetriaminepentaacetic acid, (DTPA). We first characterized our nano electrochemical sensor in KCl and then in a more complex matrix resembling artificial seawater (ASW). We incorporated phen as the ionophore in our sensor as it shows the best sensitivity among all the reported ionophores for Cd(II) detection with ITIES³⁸. Furthermore, we quantified the dissolved Cd(II) ions in a water sample collected from the Indian River Lagoon, Melbourne, FL. To the best of our knowledge, this is the first time anyone has reported the use of nano-ITIES-based electrochemical sensors to study the speciation of Cd(II) in a complex matrix and actual environmental samples. This

study provides excellent insights into future applications of nano-ITIES electrochemical sensors, particularly in detecting heavy metals in environmental and biological samples as implantable sensors.

2.2. Materials and Methodology

Chemicals

All chemicals were purchased from Sigma-Aldrich (St. Louis, MO) unless otherwise specified. CdCl₂ was used as the Cd(II) source. Cd(II) solutions were prepared in different matrices, including KCl (0.3 M), ASW, TRIS buffer, and phosphate buffer solution (PBS). TRIS buffer was composed of tris hydrochloride (15 mM), NaCl (140 mM), KCl (3.25 mM), CaCl₂ (1.2 mM), NaH₂PO₄ (1.25 mM), MgCl₂ (1.2 mM), and Na₂SO₄ (2.0 mM) at pH 7.4. The composition of ASW was NaCl (402 mM), MgCl₂ (48 mM), Na₂SO₄ (26 mM), and HEPES (10 mM) at pH 7.0. EDTA, DMSA, DTPA, and nitrilotriacetic acid (NTA) were used as model ligands to prepare Cd(II)–ligand samples by mixing Cd(II) and ligand in a 1:1 ratio in ASW at pH 7. CuSO₄·5H₂O, Fe(NO₃)₃·9H₂O, FeSO₄·7H₂O, Ni(NO₃)₂·6H₂O, Co(OOCCH₃)₂·4H₂O, CaCO₃, MgCl₂·6H₂O, and PbCl₂ were used as the sources for the selectivity test in KCl.

Electrode fabrication

Borosilicate glass capillaries (O.D. $\frac{1}{4}$ 1.0 mm, I.D. $\frac{1}{4}$ 0.58 mm, Sutter Instruments, CA, USA) were pulled using a P-2000 laser puller (Sutter Instruments, CA, USA) to obtain nanopipets with a tip diameter of \sim 600 nm. Nanopipets were imaged with a scanning electrochemical microscope, JEOL JSM-6380LV (JEOL Ltd, Tokyo, Japan), to accurately measure the pipet tip diameter (Fig. S1). The inner walls of the pulled pipets were silanized with chloromethylsilane prior to being filled with the organic phase. The silanization of glass pipettes is crucial⁴⁸ in experiments where the organic phase is placed inside a glass pipette. The inner wall of the glass pipets is hydrophilic; thus, the outer aqueous phase penetrates inside the pipet and moves the organic phase upward from the tapered end, altering the electrochemical measurements. This issue is avoided by depositing a hydrophobic material such as chloromethylsilane on the inner walls of the glass pipets, hence making it more hydrophobic and resistive to aqueous solutions. Here, the pipets (maximum of 6 pipets at once) were placed inside a desiccator connected to a vacuum pump. After a sufficient vacuum was established inside the desiccator, chlorotrimethyl silane (500 mL) was introduced for 30 min to 1 h. The silanization time varied depending on the relative humidity and the temperature of the surroundings. Silanized nanopipets were filled with the organic phase. The organic phase (dichloroethane) consisted of 10 mM 1,10-phenanthroline (phen) as the ionophore and tetradodecylammoniumtetrakis(pentafluorophenyl)borate (TDDATFAB, 0.1 M) as the electrolyte. TDDATFAB was synthesized as previously described⁴⁹.

Electrochemical experiments

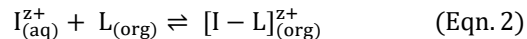
All electrochemical experiments were conducted with a CHI660E potentiostat (CH Instruments, TX, USA) in a three-electrode system using a lab-built Ag/AgCl electrode as the reference electrode and a Pt wire (Alfa Aesar, MA, USA) as the counter electrode. Each experiment was conducted with at least 4 nanopipets in triplicate (at least 12 runs in total).

2.3. Results and Discussion

2.3.1 Cyclic voltammogram of Cd(II) at nano-ITIES

Ion transfer across ITIES was first introduced by Koryta³⁵. The fundamental mechanism of electrochemistry at ITIES is that ion transfer is ruled by the ion's Gibbs energy of transfer for a specific aqueous-organic solvent system. Further, ions (with $z+$ charge) are transferred across the interface by imposing a potential difference (using a potentiostat) greater than the Gibbs energy for transfer between the two phases (Eqn. (1)), and the resultant current can be measured as a function of applied potential.





When the Gibbs energy for ion transfer is too high (compared to that of the background electrolyte solution), the presence of a suitable ionophore, L, in the organic phase lowers the required applied energy via the external circuit by forming a stable metal–ionophore complex (Eqn. (2)). Moreover, the second approach, facilitated ion transfer, provides greater selectivity for a particular target ion in the presence of a mixture of other ions. The steady-state current, i_d , obtained for ion transfer at nanoITIES formed at the tip of a nanopipette can be equated as follows (Eqn. (3)),

$$i_d = 4xzFDCr \quad (\text{Eqn. 3})$$

where z is the charge of the analyte, C is the concentration, D is the diffusion coefficient in the phase of origin, r is the radius of the pipette, x is a parameter that accounts for the thickness of the glass wall, and F is the Faraday constant.

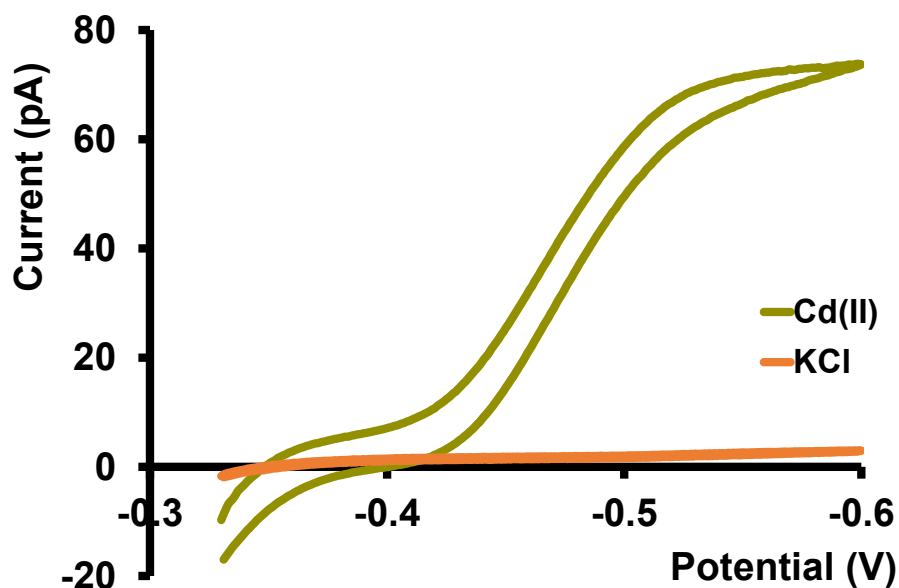


Figure 1 Yellowish-green trace is a representative CV of Cd(II) transfer and between water and DCE at 10 mV s^{-1} . Aqueous phase: $400 \text{ }\mu\text{M}$ Cd(II) in 0.3 M KCl. Organic phase: 10 mM phen and 0.1 M TDDATFAB.

Before moving into more complicated matrices, we tested our nanopipet ITIES sensor with Cd(II) dissolved in a simple electrolyte solution, KCl. Upon optimizing the potential window for the detection of Cd(II), we didn't observe any cyclic voltammograms (CV) in the absence of phen (data not shown here). We obtained a sigmoidal-shaped CV with an $E_{1/2}$ value of -0.46 V after adding excess phen to the organic phase (Fig. 1). Since the preliminary work by Koryta,³⁵ it was well established that the presence of ionophore in the organic phase lowers the solvation energy of the hydrophilic metal ions, subsequently reducing the Gibbs energy for the transfer across ITIES, resulting in a CV at a less negative potential. Conversely, in the absence of such an ionophore, the transfer energy of metal ions surpasses or

overlaps with the energy of the ions in the background electrolyte; hence a well-resolved CV is not obtainable.

Different mass transport mechanisms at nano-ITIES define the shapes of both the forward and backward waves in a CV. In general, when excess ionophore is present in the inner organic solution and a simple ion is present in the outer aqueous solution, ingress transfer is controlled by hemispherical diffusion; thus, a steady-state sigmoidal forward wave results⁴¹. Subsequently, the egress transfer of the ions or ion– ionophore complexes from the inner solution to the outer solution is controlled by linear diffusion; hence, a peak-shaped backward wave results³⁸.

However, in more recent studies, steady-state sigmoidal CVs for both ingress and egress transfer at micropipet and nanopipet ITIES have been reported^{42,50} similar to our CV shown in Fig. 1. The lack of a peak on the backward wave is due to the steady-state nonlinear mass transport in the inner solution as a result of the unique tip geometry of the glass pipet. Rodgers and Amemiya used finite elemental simulations to show that the steady-state sigmoidal wave could be achieved for egress transfer with a small tip inner angle at tapered glass pipets.⁴¹ Establishing a mass-transport controlled steady-state voltammogram at nano-ITIES is very important, particularly in studying the kinetics of ion transfer. We found Cd(II)'s

diffusion coefficient in the aqueous phase to be $8.8(\pm 0.4) \times 10^{-6} \text{ cm}^2 \text{ s}^{-1}$, which is in close agreement with the literature reported values^{38,51}.

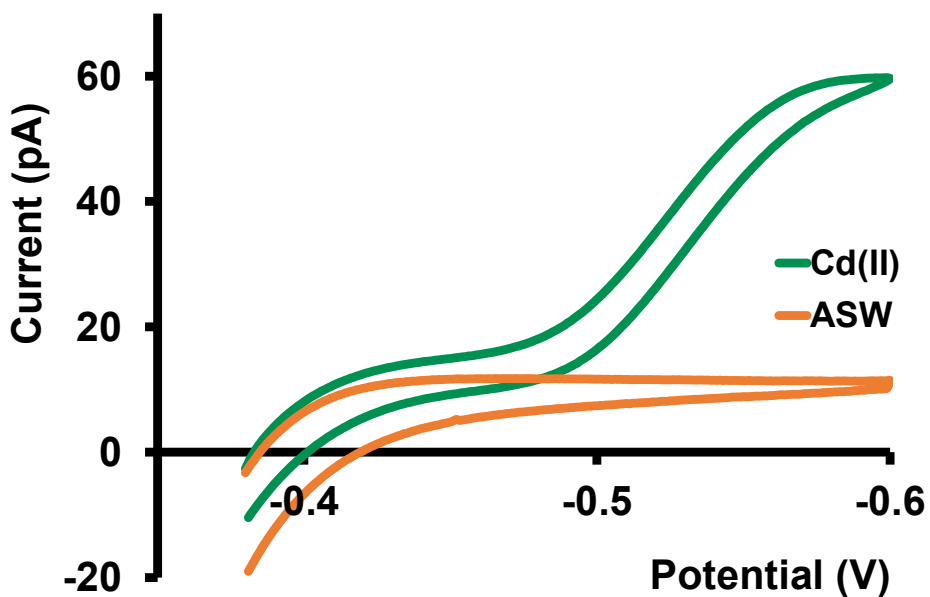


Figure 2 Green trace is a representative CV of Cd(II) transfer between water and DCE at 10 mV s^{-1} . Aqueous phase: $400 \mu\text{M}$ Cd(II) in ASW buffer, Organic phase: 10 mM phen and 0.1 M TDDATFAB.

We then tested our sensors in three different buffer solutions at pH 7; TRIS buffer (resembles artificial cerebellum fluid), PBS (Fig. S2 and S3), and a buffer solution designed to mimic the composition of seawater⁵⁰ (Fig. 2). Among all three buffer solutions, the steady-state current we obtained in ASW is most similar to that in

KCl; thus, the D in ASW, $8.5(\pm 0.2) \times 10^{-6} \text{ cm}^2 \text{ s}^{-1}$, is within experimental error of the D in KCl. As predicted for the PBS solution, we obtained a low Cd(II) transfer response. We attribute this mainly to the formation of an insoluble Cd-phosphate complex. Furthermore, nanoscopic particles of this insoluble complex can interfere with our nano-ITIES, thus blocking the passage for Cd(II) transfer. Response in TRIS buffer was not as low as in PBS; however, it wasn't as high as in KCl or ASW, resulting in a lower diffusion coefficient, $4.5 \times 10^{-6} \text{ cm}^2 \text{ s}^{-1}$. Moreover, we observed a relatively larger background current in the TRIS buffer, presumably due to the transfer of its background electrolyte ions.

2.3.2 Calibration, stability, and selectivity

We performed calibration studies in KCl, tris buffer (Fig. S5 and S6), and ASW (Fig. 3) to find the sensitivity and LOD of our nanopipets. As seen in Fig. 4, the sensitivity in ASW was 0.127 pA mM^{-1} whereas in KCl, it was 0.162 pA mM^{-1} (Fig. S5). Although there is a notable change in the solution composition, the sensitivities are not drastically different; thus, the matrix effect from ASW on our sensor's performance is negligible. However, we noticed the sensitivity in TRIS buffer was much lower (0.085 pA mM^{-1}) compared to the other two solutions; 1.5 times and 2 times lower compared to ASW and KCl, respectively. Furthermore, LOD in both KCl and ASW was 5 mM (0.56 ppm), whereas, in TRIS buffer, it was 10 mM (1.12 ppm). Moreover, a relatively high background current was obtained in TRIS buffer (Fig. S6). We ascribe the higher LOD and reduced sensitivity in

TRIS to its solution composition that yields a high background current. Moreover, studies have reported that Cd(II) makes strong complexes with TRIS⁵². Thus, removing some free Cd(II) ions in the solution subsequently decreases the measured current in our potential window. Based on these results, we performed most of our experiments in ASW, thus making our sensor the first nano- pipet based electrochemical sensor that can detect Cd(II) in complicated matrices.

Previously reported ITIES based studies were performed with macropipets or macro ITIES³⁶⁻³⁸ in a simple electrolyte solution composed of one salt.

Furthermore, these studies are primarily focused on theoretical aspects compared to applications of these sensors to aid in solving real-world problems; thus, no calibration studies were performed, nor was LOD reported. Conversely, our primary goal was to determine whether this sensor could be utilized to detect Cd(II) samples first in environmental samples and then in biological samples.

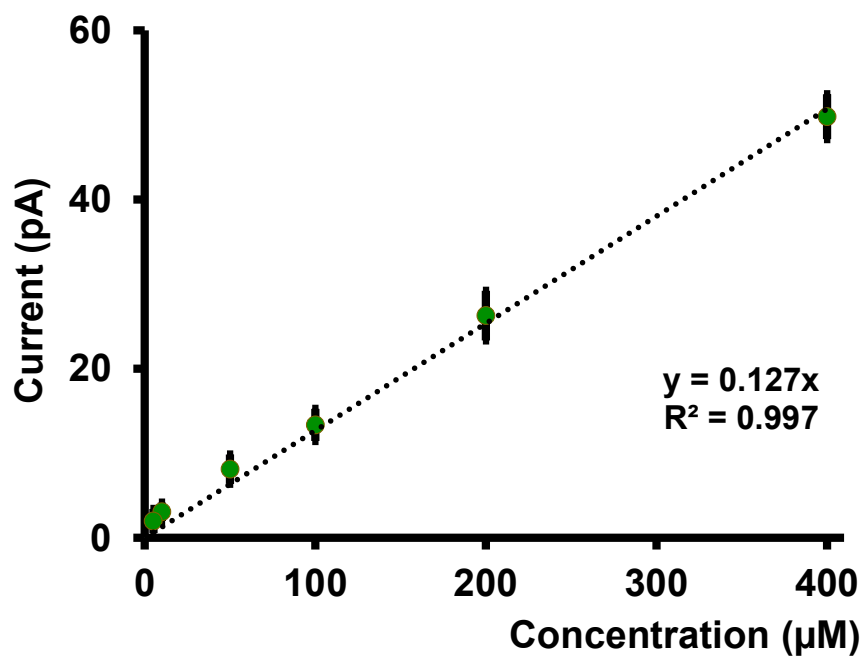


Figure 3 Calibration curve in ASW for Cd(II) transfer. Aqueous phase: x mM Cd(II) in ASW buffer, where x= 5, 10, 50, 100, 200 and 400. Organic phase: 10 mM phen and 0.1 M TDDATFAB.

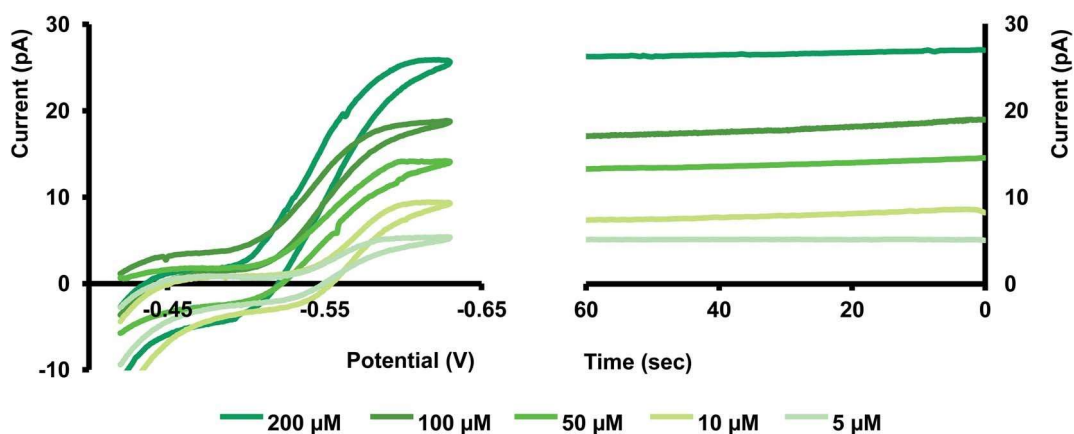


Figure 4 Left: representative CVs for different concentrations of Cd(II) transfer in ASW. Right: current vs. time (i-t) traces for each concentration.

We tested the stability of our sensor amperometrically by holding each nanopipet at the plateau potential. Although the actual measurement requires only a few seconds, as seen in Fig. 4, the current was stable for over a minute. Maintaining a constant current at nano-ITIES is often challenging, mainly due to fouling that occurs from the adsorption of nanoscopic particles at the ultra-small interface. Our finding showcases the robustness of our sensor to overcome that obstacle, thus making it an excellent tool for real sample analysis. Moreover, our data is in good agreement with a similar study performed by Colombo *et al.*; hence, validating our sensor's stability⁵⁰. We also assessed the selectivity of our nanopipet towards Cd(II) ions over some potential interfering ions; Co(II), Fe(II), Fe(III), Ni(II), Pb(II), Ca(II), Cu(II), and Mg(II) (Fig. S7).

Here, we tested each individual ion (400 mM; upper limit of our linear range) in KCl using phen (10 mM). Although it is known that phen is not selective only for Cd(II) ions,⁵³ the rationale for this experiment was that $E_{1/2}$ for each metal ion would be unique; therefore, it is still possible to distinguish Cd(II) ions from other ions. Interestingly, only Cu(II), Ca(II), and Pb(II) resulted in quasi-steady state CVs. However, all three metal ions showed a significantly lower current and high negative $E_{1/2}$ compared to Cd(II), see Figure 37. Other metal ions didn't significantly respond within the potential limit we tested for Cd(II). This is an exciting finding as our nanopipet can differentiate Cd(II) with appreciable selectivity even using a non-selective ionophore.

2.3.3 Cd(II)–ligand complexes

Metals in environmental samples exist in complex forms with naturally present ligands, thus lowering the concentration of free metal ions. However, free metal ions are readily accessible for chemical reactions and therefore are more responsible for toxicity. Hence, it is vital to detect free metal ions in a system compared to bound metal ions. Before we tested our nanopipets with natural water samples, we performed a pilot study to verify our sensor's ability to detect free Cd(II) ions in the presence of known ligands. We chose EDTA, DTPA, DMSA, and NTA as four model ligands. These were chosen based on their usage as Cd(II) detoxifying agents in the medical field. These ligands have been tested for their efficacy by several research groups, primarily to administer them to remove ingested Cd(II) from the body^{54–58}. We first mixed Cd(II) and each ligand in 1:1 molar ratio in ASW and let the mixtures equilibrate for ~24 h. Then we analyzed these samples with our nanopipets by running CV experiments. At pH 7, deprotonated forms^{59–61} of ligands exist as EDTA³⁻, DTPA³⁻, NTA³⁻ and DMSA²⁻; thus, we expected to observe prominent CVs corresponding to [Cd–EDTA]⁻¹, [Cd–DTPA]⁻¹, [Cd–NTA]⁻¹ appearing with an increase in the negative current on the forward scan, and almost no CV for [Cd–DMSA]⁰ since the overall charge of the complex is zero at pH 7.0. However, as seen in Fig. 5, we observed quasi-steady-state CVs for all four Cd–ligand mixtures resembling positively charged, free Cd(II) ions in ASW. We expanded our potential window beyond the limits shown

in Fig. 5 to observe any [Cd–ligand] complexes; however, no such feature was observed for any of these complexes (Fig. S8 in ESI†).

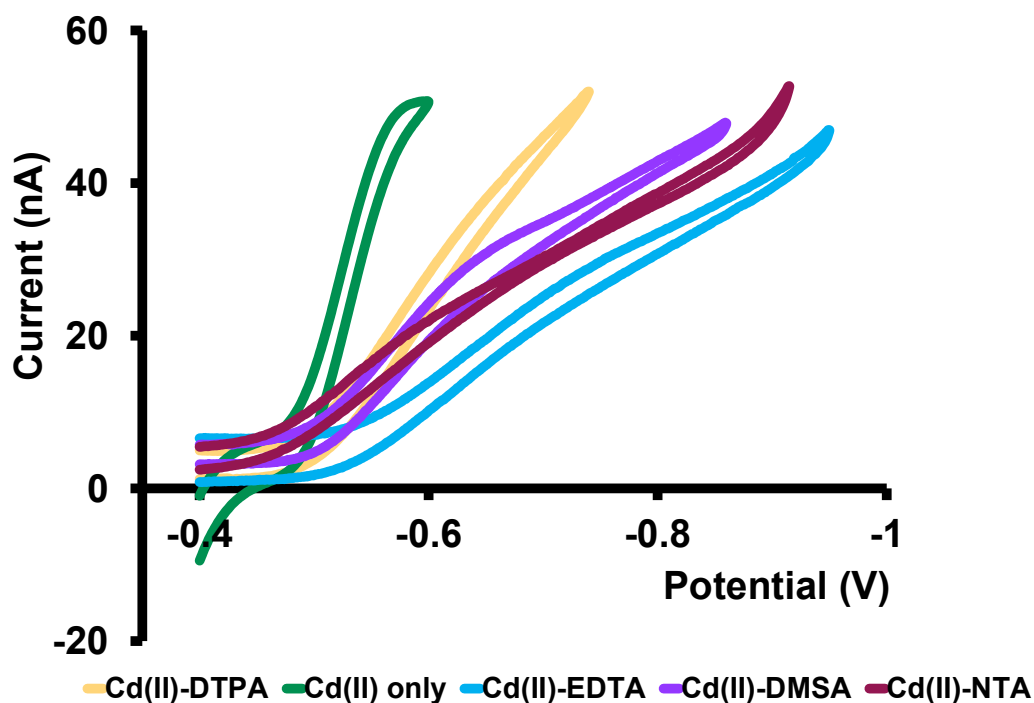


Figure 5 Representative CVs obtained for Cd(II) ion transfer in the absence (green) and in the presence of EDTA (light blue), DTPA (yellow), NTA (dark purple), and DMSA (light purple) in ASW at pH 7.0.

Furthermore, the current at the quasi-steady state is lower, and CVs are less steep than the CVs collected for Cd(II) in ASW. Interestingly, the $E_{1/2}$ of all four samples shifted to higher negative potentials compared to that of Cd(II). Therefore, we attribute these CVs to free Cd(II) ions in equilibrium with Cd–ligand complexes. Lower current, less steepness, and higher $E_{1/2}$ values are presumably due to the competition between the ligands and the applied potential. The presence of phen in

the organic phase will favor the movement of free Cd(II) ions to the organic phase, pulling more free Cd(II) ions from the Cd–ligand complex. Moreover, because Cd(II) ions are bound to ligands, the required energy for their ion transfer is higher than that in the absence of ligands; thus, $E_{1/2}$ values are shifted more towards the high negative potentials. To the best of our knowledge, this is the first time reporting a Cd(II)–ligand study with an ITIES-based nanopipet. This is an exciting finding as it showcases the power of our sensor to identify free Cd(II) ions in the presence of strong complexing agents.

2.3.4 Analysis of an environmental sample

We tested a water sample obtained from the Indian River Lagoon, Melbourne, FL, with our nanopipets. Here, we quantified the concentration of Cd(II) ions in this water sample using the standard addition approach. We first let the river water sample settle for ~48 hours and removed debris by filtration. A series of Cd(II) concentrations were prepared by mixing a known volume of filtered river water sample with different concentrations of Cd(II) in ASW (see Table S6 for more details). The corresponding CVs were taken with at least 4 nanopipets, each with three runs. As depicted in Fig. 6, the average current for at least 12 replicates for each concentration was plotted against the concentration of Cd(II). The extrapolation of the graph yielded the concentration of Cd(II) in the analyte sample, and by adjusting the dilution factor, we found the concentration of Cd(II) in the Indian River Water Lagoon to be 0.27 ppm.

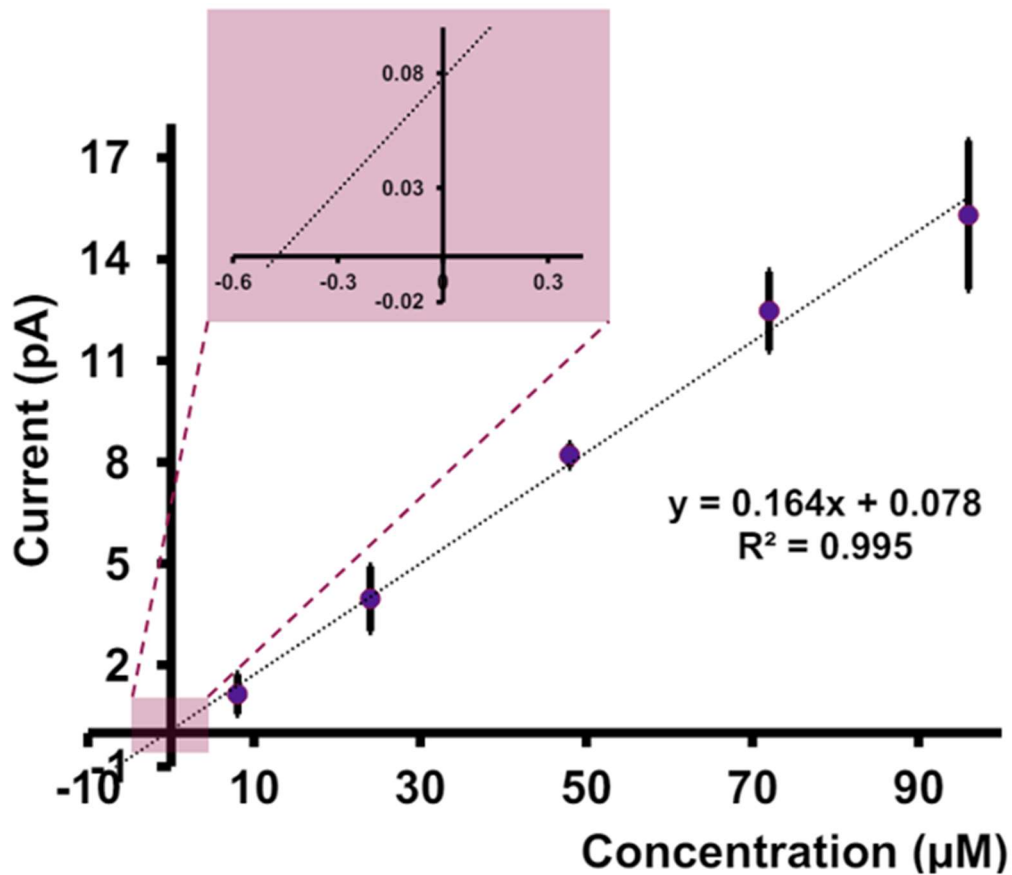


Figure 6 Plot between the concentration of Cd(II) ions added and the steady-state current. Inset shows where the graph meets the x-axis and thus, Cd(II) concentration in the analyte sample.

Interestingly, our finding agrees well with the literature. Trefry and Trocine reported Cd(II) concentrations (0.62–0.26 ppm) at different locations in the lagoon⁶². Furthermore, the authors used inductively coupled plasma mass spectrometry as their analysis tool, thus confirming our sensor's great potential for use as an environmental monitoring tool.

2.4. Conclusion

In this paper, we described the use of a nanopipet-based electrochemical sensor to detect Cd(II) ions in aqueous samples. Our electrode is a borosilicate glass electrode with an inner radius of 300 nm. It follows a hemispherical diffusion regime, owing to its nanoscale interface that allows fast measurements. Phen was used to facilitate the Cd(II) transfer across the nano-interface. We performed ITIES-based cyclic voltammetry and amperometry experiments with our nanosensor in various matrices, including simple electrolytes like KCl and complicated buffer solutions such as artificial seawater and artificial cerebellum fluid. We also tested the strength of our sensor against other standard ligands such as EDTA, NTA, DTPA, and DMSA. We found out that our electrode shows excellent stability and can withstand complex matrices without fouling, an attractive feature of an exemplary sensor. We tested our sensor with Cd(II) dissolved in a water sample collected from the Indian River Lagoon, Melbourne, FL; thus, we showcase our sensor's power as an environmental monitoring tool. To the best of our knowledge, this is the first time reporting a glass electrode with a nanometer scale for Cd(II) detection in a natural environmental sample using ITIES. Our ultra-small electrode will enable us to study the kinetics of ion transfer across ITIES; thus, allowing us to modify the sensor to enhance the sensitivity and selectivity in our future studies.

Chapter 3

Simplified Nano-ITIES System for Simultaneous Detection of Metal Ions in Aqueous Samples

This dissertation content covers research objective ii. It is in preparation for publication in the journal of Applied Sciences. Authors: Muzammil M.N. Ahmed, Nishal M. Egodawaththa, Anthi Savvidou, Nasri Nesnas and Pavithra Pathirathna*

*Corresponding Author: Pavithra Pathirathna (ppathirathna@fit.edu); 150 W. University Blvd, Melbourne, FL 32904

Abstract

Electrochemical sensors capable of trace metal detection in environmental samples are critically needed to assess exposure and prevent toxic effects. In our previous work, we developed a Cd(II) sensor capable of detecting trace amounts of Cd(II) in environmental samples using ion transfer between two immiscible electrolyte solutions (ITIES). The sensor showed exceptional performance that was on par with that of the ICP-MS. The development of ITIES technology toward the simultaneous detection of numerous metal ions will mark a significant advancement in the usefulness of the sensor and position it as a resourceful instrument for a range of uses, including environmental monitoring and biomedical diagnostics. In this work, we expand on our previous studies to create an electrochemical sensor that is reliable, fast and easy to fabricate for the

simultaneous quantitative and qualitative detection of metal ions, specifically Cd(II) and Ca(II), in complex matrices such artificial blood (AB) and artificial urine (MP-AU). In contrast to multi-bore arrangements, the suggested sensor uses a single-bore, single-ionophore configuration, which streamlines the fabrication process and lowers the number of variables, reducing uncertainty and the load for theoretical modeling. To determine the sensor's applicability for practical uses, its performance is assessed in intricate matrices like MP-AU and AB. Our sensor is characterized in the presence of EDTA calcium disodium(EDTA), a chelating agent, in AB, and the conditional stability constants in these intricate systems are evaluated. This study aims to develop a practical and efficient technique for simultaneous metal ion detection, especially in situations where Cd(II) monitoring is necessary. Faster and more accurate detection of metal ions in aqueous solutions is made possible by the straightforward single bore, single ionophore arrangement, which presents a viable substitute for more intricate sensing devices. This work advances the potential for ITIES to be utilized as a simultaneous metal ion detection technique in practical applications.

3.1. Introduction

Concerns about environmental heavy metal poisoning and its harmful consequences on human health are ever-increasing in the world. Cadmium is one of the most hazardous heavy metals and has been connected to a number of illnesses, including cancer, bone fragility, and kidney impairment⁶³⁻⁶⁶. The main industrial

pollutants that cause anthropogenic sources of environmental cadmium pollution are paints, batteries, electronic components, and waste from electroplating⁶³⁻⁶⁶. Due to the world's rapidly growing consumption of cadmium and the lack of effective cadmium recycling techniques, there is a significant risk that humans will be exposed to cadmium from a variety of sources⁶⁷⁻⁶⁹. When cadmium enters the human body, it tends to accumulate in soft tissues because of its poor excretion rate and long biological half-life (around 20–30 years)⁷⁰. This build-up can cause detrimental health issues, especially in the liver and kidneys. Exposure to cadmium can result in proximal tubular dysfunction in the kidneys, which can induce glucosuria, aminoaciduria, and proteinuria¹, while renal failure may develop as a result of glomerular damage⁷¹ brought on by prolonged exposure to cadmium. Hepatocyte necrosis and apoptosis are two signs of hepatocellular injury caused by cadmium buildup in the liver⁷². Furthermore, cadmium has been linked to the development of chronic liver disorders by inducing oxidative stress, inflammation, and fibrosis in the liver⁷³. In addition, cadmium has been connected to a number of other health problems, such as osteoporosis, endocrine and reproductive toxicities, and several forms of cancer⁶³. A number of neurodegenerative illnesses, such as Parkinson's and Alzheimer's, have also been linked to it because of its blood-brain barrier penetration⁷⁴. The main pathway that people get exposed to cadmium is through their diet, especially in places where the soil and water are contaminated⁷⁵. In order to lower the effects of cadmium poisoning and safeguard human health,

precise and effective techniques for monitoring cadmium levels in biological and environmental samples must be used.

Several research groups have created Cd(II) monitoring devices for application in biological samples. Certain systems depend on biomarkers, like urine levels of β 2-microglobulin, to determine the extent of Cd(II) exposure in the body^{76,77}.

However, the reliability of such biomarkers as sole indicators of Cd(II) levels is questionable because their concentrations in urine can fluctuate due to various factors unrelated to Cd(II) exposure, potentially leading to misinterpretation of results. Elevated levels of β 2-microglobulin in the urine, for example, have been linked to a number of illnesses, such as inflammatory disorders, cancer, and renal failure, making it difficult to interpret Cd(II) exposure solely based on this biomarker⁷⁸. Thus, to guarantee an accurate assessment of Cd(II) levels in biological systems, biomarker-based techniques should be employed in conjunction with direct measurement techniques of Cd(II) in biological systems. Many sensors have been developed to detect Cd(II) for biological application. However, traditional techniques such as atomic absorption spectrometry^{13,79} and inductively coupled plasma mass spectrometry^{18,19} require expensive equipment and are difficult to operate, making them inaccessible to many. Moreover, the pretreatment steps involved in these techniques, such as acid digestion and extraction, limit real-time detection and can alter metal speciation, which is a critical factor in determining metal toxicity. Metal speciation determines the uptake, transport, and

interaction of metals with biological molecules, which directly influences their toxicodynamics⁸⁰⁻⁸². Therefore, for accurate toxicity assessment, it is important that the original speciation state is maintained. The need for low-cost, portable, and reliable sensors that can provide real-time information while preserving metal speciation has fueled the development of electrochemical sensors for detecting Cd(II) in aqueous solutions⁸³⁻⁸⁶. These sensors offer various advantages such as high sensitivity, selectivity, and the ability to perform on-site detection without any tedious sample pre-treatment procedures. Liao *et al.* developed a novel electrochemical sensor with a TiO₂ nanocrystal fabricated glassy carbon electrode for the detection of Cd(II) and Pb(II) ions using SWASV⁸⁷. They concluded that by increasing the exposed percentage of the (001) facet, the sensitivity of the sensor toward the heavy metal ions increases, achieving a low limit of detection. Bi *et al.* developed a disposable electrochemical sensor using double-sided conductive carbon tape coated with a thin layer of gold as the working electrode for the stripping analysis of Cd(II) coupled with in situ electrodeposition of bismuth⁸⁸. With an optimized gold sputtering time of just 10 seconds to retain the nanostructure of the carbon tape, the sensor achieved a low detection limit of 0.1 µgL⁻¹ for Cd(II) using differential pulse voltammetry (DPV). It was successfully applied for detecting Cd(II) in rice samples. Manring *et al.* developed a novel electrochemical sensor using gold nanoparticle-modified carbon-fiber microelectrodes for the detection of Cd(II) ions via fast-scan cyclic voltammetry⁷⁴.

With optimized parameters, the sensor achieved a low detection limit of 0.01 μM (1.12 ppb) for Cd(II) and demonstrated excellent selectivity even in the presence of interfering metal ions such as Cu(II), Co(II), Mn(II) and Pb(II). However, conventional electrochemical techniques, such as cyclic voltammetry, anodic stripping voltammetry, and linear sweep voltammetry have certain limitations. These techniques typically require the target analyte to undergo facile oxidation-reduction processes, which can restrict their use to electroactive species. Moreover, fabricating electrodes for these techniques often involves complex procedures, further limiting their versatility and widespread adoption.

In this light, ion transfer in the interface of two immiscible electrolyte solutions (ITIES) has emerged as an aspiring branch of electroanalytical chemistry. This technique does not involve complex redox reactions in the system and relies on simple or assisted ion transfer. The addition of an ionophore to the organic phase allows for more selectivity and sensitivity while achieving assisted ion transfer³⁷. Several studies have been performed using ITIES designed for both environmental and biological systems^{30–36,40,42,89}. Mastouri *et al.* developed a liquid-liquid micro interface array with micropores drilled by laser in polyimide membranes for the detection of cadmium ions using cyclic voltammetry and square wave voltammetry⁸⁹. They demonstrated the perfect additivity of currents from 1 to 256 micropores, independent of array geometry, and achieved a low limit of detection of 11 ppb (100 nM) for cadmium ions using a 64 micropore array. This study

illustrates a significant gain in sensitivity compared to a single micropore. Viada *et al.* developed a novel electroanalytical approach for the detection of perfluorooctanesulfonate (PFOS⁻) using differential pulse stripping voltammetry (DPSV) at an array of micro-interfaces between two immiscible electrolyte solutions (μ ITIES)⁹⁰. By employing a 5-minute preconcentration step to accumulate PFOS⁻ into the organic phase held within the μ ITIES array, they achieved a limit of detection of 0.03 nM (0.015 μ g L⁻¹). Lu *et al.* investigated the detection of ametryn, a model lipophilic herbicide, at a single micro-interface between two immiscible electrolyte solutions (μ ITIES) fabricated using a glass capillary⁹¹. They developed a two-step method involving accumulation of the neutral form of ametryn in the organic phase at open-circuit potential followed by AC voltammetry detection of the proton transfer assisted by ametryn, achieving a limit of detection of 0.2 μ M in real river water samples. In our previous work, we developed a nanopipet-based electrochemical sensor with an inner radius of 300 nm for the detection of Cd(II) ions using cyclic voltammetry and amperometry at the interface between two immiscible electrolyte solutions (ITIES)⁹². Employing 1,10-phenanthroline as the ionophore in the organic phase (dichloroethane), we achieved a limit of detection of 5 μ M (0.56 ppm) for Cd(II) in complex matrices such as artificial seawater. We also quantified the dissolved Cd(II) concentration in an environmental water sample from the Indian River Lagoon to be 0.27 ppm, showcasing the sensor's potential for environmental monitoring applications. As an example of a study that

used ITIES for biological application, Iwai *et al.* developed a novel strategy for the electrochemical detection of γ -aminobutyric acid (GABA) at biological pH using nano-ITIES pipet electrodes with radii of 320-340 nm, fabricated by laser pulling of quartz capillaries⁹³. By introducing octanoic acid to the organic phase, they enabled the detection of GABA, a zwitterion, via assisted ion transfer, achieving a limit of detection of 22.4 μ M. However, the studies mentioned above do not characterize their sensors in a mixture of analytes and possible interfering ions. Among the limited attempts of co-detection of metals using ITIES, Mastouri *et al.* investigated the assisted transfer of Pb(II), Cd(II), and Zn(II) ions using a micropore drilled in polyimide plates as the working electrode and 8-hydroxyquinoline as a ligand in the organic phase, employing cyclic voltammetry and square wave voltammetry techniques⁹⁴. They achieved a limit of detection of 0.2 ppm for lead, which is significant for monitoring heavy metals in industrial effluents. However, they conclude that co-detection leads to signal overlap without proper discrimination, leading to an overall combined response, which results in ambiguity in assigning the signal to individual analytes.

Furthermore, many studies designed for metal ion detection face significant challenges in mitigating the interfering effects of Ca(II), a prominent ion in blood. This is of significance as Ca(II) is an abundant ion in environmental and biological samples⁹⁵. In this study, for the first time, we propose a single-channel nano-ITIES-based electrochemical sensor capable of distinctly detecting multiple ions in

aqueous solutions. We employ a simple single bore-single ionophore configuration and characterize our sensor in complex matrices such as artificial urine (AU) and artificial blood (AB). We use 1,10-phenanthroline as the ionophore in the organic phase as it shows affinity towards both Cd(II) and Ca(II)⁹² and demonstrate that our sensor is capable of producing unique signals for Cd(II) and Ca(II) when both are present in a mixture with Ca(II) in excess. This demonstrates the practical application of our sensor in biological samples in which the concentration of Ca(II) is always sufficiently larger than Cd(II). We further characterize the performance of our sensor in the presence of chelating agents such as EDTA calcium disodium (EDTA) in AB. We calculated the conditional stability constant of Cd-EDTA in AB. The proposed configuration in this study will simplify the simultaneous ion detection process and reduce the number of variables, thereby minimizing uncertainties and making theoretical modeling more straightforward, and it shows great potential to be employed in biological samples.

3.2. Materials and Methodology

Chemicals

Unless otherwise specified, all chemicals were purchased from Sigma-Aldrich (St. Louis, MO). CdCl₂ was used as the Cd(II) source. Cd(II) solutions were prepared in artificial urine and artificial blood. CaCl₂ at physiological concentration was used as the interfering ion while detecting Cd(II) in artificial blood. EDTA was

purchased from Sigma Aldrich and used as a model ligand to prepare Cd(II)–ligand samples by mixing Cd(II) and EDTA in a 1:1 ratio in AB at pH 7.4

Preparation of artificial urine

The artificial urine used for this study was prepared according to the procedure described by Sarigul *et al.*⁹⁶. The ingredients are listed in Table 1. The components were dissolved in deionized water and stirred using a magnetic stirrer.

Table 1 Ingredients of Artificial Urine

Components	Molarity (mM)
Na ₂ SO ₄	11.965
C ₅ H ₄ N ₄ O ₃	1.487
Na ₃ C ₆ H ₅ O ₇ ·2H ₂ O	2.450
C ₄ H ₇ N ₃ O	7.791
CH ₄ N ₂ O	249.750
KCl	30.953
NaCl	30.053
CaCl ₂	1.663
NH ₄ Cl	23.667
K ₂ C ₂ O ₄ ·H ₂ O	0.19
MgSO ₄ ·7H ₂ O	4.389
NaH ₂ PO ₄ ·2H ₂ O	18.667
Na ₂ HPO ₄ ·2H ₂ O	4.667

Preparation of artificial blood

The artificial blood used for this study was prepared according to the procedure described by Li *et al.*⁹⁷.

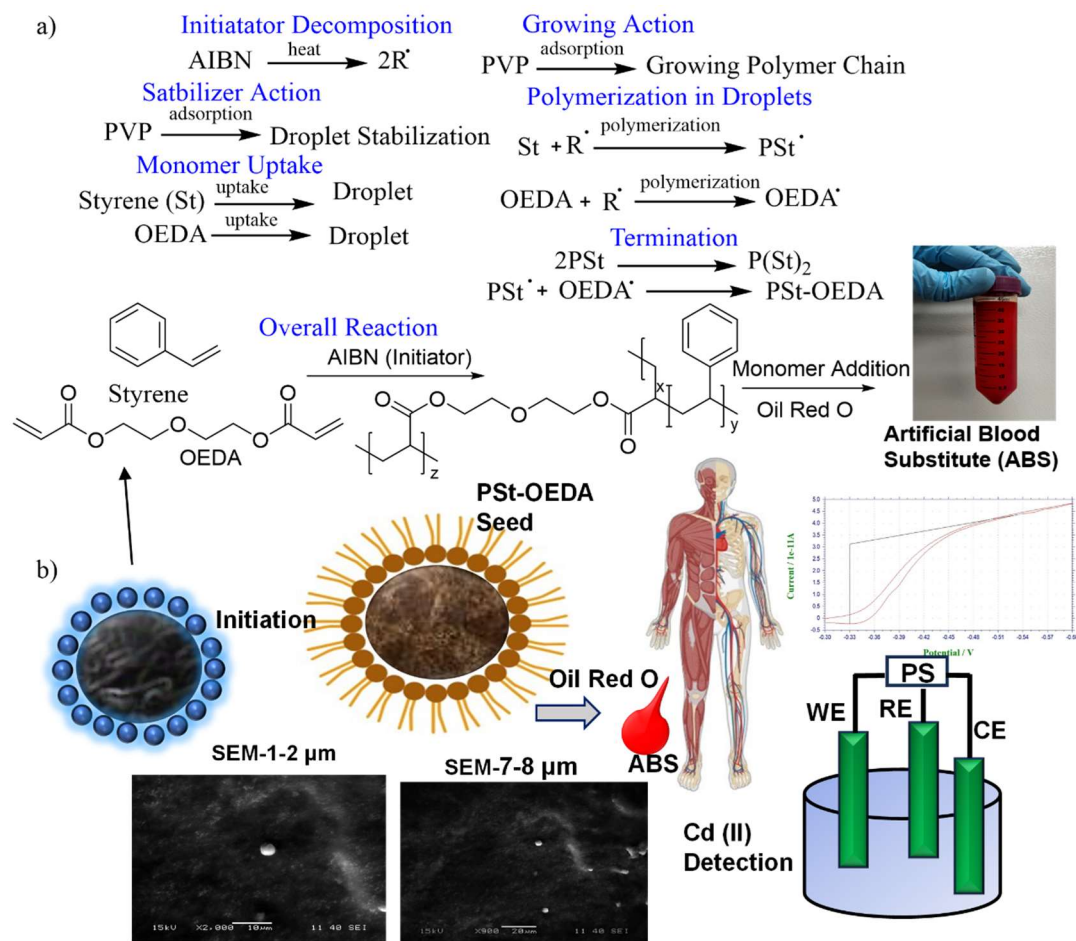


Figure 7 Representation of synthesis of artificial blood a) step by step mechanism of polymerization leading to PSt-OEDA seed b) Explore the graphical depiction of ABS formation and, Scanning Electron Microscopy (SEM) images, showcasing the emergence of Artificial Blood (AB) particles in sizes ranging from 1-2 μm to 7-8 μm . (St - Styrene, OEDA - Di(ethylene glycol)diacrylate (75%), PVP - Polyvinylpyrrolidone (M=40,000), AIBN - 2,2'-Azobis(2-methyl-propionitrile) (98%).)

Materials used

Styrene (St, ReagentPlus®, ≥99%), di(ethylene glycol)diacrylate (OEDA, 75%), polyvinylpyrrolidone (PVP, M=40,000), and 2,2'-Azobis(2-methyl-propionitrile) (AIBN, 98%) were purchased from Sigma-Aldrich. Ethyl alcohol (99.5%) was obtained from EMD Millipore Corporation, while n-heptane (99%) was purchased from Fisher Chemical.

Formulating Artificial Blood: A Refined Step-by-Step Process

In the synthesis of artificial blood, a precise procedure was followed. Initially, a mixture of 10g styrene, 0.2g OEDA, 0.3g AIBN, and 10g PVP was dissolved in a 45/15mL ethanol/n-heptane medium within a 250mL 3-neck roundbottom flask under a nitrogen atmosphere. The solution was stirred at a constant rate (150 RPM) using a magnetic stirrer, and the flask was submerged in a water bath with a controlled temperature of 52°C. The reaction was allowed to proceed for 3 hours to form St-OEDA seeds. After this initial phase, an additional solution containing 45/15mL ethanol/n-heptane, 10g styrene, 0.2g OEDA, 0.3g AIBN, and 0.5% (wt. % to styrene) Oil Red O was prepared and loaded into a syringe. Using a syringe pump, the chemicals were gradually added to the flask at a constant rate over a 5-

hour period. The reaction was then allowed to continue for a total of 12 hours. To create the artificial blood substitute, the synthesized particles were dispersed into deionized water. Initially, the particles were separated from the polymerization medium through centrifugation. Subsequently, the particles were removed, dispersed into deionized water, and subjected to multiple cycles of centrifugation and re-dispersion for thorough washing. Following washing, the particles were dispersed in deionized water at a volume concentration of 40%-50%, resembling the hematocrit value of porcine blood. This meticulous process resulted in the production of an artificial blood substitute with the desired characteristics.

The Effect of Stabilizer Concentration on Particle Size

The introduction of a small percentage of suitable stabilizers is essential for achieving particle dispersion stability. The primary function of these stabilizers is to establish a protective layer on each particle surface, preventing direct contact between particles. This form of stabilization is commonly referred to as "steric stabilization." Optimal stabilizers for dispersion polymerization are polymer and oligomer compounds with low solubility in the polymerization medium and a moderate affinity for polymer particles. In alcohol or other polar solvent-based dispersion polymerization, various polar organic polymers, including polyvinylpyrrolidone (PVP), poly(vinyl alcohol), and cellulose derivatives, are employed as stabilizers, either independently or with co-stabilizers. The resulting particle size is intricately influenced by factors such as temperature, initiator

concentration, stabilizer concentration, monomer concentration, and the type of stabilizer used. Additionally, the solvency of the medium plays a role in determining particle size. Notably, the particle size distribution exhibits a narrow range, and the average particle sizes demonstrate a modest decrease with increasing PVP concentration. Remarkably, the particle sizes achieved through dispersion polymerization align with the dimensions of human red blood cells. This nuanced control over particle size is crucial for tailoring the properties of synthesized polymers for specific applications. In the synthesis of formulating artificial blood, the chemical interaction between di(ethylene glycol)diacrylate (OEDA) and styrene initiates a copolymerization process facilitated by the radical initiator azobisisobutyronitrile (AIBN; see Fig. 7). This process leads to the formation of copolymer chains with incorporated diethylene glycol and acrylate functionalities. OEDA's acrylate groups contribute to cross-linking within the copolymer structure, while diethylene glycol units may enhance hydrophilicity. The copolymer growth, termination reactions, and the stabilizing role of polyvinylpyrrolidone (PVP) are integral to the synthesis. Additionally, Oil Red O serves as a dye or modifier, influencing the final characteristics of the artificial blood substitute. Particles were synthesized using the procedure described in the above section with 1g and 10g PVP, respectively. Optical microscope imaging along with ImageJ analysis shows that the particles that were produced using 1g PVP formed suspended organic particles with an average diameter of 7-8 μm , while the ones produced using 10g

PVP had an average particle size of 1-2 μm . This meticulously designed process aims to replicate specific features of natural blood cells, presenting a versatile synthetic material potentially suitable for biomedical applications.

Incorporate Oil Red O

Oil Red O dye was purchased from Sigma-Aldrich. In the initial phase, St-OEDA seeds were allowed to form during the first 3 hours of polymerization.

Subsequently, a continuous addition of 0.5% (wt. % to styrene) Oil Red O, along with the remaining chemicals, was performed using a syringe. The reaction was then allowed to progress for a total duration of 12 hours.

Electrode fabrication

Borosilicate glass capillaries (O.D. $\frac{1}{4}$ 1.0 mm, I.D. $\frac{1}{4}$ 0.58 mm, Sutter Instruments, CA, USA) were pulled using a P-2000 laser puller (Sutter Instruments, CA, USA) to create nanopipets with a tip diameter of 851 nm as seen in Figure S39. The nanopipet tip diameters were precisely measured using a scanning electrochemical microscope, JEOL JSM-6380LV (JEOL Ltd, Tokyo, Japan). Prior to filling the nanopipets with the organic phase, the inner walls were silanized with chloromethylsilane. Silanization of glass pipettes is essential when the organic phase is placed inside a glass pipette. The hydrophilic nature of the inner wall of glass pipets allows the outer aqueous phase to penetrate inside the pipet, displacing the organic phase upward from the tapered end and interfering with electrochemical

measurements. This problem is circumvented by coating the inner walls of the glass pipets with a hydrophobic material such as chloromethylsilane, making them more hydrophobic and resistant to aqueous solutions. This study placed pipets inside a desiccator connected to a vacuum pump, and after establishing sufficient vacuum inside the desiccator, chlorotrimethylsilane (500 mL) was introduced for 30 min to 1 h, with the silanization time varying based on the relative humidity and ambient temperature. The silanized nanopipets were then filled with the organic phase, which consisted of dichloroethane containing 10 mM 1,10-phenanthroline (phen) as the ionophore and 0.1 M tetradodecylammoniumtetrakis(penta-fluorophenyl)borate (TDDATFAB) as the electrolyte, which was synthesized according to a previously described method⁴⁹.

Electrochemical experiments

Electrochemical experiments were performed using a CHI660E potentiostat (CH Instruments, TX, USA) in a three-electrode configuration. A custom-made Ag/AgCl was used as the reference electrode, while a Pt wire (Alfa Aesar, MA, USA) was used as the counter electrode. Each experiment was carried out using a minimum of 4 nanopipets, and each nanopipet was used for three runs, resulting in at least 12 runs for each experimental condition, ensuring reproducibility.

3.3. Results and Discussion

Developing an electrochemical sensor for metal monitoring poses certain challenges, particularly in achieving the necessary sensitivity and selectivity to detect the target analyte accurately. This becomes more challenging when conducting *in vivo* measurements in complex matrices like blood, where interfering ions such as Ca(II) and other charged molecules are present. Therefore, it is essential to develop a sensor capable of detecting the target analyte Cd(II) along with Ca(II), providing distinct, assignable signals or peaks for each. There have been many attempts at simultaneous detection of analytes using electrochemical sensors. In these, the studies either make use of multi-channels^{98,99} or single-channels⁸³⁻⁸⁶. However, single-channel sensors have distinct advantages over multi-channel sensors in that they have fewer electrode preparation steps, translating to cheap and easy fabrication. They have no dimensional discrepancies between channels, which reduces the number of variables, thereby minimizing uncertainties and making theoretical modeling more straightforward. Among the electrochemical sensors that are capable of simultaneous detection of metal ions using single channels, most of them employ traditional electrochemical techniques such as SWV, SWASV, and DPV with a single working electrode configuration. While these studies show great selectivity and sensitivity, they require cumbersome electrode fabrication steps, which are expensive to mass produce, and do not have Ca(II) in the metal ion mixture. They also require the metal to undergo complex

redox electrochemistry, making the simple ion transfer mechanism of ITIES an attractive alternative. Out of the limited recent studies focusing on the simultaneous detection of metal ions using ITIES, Mastouri *et al.* demonstrated the concurrent detection of Pb(II), Cd(II), and Zn(II) by employing an ITIES assisted by an 8-hydroxyquinoline ionophore⁹⁴. However, their findings revealed that the mixture of ions produced only a single electrochemical process, with the stationary currents increasing in direct linear proportion to the total concentration of M(II) ions added to the water. This approach enables an overall detection of heavy metals rather than distinguishing between individual metal ions. This may lead to significant uncertainty in uncontrolled studies, such as detecting metal ions in biological samples, due to interference from other metal ions. In this study, we employ 1,10-phenanthroline (phen) for the assisted nano-ITIES to detect Cd(II) in the presence of Ca(II). We have previously reported that phen has a great affinity towards Cd(II), and our sensor showed great analytical ability⁹². We now sought to explore the same single bore single ionophore configuration for the detection of Cd(II) in the presence of Ca(II) in excess in intricate matrices such as artificial urine (AU) and artificial blood (AB).

3.3.1 Testing in MP-AU

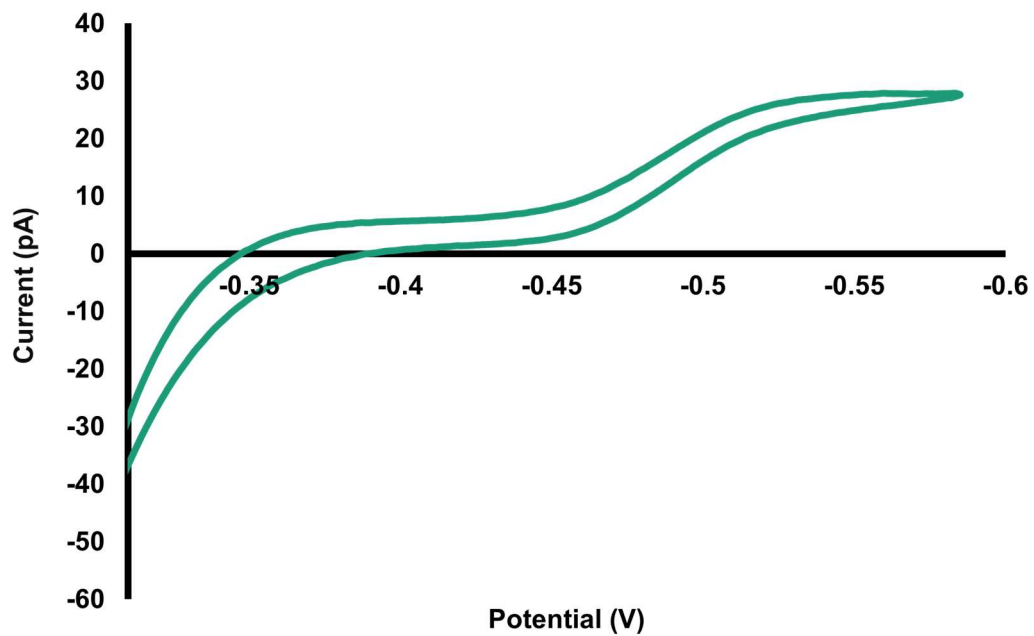


Figure 8 A representative CV of Cd(II) transfer between MP-AU and DCE at a scan rate of 20 mV/s. Aqueous phase: 0.4 mM Cd(II) in MP-AU. Organic phase: 10 mM phen and 0.1 M TDDATFAB in DCE.

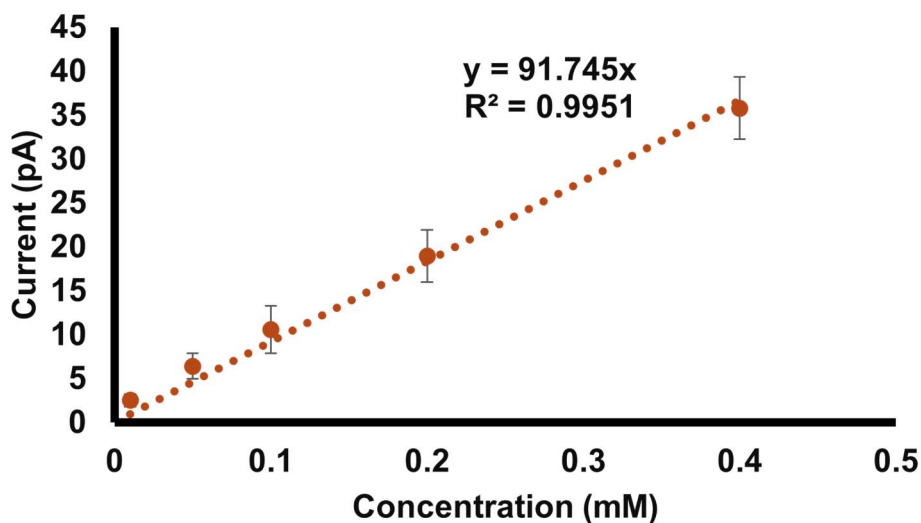


Figure 9 Calibration curve in MP-AU for Cd(II) transfer. Each data point represents the average current \pm standard error of the mean. Aqueous phase: x mM Cd(II) in MP-AU, where x = 0.01, 0.05, 0.1, 0.2 and 0.4. Organic phase: 10 mM phen and 0.1 M TDDATFAB.

Many options for the preparation of artificial urine were considered¹⁰⁰⁻¹⁰².

However, Sarigul *et al.* developed a new artificial urine protocol (MP-AU) that closely mimics the chemical composition of human urine at the molecular level, as confirmed by ATR-FTIR spectroscopy⁹⁶. They compared MP-AU with two other commonly used artificial urine formulations and found that MP-AU showed the closest similarity to the average spectrum of urine samples from 28 healthy individuals, demonstrating its potential as a reliable and economical substitute for human urine in various research applications. Therefore, we proceeded with MP-AU for further electrochemical analysis. After the fabrication and preparation of the electrodes, we performed calibration studies for the detection of Cd(II) in MP-AU.

Figure 8 shows a typical cyclic voltammogram (CV) for Cd (II) in MP-AU. It is

observed that the nano-ITIES electrode provides a steady state sigmoidal forward and backward scan. The calibration curve of Cd(II) in MP-AU is shown in Figure 9 depicts a sensitivity of 91.745 pA mM⁻¹ and a limit of detection (LOD) of 0.01 mM. We examined the stability of the interface of our sensors by performing amperometric measurements for a span of 50 sec. The results can be seen in Figure S40, where we find that the current does not deteriorate over time. This is of great significance as most studies that perform ITIES measurements tend to use simple matrices, which facilitates a stable interface, whereas, from the stability study, we find that our sensor is able to maintain a stable interface for extended periods of time in MP-AU, which is made using a combination of 13 different components. From the tests performed in MP-AU, we find that our nano-ITIES sensor's performance is largely similar to our previous studies that have been performed in various complex matrices, showcasing the robustness of our sensor.

3.3.2 Testing in AB

Human blood composition consists of 45% blood cells and 55% blood plasma. It can be considered as a suspension of cells in aqueous solution containing 90% water by weight⁹⁷. Among the suspended particles are predominantly red blood cells (RBC), followed by platelets and white blood cells (WBC)¹⁰³. While the shape and size of the red RBC and plasma are fairly constant, the WBC has various subtypes that have different shapes and sizes¹⁰⁴. Furthermore, the WBC varies in concentration depending on the physiological conditions of the body, such as the

presence or absence of pathogens, whereas the concentration of RBC and platelets remains constant. Therefore, we designed our artificial blood with molecules that mimic RBC and platelets by synthesizing organic molecules that mimic the size of RBC and plates, which are 7-8 μm and 1-2 μm , respectively. A scanning electron microscope image of the synthesized organic molecules confirmed these dimensions, as seen in Figure 7, and the image distribution was also confirmed separately with an optical microscope (not shown). These organic molecules were suspended in an artificial blood medium, as described in the experimental methods. Many electrochemical experiments have been performed in blood substitutes, such as artificial blood serum and artificial blood media¹⁰⁵⁻¹⁰⁹. However, all of these diluted the blood substitute at least 5-10 times to achieve a higher signal-to-noise ratio. In our experiments, we diluted our artificial blood samples 5 times with 0.3 M KCl to increase the signal-to-noise ratio, as it was observed that non-conventional response, with a pre-peak, was observed with undiluted blood, as seen in Figure S41. A typical CV for 0.4 mM Cd(II) in AB is shown in Figure 10, which has a slightly higher ohmic loss and hysteresis, which can be attributed to a matrix effect on the sensor. The responses in AB were also, in general, noisier than the response in MP-AU, which can be attributed to slight instability of the interface, which may be caused due to interactions of the interface with the synthesized organic molecules. However, a steady-state sigmoidal forward and backward scan is still observed. The calibration curve of Cd(II) in AB is shown in Figure 11

depicts a sensitivity of $144.16 \text{ pA mM}^{-1}$ and a limit of detection (LOD) of 0.01 mM .

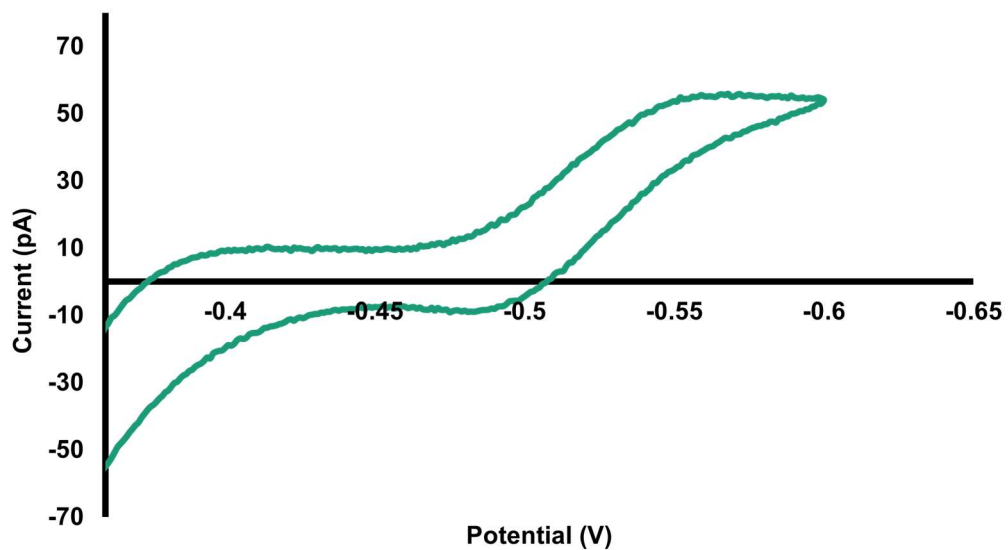


Figure 10 A representative CV of Cd(II) transfer between AB and DCE at a scan rate of 20 mV/s . Aqueous phase: 0.4 mM Cd(II) in AB. Organic phase: 10 mM phen and 0.1 M TDDATFAB in DCE.

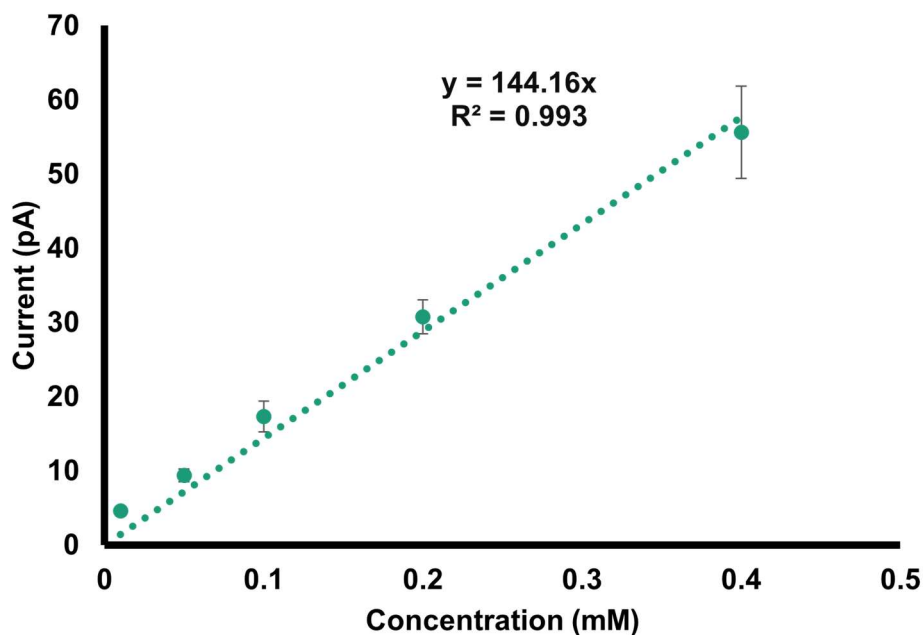


Figure 11 Calibration curve in AB for Cd(II) transfer. Each data point represents the average current \pm standard error of the mean. Aqueous phase: x mM Cd(II) in AB, where x= 0.01, 0.05, 0.1, 0.2, and 0.4. Organic phase: 10 mM phen and 0.1 M TDDATFAB.

3.3.3 Detection of Ca(II) in AB

Blood contains prominent levels of Ca(II) with an average concentration of 2.5 mM⁹⁵. This is of major concern for electrochemical systems that are designed to detect Cd(II) in blood, as Ca(II) can be a potential interfering ion in the electrochemical process. It is important to study the response of the proposed electrochemical sensor toward Ca(II) and determine the effects, it has on the detection of Cd(II) in AB. Ideally, developing a sensor capable of detecting both these metal ions will be well-suited for biological application. A typical CV for 2.5 mM Ca(II) in AB can be seen in Figure 12, where we see a sigmoidal response with a plateau current of 15.59 pA and plateau potential of -0.8 V, which is more

negative than that of Cd(II) at -0.53 V. This huge difference in plateau potential can serve as a beneficial signal separator between these two metal ions.

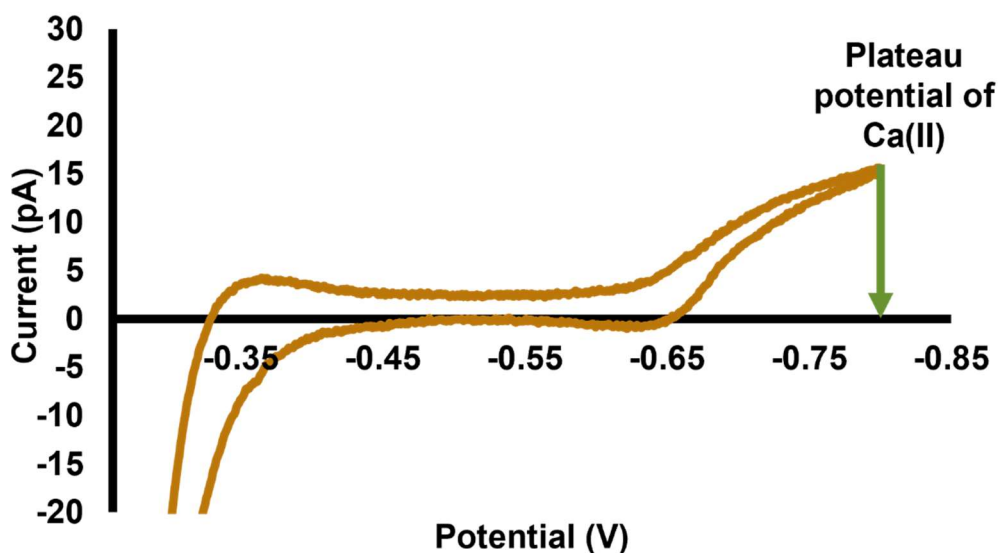


Figure 12 A representative CV of Ca(II) transfer between AB and DCE at a scan rate of 20 mV/s. Aqueous phase: 0.4 mM Ca(II) in AB. Organic phase: 10 mM phen and 0.1 M TDDATFAB in DCE.

3.3.4 Simultaneous detection of Cd(II) and Ca(II) in AB

After establishing the response of Cd(II) and Ca(II) separately in AB, we now examine the response of our sensor for both these metal ions in a mixture in AB.

The steady-state diffusion limiting current for our sensor is given by equation 3:

$$i_d = 4xzFDCr \quad (\text{Eqn 3})$$

where, i_d , the diffusion limiting current is directly proportional to the concentration, C , in the electrochemical cell, D is the diffusion coefficient of the phase of origin, F

is the Faraday constant, z is the charge of the analyte, x is the parameter that accounts for the thickness of the glass wall, and r is the internal radius of the working electrode.

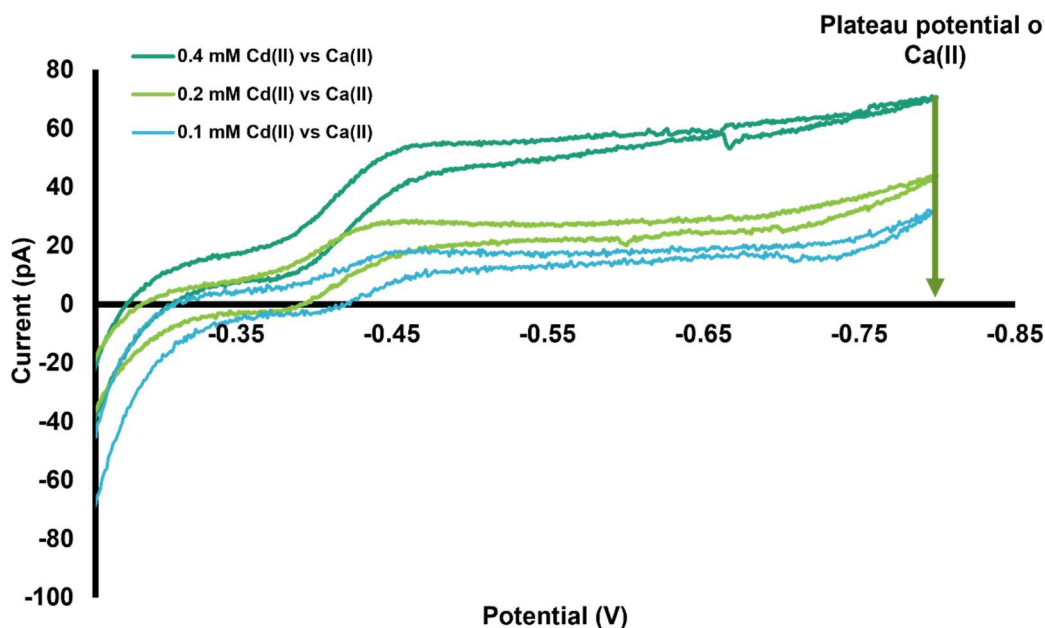


Figure 13 Representative CVs obtained for the simultaneous detection of Cd(II) and Ca(II) in AB, at a scan rate of 20 mV/s. Aqueous phase: x mM Cd(II) in AB, where $x = 0.1, 0.2, \text{ and } 0.4$, and 2.5 mM Ca(II) in each case. The green arrow indicates the plateau potential region of Ca(II).

Mastouri *et al.* previously demonstrated perfect additivity of currents from 1 to 256 micropores for the detection of Cd(II) using ITIES⁸⁹. Based on this study and equation (1), we expect the currents to have an additive nature. The results from the simultaneous detection of Cd(II) and Ca(II) can be seen in Figure 13, which was performed with three different concentrations, 0.1, 0.2 and 0.4 mM of Cd(II) with plateau potential of -0.53 V, and a single concentration of Ca(II) at 2.5 mM with

plateau potential of -0.8 V. It can be seen that the response from Cd (II) and Ca(II) are completely separate from each other, and their salient electrochemical features are preserved. The plateau potential is consistent among the individual and simultaneous runs, and the currents in the simultaneous runs display an additive behavior of the currents observed in the individual runs. From the calibration curve, we see that the average plateau current for Cd(II) for the concentrations 0.4, 0.2, and 0.1 mM is 55.62 pA, 30.78 pA, and 17.33 pA, respectively, while the plateau current for 2.5 mM Ca(II) in AB is 15.59 pA. In the simultaneous runs, we see that the plateau current measured for Cd(II) at -0.53 V for concentrations 0.4, 0.2, and 0.1 mM are 55.56 pA, 27.08 pA, and 17.97 pA, respectively, while the corresponding response for Ca(II) for these three runs are 70.65 pA, 43.71 pA, and 32.60 pA respectively. The difference in current between the response for Cd(II) and Ca(II) for each run is calculated to be 15.09 pA, 16.63 pA, and 14.63 pA, respectively, which averages to 15.45 pA, which is the expected current for 2.5 mM Ca(II) in AB. This provides new insights into the potential of utilizing phen as an effective ionophore in the detection of Cd(II) ions in the presence of excess, physiologically relevant Ca(II) ions using nano-ITIES. This approach greatly simplifies the potential simultaneous detection of metal ions using ITIES and alleviates the need for complicated fabrication of double bores, thus simplifying the fabrication process, minimizing uncertainty, cutting costs, and reducing the caveats for theoretical modeling.

3.3.5 EDTA calcium disodium as a binder for Cd(II)

Early treatment of cadmium toxicity in humans is crucial to prevent organ damage and long-term health consequences. Chelation therapy is a primary treatment approach that involves administering chelating agents to bind and remove cadmium from the body¹¹⁰. Common chelating agents used for cadmium toxicity include calcium disodium ethylenediaminetetraacetic acid (EDTA), which has shown efficacy in reducing toxic metal burden and improving symptoms in patients with neurodegenerative diseases¹¹¹. Other chelators such as desferrioxamine (DFO), deferasirox (DFX), and deferiprone (DFP) have been studied in animal models, demonstrating their ability to enhance urinary and biliary excretion of cadmium and restore altered levels of essential metals like iron¹¹². In addition to intravenous chelation therapy, oral tablets such as D-penicillamine and succimer have been used as treatment options for cadmium toxicity¹¹⁰. These oral chelators can easily be administered at home, making them more convenient and effective for patients.

To examine the efficiency of such chelation therapy, a common chelation agent, EDTA was added in a 1:1 ratio with Cd(II) in AB, and the solution was adjusted to a pH of 7.4 by adding the required amount of sodium hydroxide to the solution. The rationale behind this study is to examine the response of our sensor for Cd(II) in the presence of EDTA and to derive the conditional stability constant of the system.

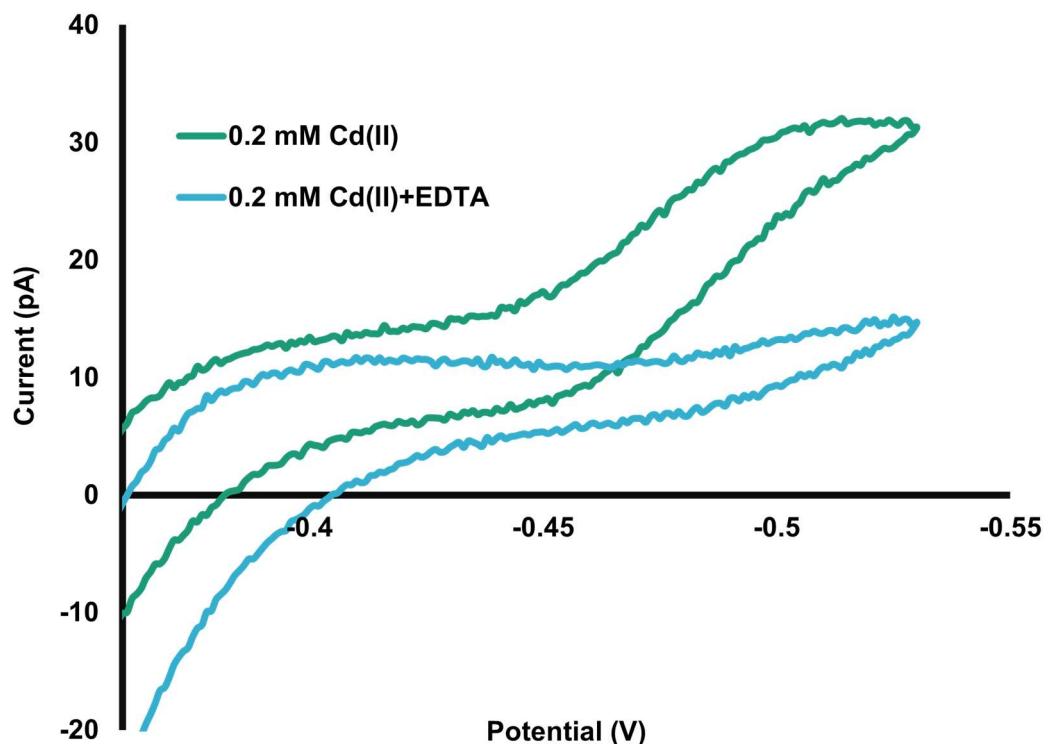


Figure 14 CV of 0.2 mM Cd(II) in AB (green) and 0.2 mM Cd(II) in AB in the presence of EDTA in the solution (light blue), with a scan rate of 20 mV/s. Organic phase: Organic phase: 10 mM phen and 0.1 M TDDATFAB in DCE.

Figure 14 shows the response of our sensor for 0.2 mM Cd(II) in the presence of equimolar EDTA. It can be observed that the plateau current of the sensor for the metal-ligand complex is much lower than that of the ligand-free system. The extended response is shown in Figures S42 and S43. From Figure S42, we infer that the response appearing after -0.53 V is interactions of ions other than Cd(II), possibly deriving from the interactions of the chelating agent and other components in AB. Similar to Figure 14, the response of our sensor for 0.4 mM Cd(II) in the presence of EDTA, as seen in Figure 15, is much lower than in the absence of the

chelating agent. The formation of complexes between Cd(II) and EDTA in AB can be affected by several phenomena, such as ligand protonation, interactions of Cd(II) with components of AB, and interaction of EDTA with components of AB. Thus, it is very difficult to calculate the theoretical stability constants in AB, as this would require extensive research and understanding of the interactions of AB with the metal and ligand. Therefore, the conditional stability constant of Cd(II)- EDTA in AB is calculated, which is given by equation 4:

$$k' = \frac{[Cd(EDTA)]}{[Cd^{2+}] [EDTA]} \quad (Eqn. 4)$$

where $[Cd(EDTA)]$ is the concentration of the complex, $[Cd^{2+}]$ is the concentration of free Cd(II), and $[EDTA]$ is the initial concentration of EDTA. Based on the response seen in Figure 14, it is seen that the plateau current of 0.2 mM Cd(II) is 31.80 pA, while the plateau current of the same in the presence of EDTA is 14.72 pA. This indicates that the ratio of free Cd(II) ions in the presence of EDTA is $14.72 / 31.80 = 0.4629$ of the initial free Cd(II) in the 0.2 mM solution. Therefore, the concentration of free Cd(II) ions is 0.093 mM, and that of Cd(EDTA) complex is 0.107 mM. Substituting these values into equation 2, we calculate the conditional stability constant to be 5.752×10^4 . The $\log(k')$ value is calculated as 3.75, which is lower than the literature-reported values for Cd(II)-EDTA complex in a simple solution⁶¹. This is understandable as EDTA interacts with other components of AB, hindering the binding ability to Cd(II), thus yielding a lower value for $\log(k')$.

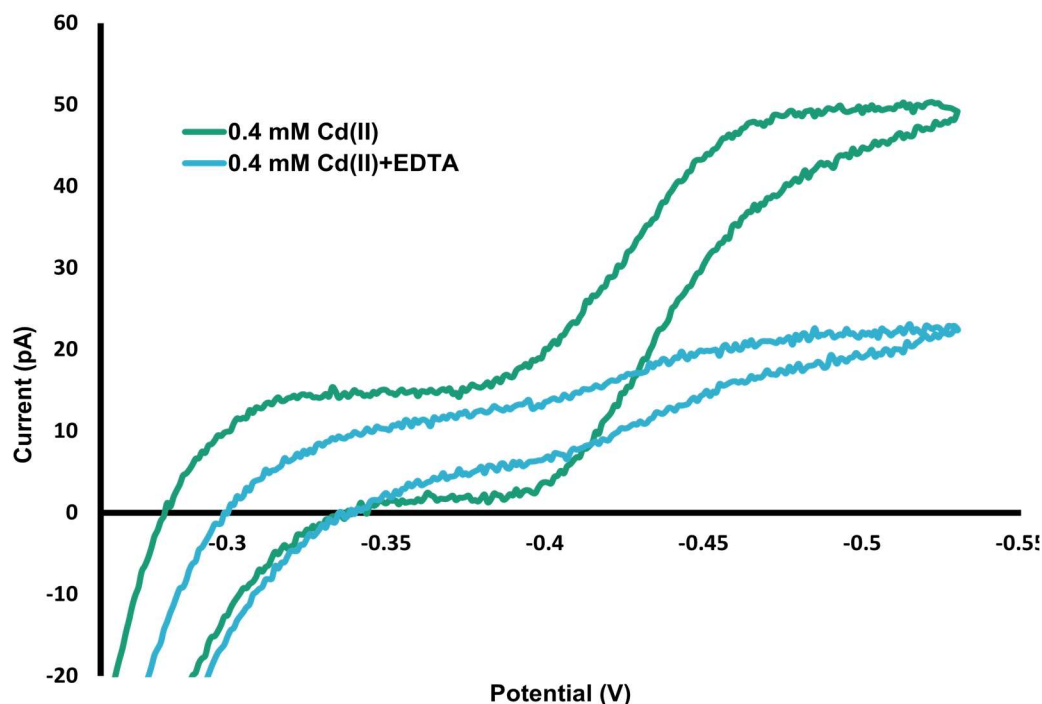


Figure 15 CV of 0.4 mM Cd(II) in AB (green) and 0.4 mM Cd(II) in AB in the presence of EDTA in the solution (light blue), with a scan rate of 20 mV/s. Organic phase: Organic phase: 10 mM phen and 0.1 M TDDATFAB in DCE.

Similar to Figure 14, it can be seen in Figure 15 that the plateau current in the absence of EDTA is 50.90 pA, and in the presence of EDTA, it is reduced to 22.63 pA. The ratio of free Cd(II) in the presence of EDTA is $22.63 / 50.90 = 0.4446$ of the initial free Cd(II) in the 0.4 mM solution. Therefore, the concentration of free Cd(II) ions is 0.178 mM and that of Cd(EDTA) is 0.222 mM. Substituting these values in equation 2, we calculate the conditional stability constant (k') to be 3.117×10^4 . The $\log(k')$ value is calculated as 3., which is similar to the one calculated earlier for 0.2 mM Cd(II). This experiment provides insights into the interaction of EDTA with Cd(II) ions in complex AB media. The significant reduction in the

plateau current indicates that a substantial amount of Cd(II) is complexed with the EDTA, providing evidence that EDTA supplements are an effective treatment for cadmium toxicity in the body. However, it must be noted that the chelation therapy medical remedy takes time to be effective against such toxicity, and early diagnosis will largely aid in the success of chelation therapy¹¹⁴. Thus, our cost-effective, smart, portable, and reliable sensor can aid in the success of such reversible metal mitigation treatments.

3.4. Conclusion

In this study, we have successfully developed a single bore, single ionophore electrochemical sensor capable of simultaneous detection of Cd(II) and Ca(II) in complex matrices such as artificial urine (MP-AU) and artificial blood (AB). The sensor uses ion transfer between two immiscible electrolyte solutions (ITIES) and demonstrates excellent sensitivity, selectivity, and stability. Compared to double-bore configurations, the streamlined fabrication process, which uses a single-bore and single-ionophore configuration, reduces the number of variables and uncertainties, allowing for easier theoretical modeling. Our sensor showed exceptional performance in MP-AU and AB, which showcases its robustness and potential for real-world applications such as healthcare monitoring. The simultaneous detection of Cd(II) and Ca(II) in AB addresses a significant caveat that may be faced during *in vivo* measurements and marks a significant advancement in ITIES technology. The sensor's ability to provide distinct,

assignable signals for each metal ion enables Cd(II) detection without interference, which greatly enhances its utility and reliability. The additive nature of the currents observed in the simultaneous detection experiments aligns with theoretical expectations, further validating the sensor's performance. The investigation of the sensor's response in the presence of a chelating agent, EDTA calcium disodium, in AB provides valuable insights into the conditional stability constants of the Cd(II)-EDTA complex in the intricate AB matrix. The significant decrease in plateau current indicates the effectiveness of EDTA supplements in treating cadmium toxicity, highlighting the importance of early diagnosis and the potential role of our sensor in aiding the success of chelation therapy.

Chapter 4

Artificial Intelligence-Enhanced Differentiation and Quantification of Metal Ions Using ITIES-Based Electrochemical Sensors

This dissertation chapter content covers research objective iii. It is in preparation for publication in an appropriate scientific journal. Authors: Muzammil M.N.

Ahmed, Parth Ganeriwala, Anthi Savvidou, Siddhartha Bhattacharyya, Pavithra Pathirathna*

*Corresponding Author: Pavithra Pathirathna (ppathirathna@fit.edu); 150 W. University Blvd, Melbourne, FL 32904

Abstract

Electrochemical sensors are an emerging field due to the ease of fabrication, the variety of techniques available, and the vast number of working electrodes that can be employed depending on the assigned task. These sensors provide numerous advantages over conventional ones in that they are very cost-effective, easy to fabricate and maintain, have high selectivity and sensitivity, and are relatively easy to use. In this realm, ITIES poses itself as one of the fastest-growing branches that depends on simple ion transfer rather than complex redox chemistry adopted by other electrochemical techniques. While ITIES sensors are comparatively easy to use, considerable improvements can be made to make them more user-friendly.

One common claim that many electrochemists have is that the shape of the cyclic voltammogram (CV) is unique for each analyte. Although experts in the field back this claim, it can be challenging for a nonexpert to spot the subtle differences, especially for certain analytes that appear very similar and have very small separations in their half-wave potentials. A method to scientifically determine the difference based on the shape has yet to be developed and implemented while doing so will expand the ease of use of such electrochemical sensors. In this study, we have developed a method based on AI that implements both ANN and CNN to help evaluate the CVs obtained from ITIES. The CNN model helps us identify any faults in the CV and differentiate the Good CVs from the faulty ones. The CNN will then be able to examine the good CV and determine if it is an electrochemical response from Cd(II) or Cu(II) based on the shape and salient electrochemical features in the sigmoidal steady state forward and backward scans. The ANN model will then be used to examine the CV with relevant information, such as plateau current and plateau potential, to determine the concentration of the analyte present. To the best of our knowledge, this is the first time a method to scientifically differentiate two analytes based on the electrochemical response from an ITIES sensor is reported. This study provides valuable insights into the integration of AI with ITIES-based sensors, and this knowledge can be transferred to build similar models for the detection of other metal ions.

4.1. Introduction

In recent years, the global problem of heavy metal contamination has compounded at an alarming rate. The number of urban industries that rely on heavy metals for various commercial processes has increased steadily, with many exploiting the catalytic abilities of such heavy metals¹¹⁵. However, economically and energetically inefficient recycling systems cause industries to overlook the possibility of recycling these heavy metals, exposing them to the environment. These heavy metals enter the food chain, and due to biomagnification, it affects all levels of the food chain¹¹⁶. One of the major pathways of exposure is through the uptake of contaminated water by plants and animals¹¹⁷. Therefore, there is a need to develop effective sensors for heavy metals in aqueous samples that will help implement and establish metal mitigation systems that will help reduce the risk of exposure to humans and the environment¹¹⁸⁻¹²⁰. Many such tools for detecting heavy metals have been developed over recent decades. Of these methods, the conventional methods include clinometry and mass spectrometric techniques such as ICPMS¹¹⁹. Although ICPMS is the golden standard for the detection of metal ions in aqueous samples due to its high accuracy and sensitivity, it has certain caveats that limit its use and widespread adoption^{121,122}. The equipment is very expensive, and bulky and requires a trained individual for operation and maintenance. They are very expensive both in terms of capital and operational costs. They require cumbersome sample pretreatment steps that can only be

performed by experts, coupled with a lengthy analysis time^{123–125}. The sample pretreatment can alter the speciation of the heavy metal ions and give no information about the speciation of the heavy metal. The instrument is not portable, which limits its ability for onsite use¹²⁶. All these factors limit the use of ICPMS within lab settings, with high capital and operational costs and lengthy analysis times.

On the other hand, electrochemical sensors, which is a fast-growing field within analytical chemistry, provide an attractive alternative^{127,128}. These sensors are fast, portable, cost-effective, and reliable and can provide accurate information on the speciation of heavy metal ions, which is invaluable information for determining the toxicity of the heavy metal. These sensors can be successfully miniaturized, which decreases the cost of the sensors and increases the portability^{129,130}. They do not need lengthy sample pretreatment and can be easily operated by non-experts in the field¹³¹. Some of the common electrochemical techniques for the detection of heavy metal ions in aqueous solutions include cyclic voltammetry, FSCV, and amperometry^{74,98,127,132,133}. Cyclic voltammetry measures the current response while sweeping the potential back and forth, providing qualitative information. Anodic stripping voltammetry involves a pre-concentration step followed by stripping of the analyte, enabling low detection limits. Amperometry uses a fixed potential to measure the current response, allowing for sensitive quantitative analysis^{134,135}. Significant research efforts have focused on developing new electrochemical

methods and modifying electrode surfaces to enhance the sensitivity and selectivity for heavy metal detection. Strategies include using chemically modified electrodes, nanostructured interfaces, and incorporating selective recognition elements like DNA, peptides, and metal-organic frameworks^{136–138}. Shan *et al.* developed an electrochemical sensor using a GR/GO-modified glassy carbon electrode for the sensitive detection of cadmium ions in water samples by differential pulse voltammetry¹³⁹. Sacara *et al.* used square wave anodic stripping voltammetry with glassy carbon electrodes modified with various ordered mesoporous silica materials and Nafion to detect Cd(II) ions in solution¹⁴⁰. Manring *et al.* reports using fast-scan cyclic voltammetry with carbon fiber microelectrodes, which were surface-modified by electrodepositing dopamine, in order to enhance the detection of Cu(II) ions in solution. The dopamine coating improved the limit of detection and sensitivity for measuring Cu(II) compared to bare, unmodified carbon fiber electrodes¹³³.

While these electrochemical methods show great sensitivity and detection limits for heavy metals, they require the target analyte to undergo complex redox reactions, achieved by tedious electrode fabrication steps. This makes the electrode fabrication process lengthy and expensive. In this light, ion transfer between two immiscible electrolyte systems (ITIES) emerges as an attractive alternative to conventional electrochemical techniques in that it does not require such redox reactions to take place within the system. ITIES exploits electrochemistry at the

interface between water and organic solvent and detects the ions that move from one phase to the other under the influence of an electric potential. The current is measured as a result of direct ion transfer in lieu of transfer of electrons. This simple yet effective electrochemical technique was initially developed to study the kinetic interactions of proteins and other biological analytes with higher oxidation states, such as proteins¹⁴¹. However, ITIES has also been employed to study the kinetics of metal ions with lower oxidation states, such as K^+ and Na^+ ¹⁴².

Shen *et al.*⁴² synthesized tris(crown ether) ionophore, TriBCE, for the assisted ion transfer of various metal ions; Mg(II), Cu(II), Cd(II), Li(i) and dopamine at nanopipette-based ITIES electrodes. Compared to the mono(crown ether) ionophore DB18C6, TriBCE enabled easier transfer of the ions, characterized by less positive half-wave transfer potentials, higher binding constants, and more negative Gibbs free energy of complexation. The stoichiometry of TriBCE complexation was 2:1 with Cd(II) and 1:1 with Li(I), providing insights into the interaction between multi-site ionophores and ions of different charges at nanoITIES electrodes. Ishimatsu *et al.*¹⁴³ used cyclic voltammetry to study the kinetics and mechanism of facilitated ion transfer of Ag(II), K(I), Ca(II), Ba(II), and Pb(II) at the interface between water and oNPOE-plasticized PVC membranes doped with selective ionophores. The membranes were supported on Au or GC electrodes modified with a PEDOT-C14 conducting polymer films. The results confirmed a one-step electrochemical (E) mechanism with standard ion transfer rate

constants of 10^{-2} to 10^{-3} cm s^{-1} , rather than a two-step electrochemical-chemical (EC) mechanism. While these studies mainly focus on the kinetics of the metal ions and their response in the forward and reverse scans, ITIES was previously used as an analytical tool for quantifying the amount of Cd(II) in an environmental sample in our previous work⁹². The nanopipet sensor was employed to detect Cd(II) in the Indian River Lagoon, Melbourne, FL, and the results were in close agreement with the analysis from ICPMS, showcasing the analytical ability of ITIES sensors.

The advancement of electrochemical sensors in recent years and the simplicity of ITIES present such sensors as an attractive alternative to conventional techniques that are not user-friendly, nor portable. However, these electrochemical sensors generate results in the form of a cyclic voltammogram (CV), which is a graph plotted between current and voltage depicting the forward and reverse scans. Although these plots can be easily analyzed by experts in the field, it is challenging for a non-expert to look at and analyze these plots. It is further challenging to differentiate the electrochemical response emerging from different metal ions that have small separations in their half-wave potential, while over-dependence on half-wave potential as the sole indicator of the identity of the metal ion may not be practical, as sensor drift may affect half-wave potential in practical applications. CVs have many salient electrochemical features that can be extracted from them, and developing a smart method to analyze them will greatly improve user-friendliness with such electrochemical sensors. There have been many recent

studies that have integrated Artificial Intelligence (AI) with electrochemical sensors^{144–149}. Many factors, such as the ease of integration, the instrumentation, and the speed of the analysis time, make it a successful combination.

Electrochemical sensors can produce a large amount of data within a short period of time, which can be processed and digested by various AI architectures to provide valuable insights. The quick operation times of these sensors make them more suitable for integration with AI than other conventional analytical methods. Wang *et al.* presents a novel dual-modal fluorescence (FL) and electrochemistry (EC) sensor combined with neural networks for simultaneous detection of cadmium Cd(II) and lead Pb(II) ions in complex water samples¹⁵⁰. The sensor uses quantum dots for FL detection of Cd(II) and sea urchin-like FeOOH modified gold electrodes for EC detection of Pb(II). A one-dimensional convolutional neural network (1D CNN) was implemented to process the combined FL spectra and EC current curves, enabling simultaneous detection without sample pretreatment. The CNN model reported mean absolute errors of $0.2176 \mu\text{g L}^{-1}$ for Cd(II) and $0.6002 \mu\text{g L}^{-1}$ for Pb(II), with R-squared values of 0.974 and 0.999 respectively.

Choi *et al.* compares deep learning and principal component regression (PCR) for analyzing fast-scan cyclic voltammetry (FSCV) data to estimate neurotransmitter concentrations¹⁵¹. They implemented a 1D convolutional neural network (CNN) using TensorFlow and Keras, with multiple convolutional and max-pooling layers followed by fully connected layers. The CNN was trained on FSCV

voltammograms from dopamine, epinephrine, norepinephrine, and serotonin at various concentrations. CNN aimed to improve neurotransmitter identification and concentration estimation, especially for mixtures. Results showed CNN outperformed PCR, reducing RMSE by 5-20% for mixtures. This study demonstrates CNN's potential to enhance FSCV data analysis, particularly for resolving complex neurotransmitter mixtures in physiological environments. Kudr *et al.*¹⁰⁵ developed an automated electrochemical system using differential pulse anodic stripping voltammetry (DPASV) with a thin-film mercury electrode for simultaneous detection of Zn(II), Cd(II), Cu(II), and Pb(II) ions in environmental samples. They implemented a multilayer perceptron artificial neural network (ANN) with 4 input, 8 hidden, and 4 output neurons to correct for interferences between metals and improve quantification accuracy. The ANN inputs were the peak heights for each metal from the voltammograms. The optimized ANN model achieved excellent performance, with R^2 values of 0.995-0.999 for predicting concentrations of all four metals in validation samples. This approach enabled accurate multi-element analysis even with overlapping voltammetric signals. Farris *et al.*¹⁵² investigate the use of machine learning models, including artificial neural networks (ANNs), to predict outcomes in electrochemical CO₂ reduction reactions. The authors implemented a multilayer perceptron ANN using the Keras library, alongside decision trees and random forests, to classify reaction outcomes based on experimental conditions. The ANN was trained on a human-curated dataset of 127

samples from the literature. Key input parameters included catalyst metal, dopant, structure, electrolyte, applied potential, and reaction conditions. The models aimed to predict electron transfer events, carbon-carbon coupling, ethylene production, and major product formation. The ANN performed comparably to shallow learning models, achieving accuracies between 0.7-0.8 for binary classification tasks. However, for multiclass product prediction, the random forest outperformed the ANN with an accuracy of 0.6. The study demonstrates that even with limited datasets, machine learning can provide insights into electrochemical CO₂ reduction, identifying important features like applied potential and electrolyte composition. The authors suggest that larger datasets could further improve predictive capabilities in this field.

Herein, we study the electrochemical response of ITIES sensors for the detection of Cd(II) and Cu(II) ions using CNN and ANN architectures. CNN will be employed to analyze the CV, identify any faults, and differentiate the faulty CVs from the good ones. This model will be trained on both the Cd(II) and Cu(II) datasets, and its performance will be evaluated against each other. It will then identify different types of faults in the CVs, giving us more insights into the electrochemical response. The CNN architecture will finally distinguish between the electrochemical response from Cd(II) and Cu(II). An ANN architecture will be employed to analyze good CVs and predict the concentration of the analytes. To the best of our knowledge this is the first time CNN or ANN is being implemented

on an ITIES based sensor, although similar studies have been performed on other electrochemical based techniques^{150,151,153}.

4.2. Materials and Methodology

Chemicals and electrode fabrication

All chemicals were purchased from Sigma-Aldrich (St. Louis, MO). CdCl₂ was used as the Cd(II) source, and CuSO₄ was used as the Cu(II) source. Aqueous solutions of the metal ions were prepared in 0.3 M KCl solution. Electrode fabrication was done based on our previous work. The nanopipette had a tip diameter of 680 nm.

Electrochemical experiments

A CHI660E potentiostat (CH Instruments, TX, USA) in a three-electrode configuration was used to perform electrochemical experiments. A custom, lab-built Ag/AgCl was used as the reference electrode, while a Pt wire (Alfa Aesar, MA, USA) was used as the counter electrode. The electrochemical experiments were run at a scan rate of 20 mV/sec.

Data acquisition and preprocessing

The CHI660E electrochemical workstation software was used to operate the potentiostat and generate raw data. MATLAB R2023b was used to generate the

images that were used to train the CNN model. It was also used to preprocess the data to reduce the dimensionality before training the ANN model. PyCharm 2024.1 was used to train the CNN and ANN models.

4.3. Results and Discussion

4.3.1 *Electrochemical Detection of Heavy Metals*

Electrochemical sensors have made huge developments in analytical chemistry in recent decades. One of the driving forces behind this is the development of electronics and electrical engineering, which enables the manufacturing of extremely miniaturized sensors that perform with great analytical integrity. The cost of making these sensors has also significantly reduced over the last decade¹⁵⁴. The widespread adoption of these sensors and their portability and affordability make them an attractive tool for commercialization and everyday use by non-experts¹⁵⁵. Many electrochemical sensors deliver the results in the form of CV, which can provide us with three electrochemical features: current intensity (plateau/ peak current), potential (half wave/ peak potential), and the shape of the CV for a particular analyte. While the current intensity is directly proportional to the concentration of the sensor, the half-wave potential is fixed for a given analyte. Therefore, many research studies use well-established half-wave potentials to identify analytes of interest¹⁵⁶. This is successful in a controlled environment such as a lab setting with less variability in experimental conditions. However, in some

electrochemical techniques, such as ITIES and many others, the half-wave potential is known to be affected by changes in the matrix of aqueous phase, such as pH or ionic strength¹⁵⁷. This limits the over-reliance of analytical techniques solely on the half-wave potential for practical application, where there can be dynamic changes to the matrix of the aqueous phase. Also, sensor drift is a common occurrence in electrochemical sensors due to stress and strain during the lifetime of the sensor¹⁵⁸. This makes reliance solely on the half-wave potential impractical for distinguishing between different analytes, especially when the separation in the half-wave potential is small. The third electrochemical feature is the shape of the CV, which is unique for each analyte. A combination of the half-wave potential and the shape of the CV can be used to identify analytes more accurately. While many researchers agree that the shape of the CV can be used to identify the analyte¹⁵⁹, a scientific method to do so has not been developed yet. While experienced researchers use their knowledge to understand the differences between the CVs of different analytes, it is very difficult for non-experts to identify the difference. Therefore, there is a need to develop a scientific method that will analyze the CVs obtained from the electrochemical sensor and predict the analyte, and doing so will greatly increase the user-friendliness of the sensor, making it more accessible and enabling widespread adoption and use.

In this study, we integrated a combination of CNN and ANN to analyze the CVs obtained for Cd(II) and Cu(II) in aqueous solutions. The electrochemical

experiments were carried out using a CHI660E potentiostat. The nanopipette was silanized and filled with the organic phase- 0.1 M tetradodecylammoniumtetrakis (penta-fluorophenyl)borate (TDDATFAB) in dichloroethane (DCE), and 10 mM 1,10 Phenanthroline (Phen) was added as the ionophore. Our earlier studies found that our phen-assisted sensor shows a response for Cd(II) and Cu(II). It must be noted that the half-wave potential for each Cd(II) and Cu(II) showed little separation, making them difficult to differentiate. The CVs also are similar in appearance; therefore, these analytes were chosen for the current study. Solutions containing different concentrations of Cd(II) and Cu(II) were made in 0.3 M KCl as the background electrolyte. The electrochemical sensor was set in a three-electrode system, and a large amount of data was collected for each concentration (>300 scans). The resulting CVs were classified as good and not good. The good CVs had a smooth sigmoidal steady state forward and backward scan, with no artifacts. The CVs classified as not good had many sub-classifications: adsorptive, cross, incomplete, and noisy. A representative CV for each classification is seen in Figure 16.

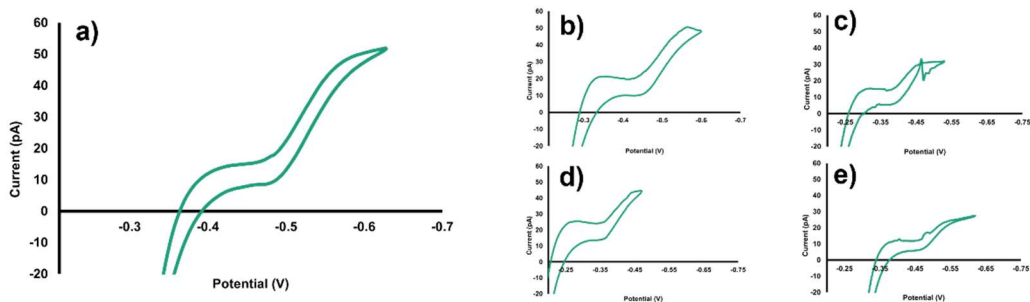


Figure 16 Representative CVs of 0.4 mM Cd(II) ion transfer between 0.3 M KCl and 0.1 M TDDATFAB in DCE: a) good, b) adsorptive, c) cross, d) incomplete, and e) noisy.

Among the classifications, a good CV indicates that the response is good in both the forward and backward scans, and there is no noise affecting the current. The plateau current reading from such a CV can be used for calibration. An adsorptive CV is one in which there is an unusually huge separation between the forward and backward scan in certain regions. This can happen due to some impurities in the interface that make the sensor deviate from the diffusion limiting behavior observed in the nanopipette due to hemispherical diffusion, and these CVs cannot be used for calibration. A cross CV represents a run in which the noise/ other impurity in the interface affects the response of the sensor significantly and the backward scan intersects the forward scan. Such a response is deemed to be unusable for calibration as it is severely affected by imperfections. An incomplete CV is one in which the electrochemical sensor was not given enough time to reach the steady state. In such a response, the plateau region is not reached, and this happens because the switching potential is set well before the plateau potential. In such a response, there is no plateau current; thus, it cannot be used for calibration.

Finally, a noisy CV is one in which the response of the sensor is affected by noise from some source, either instrumental, static, or electrochemical. Such a response may contain random spikes that appear in many parts of the CV. This imperfection, although not as severe as some of the others, makes the response unusable for calibration. Such classifications were made for CVs of 0.4 mM, 0.2 mM, 0.1 mM, and 0.05 mM Cd(II), and 0.2 mM, 0.1 mM, 0.05 mM Cu(II). Figure 17 shows the representative CV for each classification.

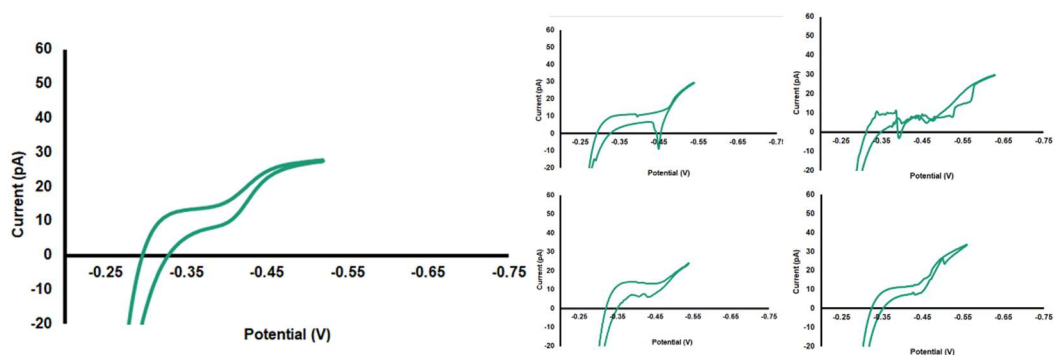


Figure 17 Representative CVs of 0.1 mM Cu(II) ion transfer between 0.3 M KCl and 0.1 M TDDATFAB in DCE: a) good, b) adsorptive, c) cross, d) incomplete, and e) noisy.

A CNN architecture was trained to identify and differentiate between the good and not-good classifications within Cd(II) and Cu(II) CVs. This will separate the good CVs of the two metal ions from the rest. Then, a CNN architecture was trained to differentiate the Cd(II) CVs from the Cu(II) CVs. Figure 18 shows a representative good CV of Cd(II) and Cu(II). To the best of our knowledge, this is the first time reporting an AI-based method to differentiate between the CV of two metal ions obtained from ITIES. We further train the CNN architecture to learn and classify

the differences between the different types of not-good CVs. This was done to explore CNN's ability to provide more insights into classifying the imperfections found in a CV. The results from this experiment have a lot of overlaps in that many CVs contained more than one type of imperfection, and the CNN model made predictions based on the more prominent imperfection found in a particular CV. Figure 19 shows some representative CVs of the not-good classification.

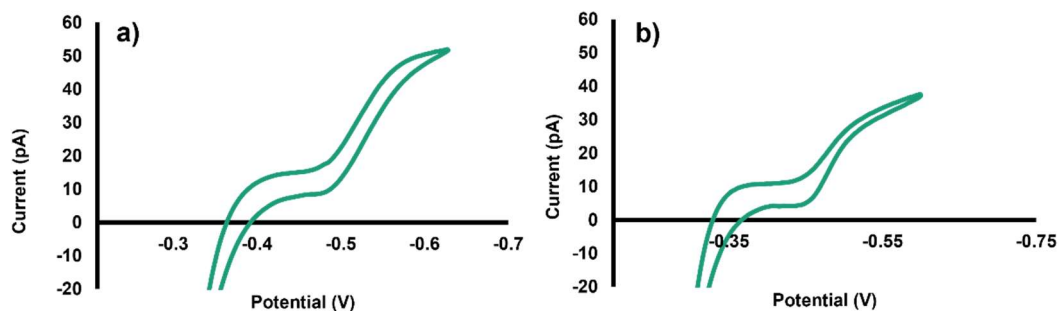


Figure 18 Representative good CVs of a) 0.4 mM Cd(II) and b) 0.2 mM Cu(II) ion transfer between 0.3 M KCl and 0.1 M TDDATFAB in DCE.

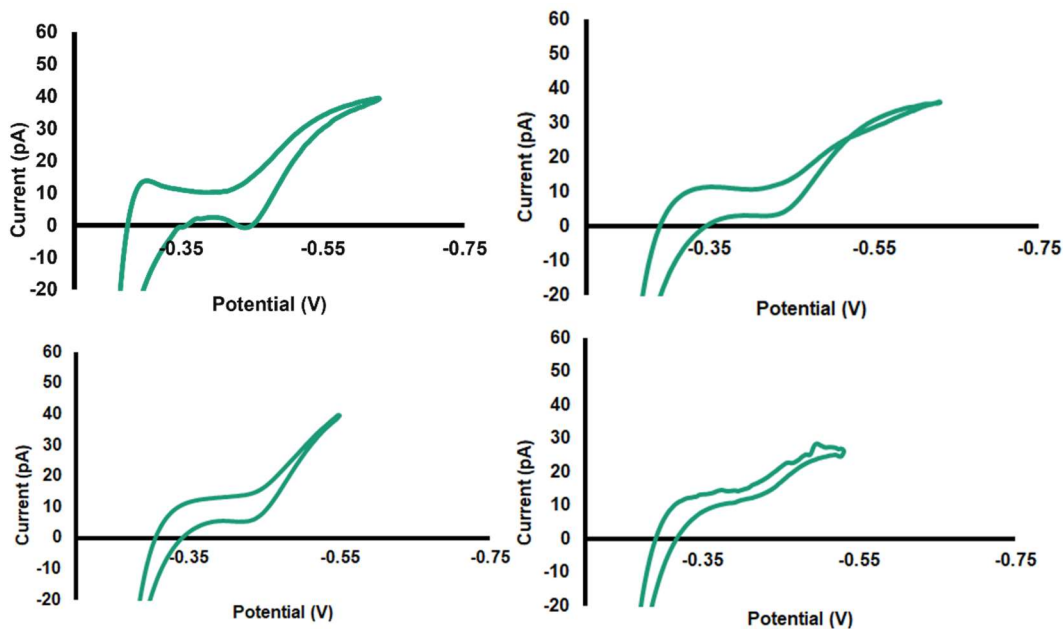


Figure 19 Representative CVs of not good classification from ion transfer of 0.2 mM Cd(II) between 0.3 M KCl and 0.1 M TDDATFAB in DCE: a) adsorptive, b) cross, c)incomplete, d) noisy.

ANN architecture was trained on good Cd(II) CVs to predict the concentration of the analyte. This process was initially done by including the entire dimension of the CV and uniformly standardizing the dimensions. This process had low accuracy and high mean square error (MSE). To minimize the computational strain and increase the accuracy of the ANN architecture, the data must undergo preprocessing in which its dimensionality is reduced. This is done by extracting the most vital information from each CV. A MATLAB code was developed to identify the plateau current point and the initial plateau before the plateau potential and extract these two points from the entire CV. Now, the entire CV will be represented by these two points. Figure 20 represents the points that were used to reduce the

dimensionality of the data. The pathway of the data will start from the data acquisition, followed by image generation using MATLAB, which will then go to CNN to differentiate between good and not good CV, which is followed by identification of the analyte (Cd(II) or Cu(II)) and then MATLAB will be used to preprocess the data to reduce dimensionality which will enter the ANN model to predict the concentration.

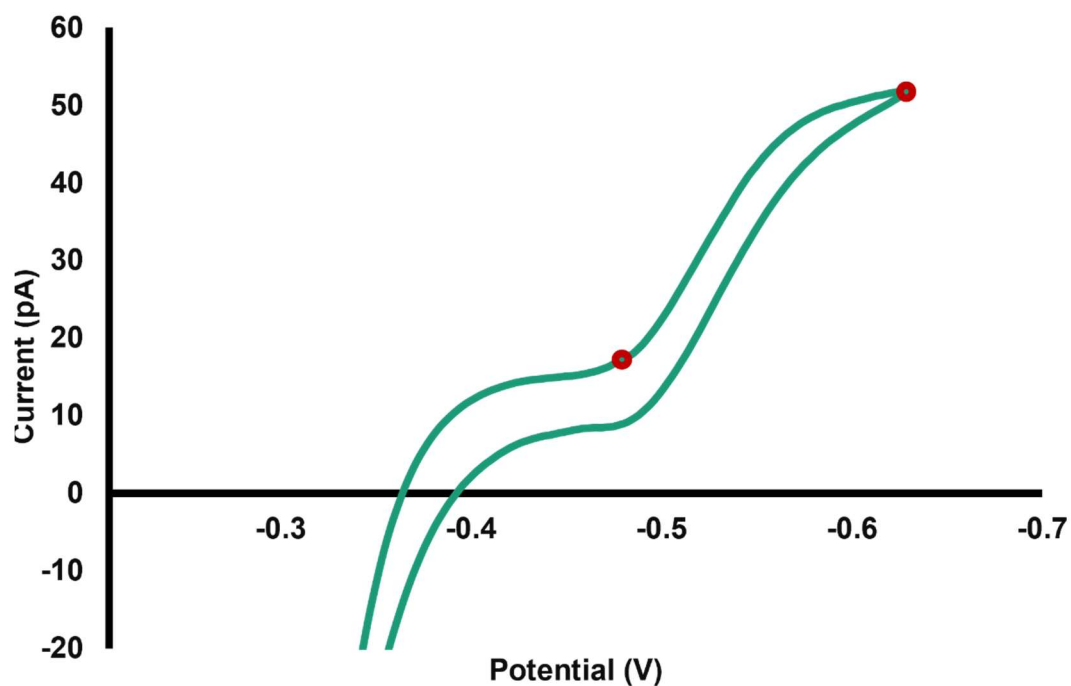


Figure 20 A representative CV depicting the points that are extracted using MATLAB. These points provide the most vital information that represents the entire CV.

4.3.2 AI Architecture

Convolutional Neural Network

Convolutional Neural Networks (CNNs) are a type of deep learning model known for their ability to extract intricate features from data¹⁶⁰⁻¹⁶⁵, particularly in tasks like image recognition. They leverage local connectivity and weight sharing, optimizing the analysis and prediction process. Notable examples include LeNet-5, which excels in recognizing handwritten digits, and AlexNet, acclaimed for its effectiveness in face recognition and pedestrian detection. Zhang *et al.* presents a novel approach for heavy-metal ion detection using a convolutional neural network (CNN) combined with square wave anodic stripping voltammetry (SWASV)¹⁵³. The authors implemented a 1D CNN model to analyze SWASV data for the simultaneous detection of Pb(II), Cd(II), and Cu(II) ions. The CNN was trained on a dataset of 1,000 SWASV curves, utilizing current, potential, and concentration as key input parameters. The model's purpose was to accurately predict heavy metal concentrations from voltammetric data, addressing challenges in traditional peak-based analysis methods. The CNN demonstrated superior performance compared to conventional techniques, achieving high accuracy ($R^2 > 0.99$) and low relative errors (<5%) for all three target analytes. Notably, the model showed robust performance in complex scenarios, including overlapping peaks and interference from other metal ions. This CNN-based approach offers a promising tool for rapid, accurate, and automated heavy metal detection in environmental and health

monitoring applications, potentially improving the efficiency and reliability of electrochemical sensing techniques.

CNNs are composed of multiple layers such as convolutional layers, pooling layers, and fully connected layers. Convolutional layers are the core building blocks of CNNs. They apply convolution operations to input data using filters (also called kernels) to extract various features. By convolving filters across the input image, CNNs can detect patterns such as edges, textures, and shapes. Pooling layers are often inserted after convolutional layers to reduce the spatial dimensions of the feature maps while retaining important information. Common pooling operations include max pooling and average pooling, which down sample the feature maps by selecting the maximum or average value within a certain window. Fully connected layers similar to those in traditional feedforward neural networks, are typically placed at the end of the CNN architecture. They receive flattened feature maps from the preceding layers and perform classification or regression tasks based on the learned features. CNNs exploit the spatial locality of data by connecting each neuron in a layer to only a local region of the input volume. This enables them to capture spatial patterns efficiently. The same set of weights (filters) is applied across different spatial locations of the input data. This parameter sharing significantly reduces the number of parameters in the model, making it more efficient and less prone to overfitting. CNNs learn hierarchical representations of data. Lower layers capture low-level features like edges and textures, while higher

layers learn more abstract features relevant to the task at hand. This hierarchical feature learning enables CNNs to achieve superior performance in tasks like image classification, object detection, and segmentation.

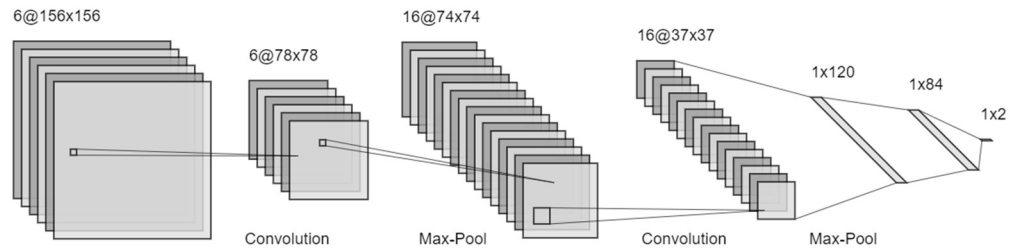


Figure 21 Modified LeNet architecture for CV classification

The CNN implementation starts by loading the dataset of PNG images from the specified folder path. It preprocesses the images by normalizing pixel values and encoding the labels. The dataset is then split into training, validation, and testing sets. A modified LeNet-5 architecture is defined as one that consists of convolutional, max-pooling, and fully connected layers. The model is compiled with binary cross-entropy loss and an Adam optimizer. Several callbacks, including early stopping, learning rate scheduling, and model checkpointing, are employed to monitor and improve the training process. After training, the code visualizes the training and validation metrics, evaluates the model on the test set, and provides a function to visualize the model's predictions on a subset of test images, comparing the true and predicted labels.

The CNN model achieved impressive results in classifying good vs. not good cyclic voltammograms (CVs) for both Cd(II) and Cu(II) analytes. The validation accuracies for these classifications were above 95%, indicating that the model learned to effectively differentiate between good and faulty CVs. Furthermore, the CNN model demonstrated exceptional performance in distinguishing between Cd(II) and Cu(II) CVs, achieving a validation accuracy of 99.15%. This remarkable result suggests that the model successfully learned the unique shapes and features of the CVs for each analyte, enabling accurate identification based solely on the CV shape.

However, the model's performance in classifying the different types of not good CVs (noisy, incomplete, adsorptive, cross) was relatively lower, with validation accuracies around 85-88%. This implies that distinguishing between these subtypes of faulty CVs posed a greater challenge for the CNN model, possibly due to similarities or subtleties in their characteristics. The ability to identify faulty CVs is a significant advantage of the CNN model, as it can help eliminate data points that may lead to inaccurate concentration predictions, improving the overall reliability of the electrochemical sensor.

Table 2 Accuracy for Different Categories of CNN Classification

CNN Classification	Train Accuracy	Validation Accuracy	Test Accuracy	Learning Rate
Cd(II) Good vs Not Good	99.96%	96.12%	95.37%	0.001
Cu(II) Good vs Not Good	99.62%	98.68%	98.34%	0.001
Cd(II) vs Cu(II)	99.20%	99.15%	99.14%	0.0005
Cd(II) – Not good	96.80%	87.71%	92.45%	0.001
Cu(II) – Not Good	93.63%	85.14%	89.19%	0.001

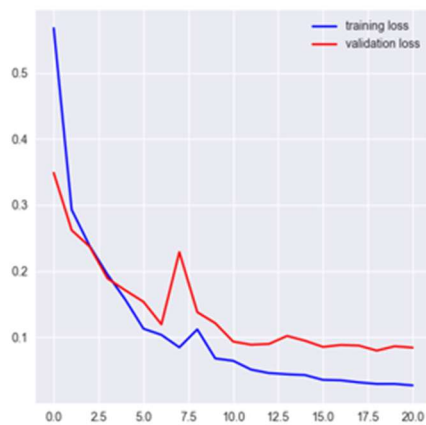
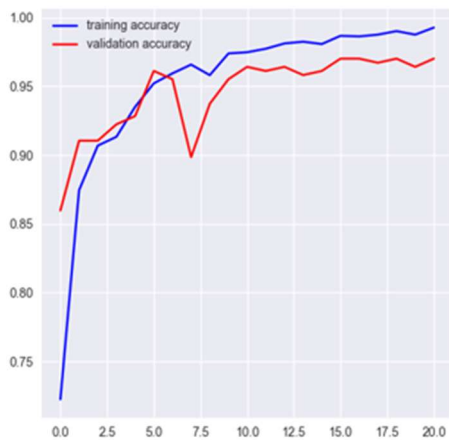


Figure 22 Line plots of the training and validation accuracy and loss values over 20 training epochs.

True: Not Good



True: Good



True: Not Good



True: Good



Predicted: Not Good



Predicted: Good



Predicted: Good



Predicted: Good



Figure 23 Cd(II) Classification of Good vs. Not Good CV Types.

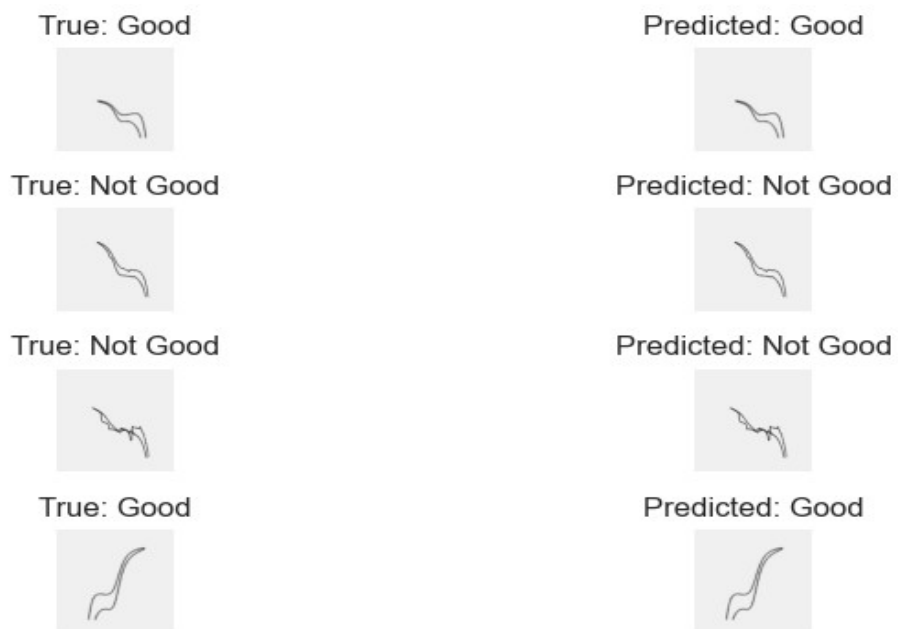


Figure 24 Cu(II) Classification of Good vs. Not Good CV Types.

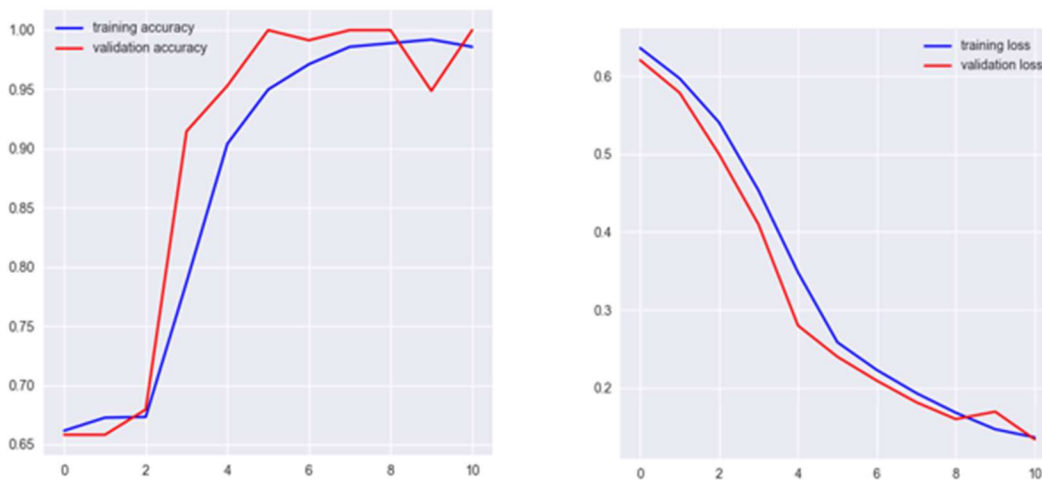


Figure 25 Line plots of the training and validation accuracy and loss values over 20 training epochs.

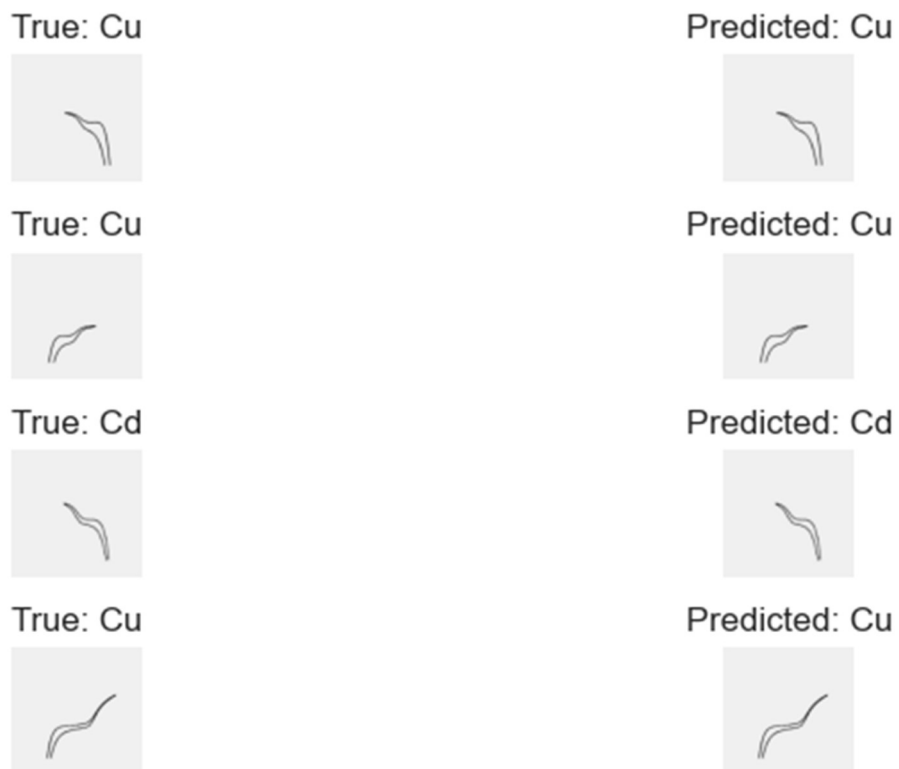


Figure 26 Classification of Cd(II) vs Cu(II) CVs.

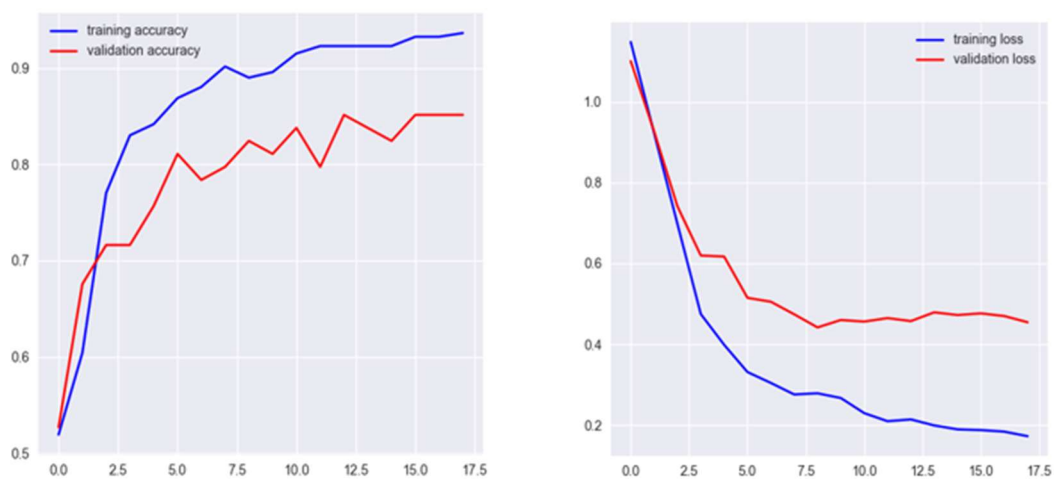


Figure 27 Line plots of the training and validation accuracy and loss values over 20 training epochs.

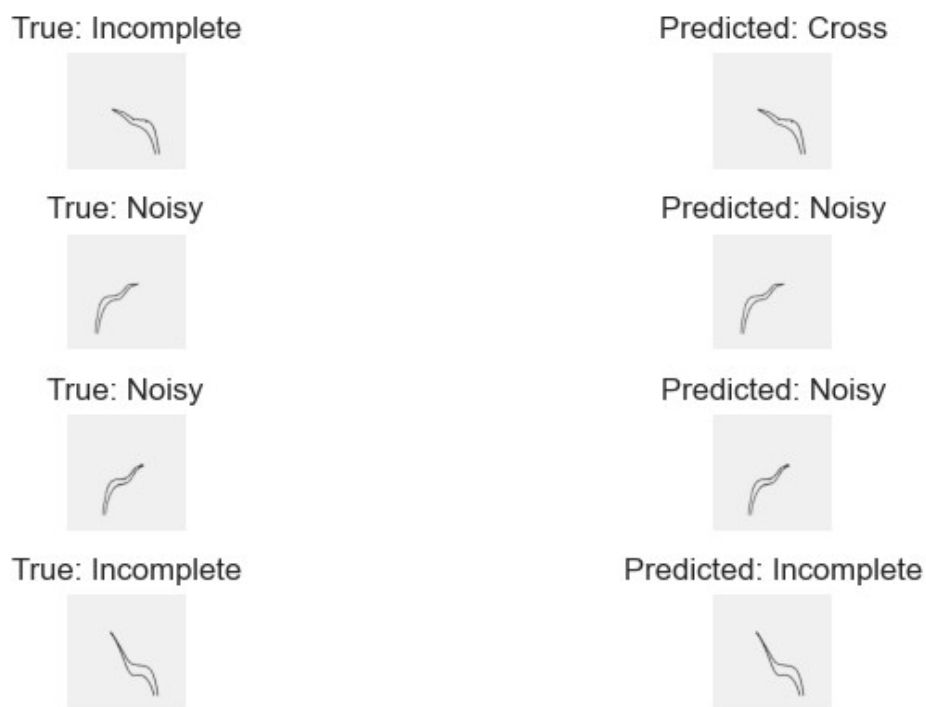


Figure 28 Cd(II) Classification of Not Good CV Types (Noisy, Incomplete, Adsorptive, Cross).

The CNN model demonstrated exceptional performance in classifying cyclic voltammograms (CVs) for both Cd(II) and Cu(II) analytes. The model achieved high validation accuracies of over 95% for distinguishing between good and faulty CVs, and an impressive 99.15% accuracy for differentiating between Cd(II) and Cu(II) responses. These results highlight the CNN's ability to effectively learn and recognize the unique shapes and features of CVs for different analytes and quality levels. While the model showed slightly lower accuracy (85-88%) in classifying specific types of faulty CVs, its overall performance underscores the potential of

CNNs in enhancing the analysis and interpretation of electrochemical sensor data. By automating the process of CV classification and analyte identification, this CNN-based approach significantly improves the user-friendliness and reliability of ITIES-based electrochemical sensors for heavy metal detection.

Artificial Neural Network

Artificial Neural Networks (ANNs) are a class of machine learning models inspired by the biological neural networks found in the human brain¹⁶⁶. They consist of interconnected nodes, or artificial neurons, organized in layers. These neurons process and transmit information through weighted connections, enabling the network to learn complex patterns and relationships in data. ANNs have found widespread applications in various fields, including image and speech recognition, natural language processing, and data analysis¹⁶⁷.

The basic building block of an ANN is the artificial neuron, which receives inputs, applies weights to them, and produces an output through an activation function. The weights determine the strength of connections between neurons and are adjusted during the learning process. The activation function introduces non-linearity, allowing the network to model complex relationships. ANNs typically consist of an input layer, one or more hidden layers, and an output layer. The input layer receives the raw data, while the hidden layers perform feature extraction and transformation. The output layer produces the final prediction or classification. The

learning process in ANNs involves adjusting the weights of connections based on the error between predicted and actual outputs. This is often done using backpropagation, an algorithm that propagates the error signal backward through the network, updating weights to minimize the error.

In the context of electrochemistry, ANNs can be employed to analyze complex electrochemical data, such as CVs¹⁶⁸. By training on a dataset of CVs with known analyte concentrations, the ANN can learn to recognize patterns and correlations between the CV features and the corresponding concentrations. Once trained, the ANN can predict the concentration of an analyte in a new, unseen CV, providing a rapid and accurate method for quantitative analysis^{169–171}. This application is particularly useful in environmental monitoring, where the rapid and accurate detection of heavy metal ions like Cd(II) and Cu(II) is crucial for assessing water quality and ensuring public safety.

The ANN implementation loads the dataset from text files containing the x and y coordinates of cyclic voltammograms (CVs). The data is split into training and testing sets. A simple feed-forward neural network architecture with two dense layers and an output layer for regression is defined. Similar to the CNN implementation, early stopping and learning rate scheduling callbacks are used. The model is compiled with mean squared error loss, Adam optimizer, mean absolute error, and mean squared error as evaluation metrics. After training, the code visualizes the training and validation loss, mean absolute error, and mean squared

error. It evaluates the model on the test set and reports the corresponding metrics. Finally, the code demonstrates making predictions on the test set and visualizes the comparison between predicted and actual values in a DataFrame. Additionally, it showcases predicting the concentration for a set of unrecognized CV data points.

```

Model: "sequential"
-----
Layer (type)                Output Shape              Param #
-----
dense (Dense)                (None, 64)                320
-----
dense_1 (Dense)              (None, 32)                2080
-----
dense_2 (Dense)              (None, 1)                 33
-----
Total params: 2,433
Trainable params: 2,433
Non-trainable params: 0
-----

```

Figure 29 ANN architecture with the training parameters.

The proposed ANN architecture is a sequential model designed for regression tasks in electrochemistry, such as predicting analyte concentrations from cyclic voltammetry data. The model consists of an input layer with 64 neurons, followed by two hidden layers with 32 neurons each, and an output layer with a single neuron making 2,433 trainable parameters in total. The hidden layers utilize the Rectified Linear Unit (ReLU) activation function for introducing non-linearity, while the output layer employs a linear activation for direct prediction of the target

value. The model is trained using the Adam optimizer with an initial learning rate of 0.01 and mean squared error (MSE) as the loss function. To prevent overfitting, early stopping is implemented with a patience of 5 epochs, restoring the best weights if no improvement is observed. Additionally, a learning rate scheduler is employed, reducing the learning rate by half every 5 epochs to fine-tune the model's performance.

Table 3 ANN Results with the Mean Absolute Error and Mean Squared Error

ANN	MAE	MSE	LR
Cd(II)	0.0158	4.09E-04	0.01
Cu(II)	0.0127	2.61E-04	0.01

Table 4 Test Results of ANN Prediction of Concentration for 10 Randomly Selected Cu(II) Values

Cu(II) Real Values	Predicted Values
0.05	0.032442
0.05	0.039273
0.05	0.056565
0.1	0.109722
0.05	0.017079
0.1	0.099719
0.2	0.209858
0.05	0.065821
0.05	0.046686
0.1	0.123535

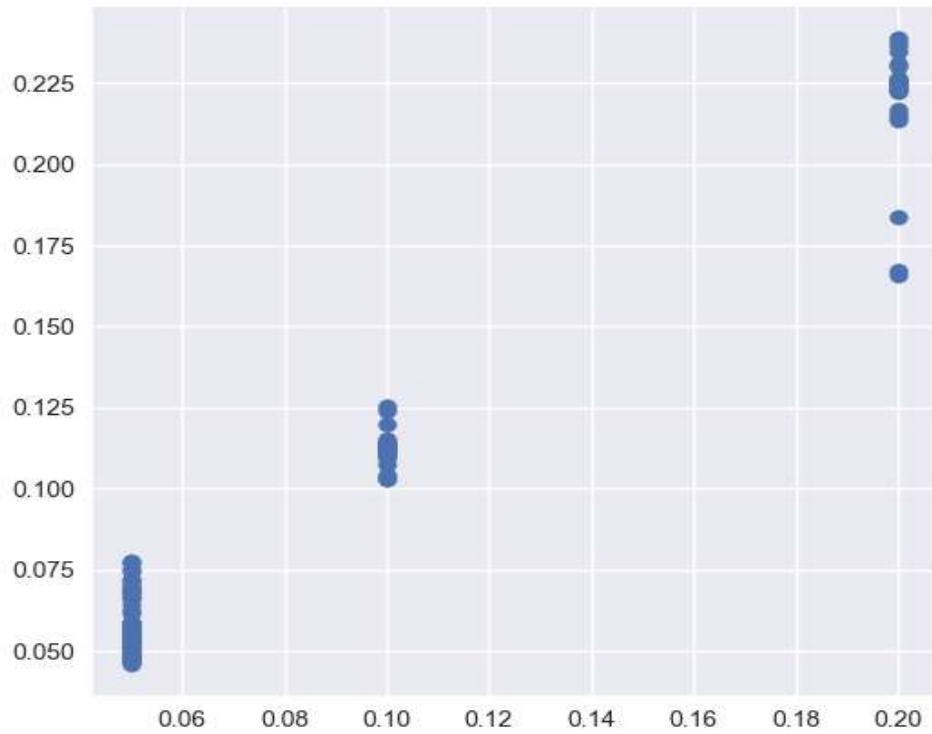


Figure 30 Variance of the concentration predictions for Cu(II).

Table 5 Test Results of ANN Prediction of Concentration for 10 Randomly Selected Cd(II) Values.

Cd(II) Real Values	Predicted Values
0.1	0.120909
0.4	0.392451
0.05	0.036781
0.05	0.036781
0.2	0.182019
0.05	0.058828
0.4	0.392429
0.4	0.392018
0.4	0.388183
0.1	0.10314

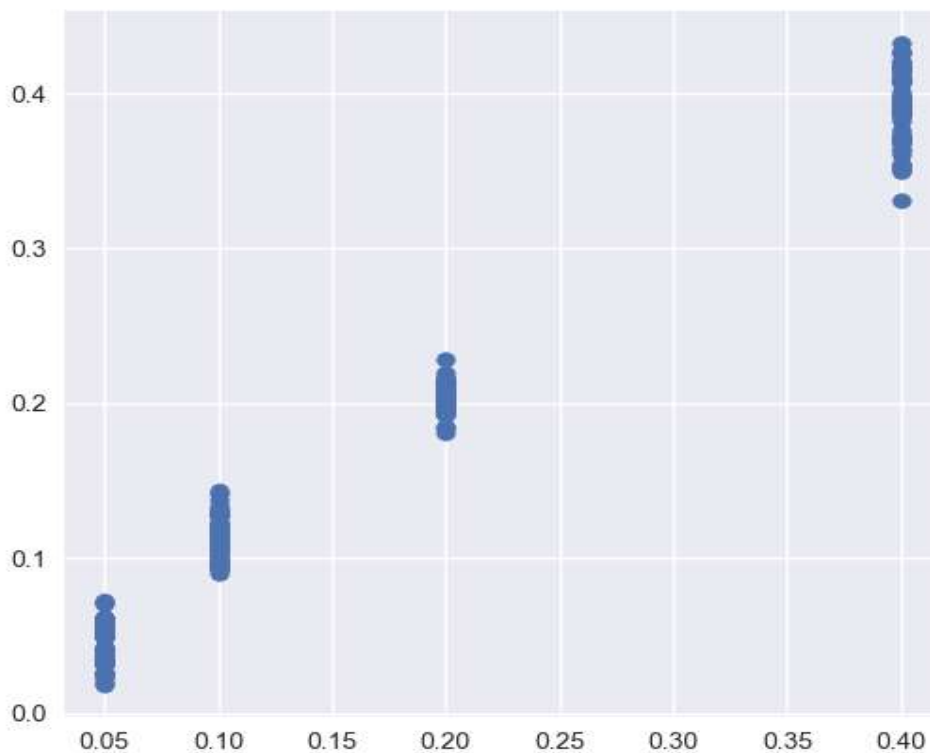


Figure 31 Variance of the concentration predictions for Cd(II).

The ANN model demonstrated promising results in predicting the concentrations of Cd(II) and Cu(II) analytes based on the CV data. The model achieved low Mean Absolute Error (MAE) and Mean Squared Error (MSE) values on the test set, indicating good performance in the regression task. Specifically, for Cd(II), the model achieved a test MAE of 0.0158 and a test MSE of 4.0896e-04, while for Cu(II), the test MAE was 0.0127, and the test MSE was 2.6129e-04. These results indicate the ANN's ability to accurately estimate analyte concentrations from preprocessed CV data. The model's performance was consistent across different

concentration ranges, as evidenced by the comparison between predicted and actual values.

The code provides a comparison of the predicted concentrations with the actual values in a DataFrame, allowing for a visual inspection of the model's performance. Additionally, it demonstrates the ability of the trained ANN model to predict concentrations for a set of unrecognized CV data points, showcasing its potential for practical applications. Overall, the combination of the CNN for classifying and identifying good CVs and the ANN for concentration prediction showcases the effective integration of AI architectures with electrochemical sensors. The CNN's ability to differentiate analytes based on CV shapes and identify faulty data, coupled with the ANN's concentration prediction capabilities, provides a robust and reliable analytical platform for accurate and user-friendly detection of heavy metal ions in environmental samples.

4.4. Conclusion

In conclusion, this study demonstrates the successful integration of artificial intelligence techniques with nano-ITIES-based electrochemical sensors for the detection and quantification of heavy metal ions, specifically Cd(II) and Cu(II). The combination of Convolutional Neural Networks (CNNs) and Artificial Neural Networks (ANNs) significantly enhances the analytical capabilities and user-friendliness of these sensors. The CNN model excels in classifying cyclic

voltammograms, achieving high accuracies of over 95% in distinguishing between good and faulty CVs, and an impressive 99.15% accuracy in differentiating between Cd(II) and Cu(II) responses. This classification step is crucial for ensuring data quality and reliability. Complementing the CNN, the ANN model demonstrates excellent performance in predicting analyte concentrations, with low Mean Absolute Errors of 0.0158 for Cd(II) and 0.0127 for Cu(II). The synergy between these AI models creates a robust analytical pipeline that automates CV classification, analyte identification, and concentration prediction. This integrated approach not only improves the accuracy and reliability of heavy metal detection but also makes ITIES-based sensors more accessible to non-expert users, potentially broadening their application in environmental monitoring and other fields requiring rapid, on-site metal ion analysis.

Chapter 5

Conclusion and Future Work

5.1 Conclusion

This dissertation presents a series of innovative advancements in the field of electrochemical sensing for metal ion detection, particularly focusing on Cd(II) ions in complex matrices. The research progressed through three interconnected projects, each building upon the findings of the previous one to address critical challenges in heavy metal analysis and sensor development. The first project successfully developed a nanopipet-based electrochemical sensor for Cd(II) detection using ITIES. The sensor demonstrated excellent stability and performance in various complex matrices, including artificial seawater and cerebellum fluid. The sensor's ability to withstand complex environments without fouling and its successful application to a real environmental sample from the Indian River Lagoon highlight its potential as a powerful tool for environmental monitoring. Building on this foundation, the second project expanded the sensor's capabilities to simultaneously detect Cd(II) and Ca(II) in complex biological matrices such as artificial urine and blood. The innovative single-bore, single-ionophore configuration simplified the fabrication process and reduced uncertainties, making it more suitable for theoretical modeling and practical applications. The sensor's performance in the presence of chelating agents provided valuable insights into conditional stability constants and showcased its potential for

healthcare monitoring and toxicity treatment assessment. The third project marked a significant leap forward by integrating artificial intelligence with ITIES-based sensors. The combination of Convolutional Neural Networks (CNNs) and Artificial Neural Networks (ANNs) greatly enhanced the analytical capabilities and user-friendliness of these sensors. The CNN model achieved high accuracies in classifying cyclic voltammograms and differentiating between Cd(II) and Cu(II) responses, while the ANN model demonstrated excellent performance in predicting analyte concentrations. This AI-integrated approach not only improves the accuracy and reliability of heavy metal detection but also makes ITIES-based sensors more accessible to non-expert users. Collectively, these studies represent significant advancements in electrochemical sensing technology. The progression from a single-ion nanopipet sensor to a multi-ion detection system, and finally to an AI-integrated analytical platform, showcases the evolution and potential of ITIES-based sensors. These developments address critical needs in environmental monitoring, healthcare diagnostics, and analytical chemistry. The sensors developed in this dissertation offer several advantages over conventional methods, including cost-effectiveness, ease of fabrication and maintenance, high selectivity and sensitivity, and improved user-friendliness. The integration of AI further enhances these benefits by automating complex data interpretation tasks and improving overall analytical accuracy.

5.2 Future Work

The research performed in this dissertation pave way to the following research work for the future:

1. Expand the range of detectable heavy metal ions to other ions such as Hg(II), Cr(II) to ensure that more heavy metals have reliable electrochemical sensors
2. Further validate the sensors performance in practical application such as industrial effluent samples to demonstrate the practical applicability of the sensor.
3. Refine AI models for wider application in signal processing by integrating other AI architectures
4. Develop a user-friendly interface and software package integrated with the developed AI model to enhance widespread usage
5. Investigate the potential for miniaturization of the sensor for integration into wearable devices

References

- (1) Sarma, H. H.; Rajkumar, A.; Baro, A.; Das, B. C.; Talukdar, N. Impact of Heavy Metal Contamination on Soil and Crop Ecosystem with Advanced Techniques to Mitigate Them. *J Adv Biol Biotechnol* **2024**, *27* (6), 53–63. <https://doi.org/10.9734/jabb/2024/v27i6865>.
- (2) Qin, G.; Niu, Z.; Yu, J.; Li, Z.; Ma, J.; Xiang, P. Soil Heavy Metal Pollution and Food Safety in China: Effects, Sources and Removing Technology. *Chemosphere* **2021**, *267*, 129205. <https://doi.org/10.1016/J.CHEMOSPHERE.2020.129205>.
- (3) Ramadan, F.; Nour, H. E.; Wahed, N. A.; Rakha, A.; Amuda, A. K.; Faisal, M. Heavy Metal Contamination and Environmental Risk Assessment: A Case Study of Surface Water in the Bahr Mouse Stream, East Nile Delta, Egypt. *Environ Monit Assess* **2024**, *196* (5). <https://doi.org/10.1007/s10661-024-12541-1>.
- (4) Xu, Y.; Liao, X.; Guo, B. Assessment of Heavy Metal Pollution in Water Sediment and Study on Pollution Mechanism—Taking the Weihe River Basin in China as an Example. *Processes* **2023**, *11* (2). <https://doi.org/10.3390/pr11020416>.
- (5) Walter, A.; Kuhri, S.; Reinicke, M.; Bocklitz, T.; Schumacher, W.; Rösch, P.; Merten, D.; Büchel, G.; Kothe, E.; Popp, J. Raman Spectroscopic Detection of Nickel Impact on Single Streptomyces Cells - Possible Bioindicators for Heavy Metal Contamination. *Journal of Raman Spectroscopy* **2012**, *43* (8), 1058–1064. <https://doi.org/10.1002/jrs.3126>.

- (6) Wei, M.; Wang, S.; Wu, B.; Cheng, H.; Wang, C. Heavy Metal Pollution Improves Allelopathic Effects of Canada Goldenrod on Lettuce Germination. *Plant Biol* **2020**, *22* (5), 832–838.
<https://doi.org/10.1111/plb.13126>.
- (7) Fierro, P.; Tapia, J.; Bertrán, C.; Acuña, C.; Vargas-Chacoff, L. Assessment of Heavy Metal Contamination in Two Edible Fish Species and Water from North Patagonia Estuary. *Applied Sciences (Switzerland)* **2021**, *11* (6).
<https://doi.org/10.3390/app11062492>.
- (8) Kubier, A.; Wilkin, R. T.; Pichler, T. Cadmium in Soils and Groundwater: A Review. *Applied Geochemistry*. Elsevier Ltd September 1, 2019.
<https://doi.org/10.1016/j.apgeochem.2019.104388>.
- (9) Yousaf, M.; Mandiwana, K. L.; Baig, K. S.; Lu, J. Evaluation of Acer Rubrum Tree Bark as a Bioindicator of Atmospheric Heavy Metal Pollution in Toronto, Canada. *Water Air Soil Pollut* **2020**, *231* (8).
<https://doi.org/10.1007/s11270-020-04758-w>.
- (10) Lubal, M. J. Health Effects of Heavy Metal Contamination in Drinking Water. *UTTAR PRADESH JOURNAL OF ZOOLOGY* **2024**, *45* (10), 16–25.
<https://doi.org/10.56557/upjoz/2024/v45i104041>.
- (11) *Morbidity and Mortality Weekly Report*; 1999.
<http://www.cdc.gov/nceh/lead/publications/books/plpyc/contents.htm>.
- (12) Al-Bagawi, A. H. Feasibility Study of the Environmental and Economic Impact of Phytoremediation of Heavy Metal-Contaminated Soil. *Chemical Papers* **2023**, *77* (9), 5541–5553. <https://doi.org/10.1007/s11696-023-02884-3>.

- (13) Sardans, J.; Montes, F.; Peñuelas, J. Determination of As, Cd, Cu, Hg and Pb in Biological Samples by Modern Electrothermal Atomic Absorption Spectrometry. *Spectrochimica Acta - Part B Atomic Spectroscopy*. February 2010, pp 97–112. <https://doi.org/10.1016/j.sab.2009.11.009>.
- (14) Ivanova-Petropulos, V.; Jakabová, S.; Nedelkovski, D.; Pavlík, V.; Balážová, Ž.; Hegedús, O. Determination of Pb and Cd in Macedonian Wines by Electrothermal Atomic Absorption Spectrometry (ETAAS). *Food Anal Methods* **2015**, *8* (8). <https://doi.org/10.1007/s12161-014-0062-x>.
- (15) Murphy, K.; Rehkämper, M.; Kreissig, K.; Coles, B.; Van De Fliedrt, T. Improvements in Cd Stable Isotope Analysis Achieved through Use of Liquid-Liquid Extraction to Remove Organic Residues from Cd Separates Obtained by Extraction Chromatography. *J Anal At Spectrom* **2016**, *31* (1). <https://doi.org/10.1039/c5ja00115c>.
- (16) Choi, K. S.; Lee, C. H.; Kim, J. G.; Kim, W. H.; Kang, J. G. Separating Ag, B, Cd, Dy, Eu, and Sm in a Gd Matrix Using 2-Ethylhexyl Phosphonic Acid Mono-2-Ethylhexyl Ester Extraction Chromatography for ICP-AES Analysis. *Talanta* **2007**, *71* (2). <https://doi.org/10.1016/j.talanta.2006.05.015>.
- (17) Zhang, M.; Liu, Y. Q.; Ye, B. C. Colorimetric Assay for Parallel Detection of Cd²⁺, Ni²⁺ and Co²⁺ Using Peptide-Modified Gold Nanoparticles. *Analyst* **2012**, *137* (3). <https://doi.org/10.1039/c1an15909g>.
- (18) Ikeda, M.; Ohashi, F.; Fukui, Y.; Sakuragi, S.; Moriguchi, J. Cadmium, Chromium, Lead, Manganese and Nickel Concentrations in Blood of Women in Non-Polluted Areas in Japan, as Determined by Inductively Coupled Plasma-Sector Field-Mass Spectrometry. *Int Arch Occup Environ Health* **2011**, *84* (2), 139–150. <https://doi.org/10.1007/s00420-010-0542-2>.

- (19) Guo, W.; Hu, S.; Xiao, Y.; Zhang, H.; Xie, X. Direct Determination of Trace Cadmium in Environmental Samples by Dynamic Reaction Cell Inductively Coupled Plasma Mass Spectrometry. *Chemosphere* **2010**, *81* (11), 1463–1468. <https://doi.org/10.1016/j.chemosphere.2010.08.056>.
- (20) Peng, G.; He, Q.; Zhou, G.; Li, Y.; Su, X.; Liu, M.; Fan, L. Determination of Heavy Metals in Water Samples Using Dual-Cloud Point Extraction Coupled with Inductively Coupled Plasma Mass Spectrometry. *Analytical Methods* **2015**, *7* (16), 6732–6739. <https://doi.org/10.1039/c5ay00801h>.
- (21) Shih, T. T.; Hsu, I. H.; Chen, S. N.; Chen, P. H.; Deng, M. J.; Chen, Y.; Lin, Y. W.; Sun, Y. C. A Dipole-Assisted Solid-Phase Extraction Microchip Combined with Inductively Coupled Plasma-Mass Spectrometry for Online Determination of Trace Heavy Metals in Natural Water. *Analyst* **2015**, *140* (2), 600–608. <https://doi.org/10.1039/c4an01421a>.
- (22) Abdelhamid, H. N.; Wu, H. F. Synthesis and Characterization of Quantum Dots for Application in Laser Soft Desorption/Ionization Mass Spectrometry to Detect Labile Metal-Drug Interactions and Their Antibacterial Activity. *RSC Adv* **2015**, *5* (93), 76107–76115. <https://doi.org/10.1039/c5ra11301f>.
- (23) Kim, Y.; Choi, H.; Shin, W. H.; Oh, J. M.; Koo, S. M.; Kim, Y.; Lee, T.; Yu, B. J.; Park, C. Development of Colorimetric Whole-Cell Biosensor for Detection of Heavy Metals in Environment for Public Health. *Int J Environ Res Public Health* **2021**, *18* (23). <https://doi.org/10.3390/ijerph182312721>.
- (24) Tajik, S.; Beitollahi, H.; Nejad, F. G.; Dourandish, Z.; Khalilzadeh, M. A.; Jang, H. W.; Venditti, R. A.; Varma, R. S.; Shokouhimehr, M. Recent Developments in Polymer Nanocomposite-Based Electrochemical Sensors for Detecting Environmental Pollutants. *Ind Eng Chem Res* **2021**, *60* (3), 1112–1136. <https://doi.org/10.1021/acs.iecr.0c04952>.

- (25) Florescu, M.; Badea, M.; Florescu, M.; Badea, M.; Coman, G.; Marty, J.-L.; Mitrica, M. *Screen Printed Electrodes Used for Detection of Ionic Heavy Metals*; 2009; Vol. 2. <https://www.researchgate.net/publication/267378077>.
- (26) Gumpu, M. B.; Krishnan, U. M.; Rayappan, J. B. B. Design and Development of Amperometric Biosensor for the Detection of Lead and Mercury Ions in Water Matrix—a Permeability Approach. *Anal Bioanal Chem* **2017**, *409* (17), 4257–4266. <https://doi.org/10.1007/s00216-017-0376-9>.
- (27) Guo, T. T.; Cao, X. Y.; An, Y. Y.; Zhang, X. L.; Yan, J. Z. Sulfur-Bridged Co(II)-Thiacalix[4]Arene Metal-Organic Framework as an Electrochemical Sensor for the Determination of Toxic Heavy Metals. *Inorg Chem* **2023**, *62* (11), 4485–4494. <https://doi.org/10.1021/acs.inorgchem.2c04197>.
- (28) Rajawat, D. S.; Kardam, A.; Srivastava, S.; Satsangee, S. P. Nanocellulosic Fiber-Modified Carbon Paste Electrode for Ultra Trace Determination of Cd (II) and Pb (II) in Aqueous Solution. *Environmental Science and Pollution Research* **2013**, *20* (5), 3068–3076. <https://doi.org/10.1007/s11356-012-1194-4>.
- (29) Keramari, V.; Papadimou, S. G.; Golia, E. E.; Girousi, S. Bismuth Film along with DsDNA-Modified Electrode Surfaces as Promising (Bio)Sensors in the Analysis of Heavy Metals in Soils. *Biosensors (Basel)* **2024**, *14* (6). <https://doi.org/10.3390/bios14060310>.
- (30) Lalmalsawmi, J.; Sarikokba; Tiwari, D.; Kim, D. J. Simultaneous Detection of Cd²⁺ and Pb²⁺ by Differential Pulse Anodic Stripping Voltammetry: Use of Highly Efficient Novel Ag⁰(NPs) Decorated Silane Grafted Bentonite Material. *Journal of Electroanalytical Chemistry* **2022**, *918*. <https://doi.org/10.1016/j.jelechem.2022.116490>.

- (31) Lu, S.; Gu, Z.; Hummel, M.; Zhou, Y.; Wang, K.; Xu, B. Bin; Wang, Y.; Li, Y.; Qi, X.; Liu, X. Nickel Oxide Immobilized on the Carbonized Eggshell Membrane for Electrochemical Detection of Urea. *J Electrochem Soc* **2020**, *167* (10), 106509. <https://doi.org/10.1149/1945-7111/ab9c80>.
- (32) Sibit, N. H.; Roushani, M.; Karazan, Z. M. Electrochemical Determination of Mercury Ions in Various Environmental Samples Using Glassy Carbon Electrode Modified with Poly (L-Tyrosinamide). *Ionics (Kiel)* **2024**, *30* (2), 1101–1112. <https://doi.org/10.1007/s11581-023-05334-y>.
- (33) IEEE Sensors Council; Institute of Electrical and Electronics Engineers. *IEEE SENSORS 2014 : Proceedings : Valencia Conference Centre, Valencia, Spain, November 2-5, 2014*.
- (34) Wei, J.; Guo, Z.; Chen, X.; Han, D. D.; Wang, X. K.; Huang, X. J. Ultrasensitive and Ultraspecific Impedimetric Detection of Cr(vi) Using Crown Ethers as High-Affinity Targeting Receptors. *Anal Chem* **2015**, *87* (3), 1991–1998. <https://doi.org/10.1021/ac504449v>.
- (35) Koryta, J. Electrochemical Polarization Phenomena at the Interface of Two Immiscible Electrolyte Solutions. *Electrochim Acta* **1979**, *24* (3). [https://doi.org/10.1016/0013-4686\(79\)85048-3](https://doi.org/10.1016/0013-4686(79)85048-3).
- (36) Wilke, S.; Wang, H. Transfer of Heavy Metal Ions across the Water Nitrobenzene Microinterface Facilitated by the Cadmium Selective Ionophore ETH1062. *Journal of Electroanalytical Chemistry* **1999**, *475* (1). [https://doi.org/10.1016/S0022-0728\(99\)00327-7](https://doi.org/10.1016/S0022-0728(99)00327-7).
- (37) Bingol, H.; Atalay, T. Interfacial Transfer of Cd²⁺ Assisted by 4' - Morpholino-Acetophenone-4-Phenyl-3-Thiosemicarbazone across the

- Water/1,2-Dichloroethane Interface. *Central European Journal of Chemistry* **2010**, 8 (5), 1134–1139. <https://doi.org/10.2478/s11532-010-0089-9>.
- (38) Benvidi, A.; Lanjwani, S. N.; Ding, Z. Cd²⁺ Transfer across Water/1,2-Dichloroethane Microinterfaces Facilitated by Complex Formation with 1,10-Phenanthroline. *Electrochim Acta* **2010**, 55 (6). <https://doi.org/10.1016/j.electacta.2009.11.056>.
- (39) Lee, S. H.; Sumranjit, J.; Tongkate, P.; Chung, B. H.; Lee, H. J. Voltammetric Studies of Cu(II) Ion Transfer Reaction with Picolinamide-Phenylenevinylene across Liquid/Liquid Interfaces and Their Sensing Applications. *Electrochim Acta* **2014**, 123. <https://doi.org/10.1016/j.electacta.2014.01.003>.
- (40) Sanchez Vallejo, L. J.; Ovejero, J. M.; Fernández, R. A.; Dassie, S. A. Simple Ion Transfer at Liquid/Liquid Interfaces. *International Journal of Electrochemistry* **2012**, 2012. <https://doi.org/10.1155/2012/462197>.
- (41) Rodgers, P. J.; Amemiya, S. Cyclic Voltammetry at Micropipet Electrodes for the Study of Ion-Transfer Kinetics at Liquid/Liquid Interfaces. *Anal Chem* **2007**, 79 (24). <https://doi.org/10.1021/ac0711642>.
- (42) Chen, R.; Yang, A.; Chang, A.; Oweimrin, P. F.; Romero, J.; Vichitcharoenpaisarn, P.; Tapia, S.; Ha, K.; Villaflor, C.; Shen, M. A Newly Synthesized Tris(Crown Ether) Ionophore for Assisted Ion Transfer at NanoITIES Electrodes. *ChemElectroChem* **2020**, 7 (4). <https://doi.org/10.1002/celec.201901997>.
- (43) Edition, F. Guidelines for Drinking-Water Quality. *World Health* **2011**, 1 (3). [https://doi.org/10.1016/S1462-0758\(00\)00006-6](https://doi.org/10.1016/S1462-0758(00)00006-6).

- (44) Satarug, S.; Moore, M. R. Adverse Health Effects of Chronic Exposure to Low-Level Cadmium in Foodstuffs and Cigarette Smoke. *Environ Health Perspect* **2004**, *112* (10). <https://doi.org/10.1289/ehp.6751>.
- (45) Genchi, G.; Sinicropi, M. S.; Lauria, G.; Carocci, A.; Catalano, A. The Effects of Cadmium Toxicity. *International Journal of Environmental Research and Public Health*. MDPI AG June 1, 2020. <https://doi.org/10.3390/ijerph17113782>.
- (46) Chen, Y.; Zhang, D.; Wang, D.; Lu, L.; Wang, X.; Guo, G. A Carbon-Supported BiSn Nanoparticles Based Novel Sensor for Sensitive Electrochemical Determination of Cd (II)Ions. *Talanta* **2019**, *202*. <https://doi.org/10.1016/j.talanta.2019.04.066>.
- (47) Abdallah, A. B.; El-Kholany, M. R.; Molouk, A. F. S.; Ali, T. A.; El-Shafei, A. A.; Khalifa, M. E. Selective and Sensitive Electrochemical Sensors Based on an Ion Imprinting Polymer and Graphene Oxide for the Detection of Ultra-Trace Cd(Ii) in Biological Samples. *RSC Adv* **2021**, *11* (49). <https://doi.org/10.1039/d1ra05489a>.
- (48) Shao, Y.; Mirkin, M. V. Probing Ion Transfer at the Liquid/Liquid Interface by Scanning Electrochemical Microscopy (SECM). *J Phys Chem B* **1998**, *102* (49). <https://doi.org/10.1021/jp9828282>.
- (49) Guo, J.; Amemiya, S. Voltammetric Heparin-Selective Electrode Based on Thin Liquid Membrane with Conducting Polymer-Modified Solid Support. *Anal Chem* **2006**, *78* (19). <https://doi.org/10.1021/ac061003i>.
- (50) Colombo, M. L.; Sweedler, J. V.; Shen, M. Nanopipet-Based Liquid-Liquid Interface Probes for the Electrochemical Detection of Acetylcholine,

- Tryptamine, and Serotonin via Ionic Transfer. *Anal Chem* **2015**, *87* (10).
<https://doi.org/10.1021/ac504151e>.
- (51) Abate, G.; Masini, J. C. Complexation of Cd(II) and Pb(II) with Humic Acids Studied by Anodic Stripping Voltammetry Using Differential Equilibrium Functions and Discrete Site Models. *Org Geochem* **2002**, *33* (10). [https://doi.org/10.1016/S0146-6380\(02\)00087-6](https://doi.org/10.1016/S0146-6380(02)00087-6).
- (52) Schroeder, G.; Łe, B.; Gierczyk, B.; Eitner, K.; Wojciechowski, G.; Róz, B.; Bartl, F.; Brzezinski, B. *Studies of Complexation of Metal Cations by Tris(3,6-Dioxaheptyl)Amine in Solution*.
- (53) Brandt, W. W.; Dwyer, F. P.; Gyarfas, E. C. *CHELATE COMPLEXES OF 1,10-PHENANTHROLINE AND RELATED COMPOUNDS AND*.
- (54) Owens, G.; Ferguson, V. K.; Mclaughlin, M. J.; Singleton, I.; Reid, R. J.; Smith, F. A. Determination of NTA and EDTA and Speciation of Their Metal Complexes in Aqueous Solution by Capillary Electrophoresis. *Environ Sci Technol* **2000**, *34* (5). <https://doi.org/10.1021/es990309m>.
- (55) Zeini Jahromi, E.; Gailer, J.; Pickering, I. J.; George, G. N. Structural Characterization of Cd²⁺ Complexes in Solution with DMSA and DMPS. *J Inorg Biochem* **2014**, *136*. <https://doi.org/10.1016/j.jinorgbio.2013.10.025>.
- (56) Silva, V. L.; Carvalho, R.; Freitas, M. P.; Tormena, C. F.; Melo, W. C. Structural Determination of Zn and Cd-DTPA Complexes: MS, Infrared, ¹³C NMR and Theoretical Investigation. *Spectrochim Acta A Mol Biomol Spectrosc* **2007**, *68* (5). <https://doi.org/10.1016/j.saa.2007.01.020>.
- (57) Wątyły, J.; Łuczkowski, M.; Padjasek, M.; Krężel, A. Phytochelatins as a Dynamic System for Cd(II) Buffering from the Micro- To Femtomolar

- Range. *Inorg Chem* **2021**, *60* (7).
<https://doi.org/10.1021/acs.inorgchem.0c03639>.
- (58) Andersen, O. Chelation of Cadmium. *Environ Health Perspect* **1983**, *VOL. 54*. <https://doi.org/10.1289/ehp.8454249>.
- (59) Peraferrer, C.; Martínez, M.; Poch, J.; Villaescusa, I. Toxicity of Metal-Ethylenediaminetetraacetic Acid Solution as a Function of Chemical Speciation: An Approach for Toxicity Assessment. *Arch Environ Contam Toxicol* **2012**, *63* (4), 484–494. <https://doi.org/10.1007/s00244-012-9788-x>.
- (60) Li, C. W.; Cheng, C. H.; Choo, K. H.; Yen, W. S. Polyelectrolyte Enhanced Ultrafiltration (PEUF) for the Removal of Cd(II): Effects of Organic Ligands and Solution PH. *Chemosphere* **2008**, *72* (4).
<https://doi.org/10.1016/j.chemosphere.2008.02.036>.
- (61) Karak, T.; Paul, R. K.; Das, D. K.; Boruah, R. K. Complexation of DTPA and EDTA with Cd²⁺: Stability Constants and Thermodynamic Parameters at the Soil-Water Interface. *Environ Monit Assess* **2016**, *188* (12).
<https://doi.org/10.1007/s10661-016-5685-5>.
- (62) TREFRY, J. H.; P.TROCINE, R. Metals in Sediments and Clams From the Indian River Lagoon , Florida : 2006 – 7 Versus 1992. *Florida Scientist* **2006**, *74*.
- (63) Patel, K. S.; Pandey, P. K.; Martín-Ramos, P.; Corns, W. T.; Varol, S.; Bhattacharya, P.; Zhu, Y. A Review on Arsenic in the Environment: Contamination, Mobility, Sources, and Exposure. *RSC Advances*. Royal Society of Chemistry March 17, 2023, pp 8803–8821.
<https://doi.org/10.1039/d3ra00789h>.

- (64) Mielke, H. W.; Powell, E. T.; Shah, A.; Gonzales, C. R.; Mielke, P. W. *Environmental Health Perspectives* • VOLUME; 2001; Vol. 109. <http://ehpnet1.niehs.nih.gov/docs/2001/109p973-978mielke/abstract.html>.
- (65) Sirikonda, C. Journal of Environmental Analytical Chemistry Chiranjeevi Sirikonda. *J Environ Anal Chem* **2021**, 8 (3), 300.
- (66) Sayadi, M. H.; Sayyed, M. R. G.; Kumar, S. Short-Term Accumulative Signatures of Heavy Metals in River Bed Sediments in the Industrial Area, Tehran, Iran. *Environ Monit Assess* **2010**, 162 (1–4), 465–473. <https://doi.org/10.1007/s10661-009-0810-3>.
- (67) Zhang, X.; Li, J.; Niu, Y. Two New 1D Supramolecular Compounds Based on PbI₂ for Efficient Iodine Capture. *Molecules* **2023**, 28 (7). <https://doi.org/10.3390/molecules28072934>.
- (68) Hou, S.; Zheng, N.; Tang, L.; Ji, X.; Li, Y.; Hua, X. Pollution Characteristics, Sources, and Health Risk Assessment of Human Exposure to Cu, Zn, Cd and Pb Pollution in Urban Street Dust across China between 2009 and 2018. *Environment International*. Elsevier Ltd July 1, 2019, pp 430–437. <https://doi.org/10.1016/j.envint.2019.04.046>.
- (69) Tigoi, C.; Sang, R.; Chepkorir, E.; Orindi, B.; Arum, S. O.; Mulwa, F.; Mosomtai, G.; Limbaso, S.; Hassan, O. A.; Irura, Z.; Ahlm, C.; Evander, M. High Risk for Human Exposure to Rift Valley Fever Virus in Communities Living along Livestock Movement Routes: A Cross-Sectional Survey in Kenya. *PLoS Negl Trop Dis* **2020**, 14 (2). <https://doi.org/10.1371/journal.pntd.0007979>.
- (70) Satarug, S.; Baker, J. R.; Urbenjapol, S.; Haswell-Elkins, M.; Reilly, P. E. B.; Williams, D. J.; Moore, M. R. A Global Perspective on Cadmium

- Pollution and Toxicity in Non-Occupationally Exposed Population. *Toxicol Lett* **2003**, *137* (1–2), 65–83. [https://doi.org/10.1016/S0378-4274\(02\)00381-8](https://doi.org/10.1016/S0378-4274(02)00381-8).
- (71) Johri, N.; Jacquillet, G.; Unwin, R. Heavy Metal Poisoning: The Effects of Cadmium on the Kidney. *BioMetals*. October 2010, pp 783–792. <https://doi.org/10.1007/s10534-010-9328-y>.
- (72) Rikans, L. E.; Yamano, T. *Mechanisms of Cadmium-Mediated Acute Hepatotoxicity*; John Wiley & Sons, Inc, 2000; Vol. 14.
- (73) Hyder, O.; Chung, M.; Cosgrove, D.; Herman, J. M.; Li, Z.; Firoozmand, A.; Gurakar, A.; Koteish, A.; Pawlik, T. M. Cadmium Exposure and Liver Disease among US Adults. *Journal of Gastrointestinal Surgery* **2013**, *17* (7), 1265–1273. <https://doi.org/10.1007/S11605-013-2210-9>.
- (74) Manring, N.; Strini, M.; Koifman, G.; Smeltz, J. L.; Pathirathna, P. Gold Nanoparticle-Modified Carbon-Fiber Microelectrodes for the Electrochemical Detection of Cd²⁺ via Fast-Scan Cyclic Voltammetry. *Micromachines (Basel)* **2024**, *15* (3), 294. <https://doi.org/10.3390/mi15030294>.
- (75) Wang, M.; Chen, Z.; Song, W.; Hong, D.; Huang, L.; Li, Y. A Review on Cadmium Exposure in the Population and Intervention Strategies Against Cadmium Toxicity. *Bull Environ Contam Toxicol* **2021**, *106* (1), 65–74. <https://doi.org/10.1007/s00128-020-03088-1>.
- (76) Sun, X. L.; Phuc, H. D.; Okamoto, R.; Kido, T.; Oanh, N. T. P.; Manh, H. D.; Anh, L. T.; Ichimori, A.; Nogawa, K.; Suwazono, Y.; Nakagawa, H. A 30-Year Follow-up Study in a Former Cadmium-Polluted Area of Japan: The Relationship between Cadmium Exposure and B2-Microglobulin in the

Urine of Japanese People. *Environmental Science and Pollution Research* **2023**, *30* (9), 23079–23085. <https://doi.org/10.1007/s11356-022-23818-8>.

- (77) Tsai, K. F.; Hsu, P. C.; Lee, C. Te; Kung, C. Te; Chang, Y. C.; Fu, L. M.; Ou, Y. C.; Lan, K. C.; Yen, T. H.; Lee, W. C. Association between Enzyme-Linked Immunosorbent Assay-Measured Kidney Injury Markers and Urinary Cadmium Levels in Chronic Kidney Disease. *J Clin Med* **2022**, *11* (1). <https://doi.org/10.3390/jcm11010156>.
- (78) Shen, X.; Cheng, J.; Yu, G.; Li, X.; Li, H.; Chen, J. Urine B2-Microglobulin and Retinol-Binding Protein and Renal Disease Progression in IgA Nephropathy. *Front Med (Lausanne)* **2021**, *8*. <https://doi.org/10.3389/fmed.2021.792782>.
- (79) Olmedo, P.; Pla, A.; Hernández, A. F.; López-Guarnido, O.; Rodrigo, L.; Gil, F. Validation of a Method to Quantify Chromium, Cadmium, Manganese, Nickel and Lead in Human Whole Blood, Urine, Saliva and Hair Samples by Electrothermal Atomic Absorption Spectrometry. *Anal Chim Acta* **2010**, *659* (1–2), 60–67. <https://doi.org/10.1016/j.aca.2009.11.056>.
- (80) Ferraro, G.; Paolillo, M.; Sciortino, G.; Pisanu, F.; Garribba, E.; Merlino, A. Implications of Protein Interaction in the Speciation of Potential VIVO-Pyridinone Drugs. *Inorg Chem* **2023**, *62* (21), 8407–8417. <https://doi.org/10.1021/acs.inorgchem.3c01041>.
- (81) Irto, A.; Cardiano, P.; Chand, K.; Cigala, R. M.; Crea, F.; De Stefano, C.; Santos, M. A. Bifunctional 3-Hydroxy-4-Pyridinones as Potential Selective Iron(III) Chelators: Solution Studies and Comparison with Other Metals of Biological and Environmental Relevance. *Molecules* **2021**, *26* (23). <https://doi.org/10.3390/molecules26237280>.

- (82) Aiello, D.; Carnamucio, F.; Cordaro, M.; Foti, C.; Napoli, A.; Giuffrè, O. Ca²⁺ Complexation with Relevant Bioligands in Aqueous Solution: A Speciation Study with Implications for Biological Fluids. *Front Chem* **2021**, *9*. <https://doi.org/10.3389/fchem.2021.640219>.
- (83) Gumpu, M. B.; Veerapandian, M.; Krishnan, U. M.; Rayappan, J. B. B. Simultaneous Electrochemical Detection of Cd(II), Pb(II), As(III) and Hg(II) Ions Using Ruthenium(II)-Textured Graphene Oxide Nanocomposite. *Talanta* **2017**, *162*, 574–582. <https://doi.org/10.1016/j.talanta.2016.10.076>.
- (84) Göde, C.; Yola, M. L.; Yilmaz, A.; Atar, N.; Wang, S. A Novel Electrochemical Sensor Based on Calixarene Functionalized Reduced Graphene Oxide: Application to Simultaneous Determination of Fe(III), Cd(II) and Pb(II) Ions. *J Colloid Interface Sci* **2017**, *508*, 525–531. <https://doi.org/10.1016/j.jcis.2017.08.086>.
- (85) Ruecha, N.; Rodthongkum, N.; Cate, D. M.; Volckens, J.; Chailapakul, O.; Henry, C. S. Sensitive Electrochemical Sensor Using a Graphene-Polyaniline Nanocomposite for Simultaneous Detection of Zn(II), Cd(II), and Pb(II). *Anal Chim Acta* **2015**, *874*, 40–48. <https://doi.org/10.1016/j.aca.2015.02.064>.
- (86) Yao, Y.; Wu, H.; Ping, J. Simultaneous Determination of Cd(II) and Pb(II) Ions in Honey and Milk Samples Using a Single-Walled Carbon Nanohorns Modified Screen-Printed Electrochemical Sensor. *Food Chem* **2019**, *274*, 8–15. <https://doi.org/10.1016/j.foodchem.2018.08.110>.
- (87) Liao, J.; Yang, F.; Wang, C. Z.; Lin, S. The Crystal Facet-Dependent Electrochemical Performance of TiO₂ Nanocrystals for Heavy Metal Detection: Theoretical Prediction and Experimental Proof. *Sens Actuators B Chem* **2018**, *271*, 195–202. <https://doi.org/10.1016/j.snb.2018.05.067>.

- (88) Bi, X. M.; Wang, H. R.; Ge, L. Q.; Zhou, D. M.; Xu, J. Z.; Gu, H. Y.; Bao, N. Gold-Coated Nanostructured Carbon Tape for Rapid Electrochemical Detection of Cadmium in Rice with in Situ Electrodeposition of Bismuth in Paper-Based Analytical Devices. *Sens Actuators B Chem* **2018**, *260*, 475–479. <https://doi.org/10.1016/j.snb.2018.01.007>.
- (89) Mastouri, A.; Peulon, S.; Farcage, D.; Bellakhal, N.; Chaussé, A. Perfect Additivity of Microinterface Arrays for Liquid-Liquid Measurements: Application to Cadmium Ions Quantification. *Electrochim Acta* **2014**, *120*, 212–218. <https://doi.org/10.1016/j.electacta.2013.12.034>.
- (90) Viada, B. N.; Yudi, L. M.; Arrigan, D. W. M. Detection of Perfluorooctane Sulfonate by Ion-Transfer Stripping Voltammetry at an Array of Microinterfaces between Two Immiscible Electrolyte Solutions. *Analyst* **2020**, *145* (17), 5776–5786. <https://doi.org/10.1039/d0an00884b>.
- (91) Lu, G.; Despas, C.; Liu, L.; Herzog, G. Ametryn Detection by Proton Assisted Transfer at a Single Micro-Interface between Two Immiscible Electrolyte Solutions. *Journal of Electroanalytical Chemistry* **2020**, 877. <https://doi.org/10.1016/j.jelechem.2020.114745>.
- (92) Ahmed, M. M. N.; Bodowara, F. S.; Zhou, W.; Penteado, J. F.; Smeltz, J. L.; Pathirathna, P. Electrochemical Detection of Cd(II) Ions in Complex Matrices with Nanopipets. *RSC Adv* **2022**, *12* (2), 1077–1083. <https://doi.org/10.1039/d1ra07655h>.
- (93) Iwai, N. T.; Kramaric, M.; Crabbe, D.; Wei, Y.; Chen, R.; Shen, M. GABA Detection with Nano-ITIES Pipet Electrode: A New Mechanism, Water/DCE-Octanoic Acid Interface. *Anal Chem* **2018**, *90* (5), 3067–3072. <https://doi.org/10.1021/acs.analchem.7b03099>.

- (94) Mastouri, A.; Peulon, S.; Bellakhal, N.; Chaussé, A. M(II) Transfer across a Liquid-Liquid Microinterface Facilitated by a Complex Formation with 8-Hydroxyquinoline: Application to Quantification of Pb(II), Cd(II) and Zn(II) Alone or in Mixture in Effluents. *Electrochim Acta* **2014**, *130*, 818–825. <https://doi.org/10.1016/j.electacta.2014.03.073>.
- (95) Evidence_for_the_relationship_ (1).
- (96) Sarigul, N.; Korkmaz, F.; Kurultak, İ. A New Artificial Urine Protocol to Better Imitate Human Urine. *Sci Rep* **2019**, *9* (1). <https://doi.org/10.1038/s41598-019-56693-4>.
- (97) Etd.
- (98) Manring, N.; Strini, M.; Smeltz, J. L.; Pathirathna, P. Simultaneous Detection of Neurotransmitters and Cu²⁺ Using Double-Bore Carbon Fiber Microelectrodes via Fast-Scan Cyclic Voltammetry. *RSC Adv* **2023**, *13* (48), 33844–33851. <https://doi.org/10.1039/d3ra06218j>.
- (99) Han, J. H.; Lee, D.; Chew, C. H. C.; Kim, T.; Pak, J. J. A Multi-Virus Detectable Microfluidic Electrochemical Immunosensor for Simultaneous Detection of H1N1, H5N1, and H7N9 Virus Using ZnO Nanorods for Sensitivity Enhancement. *Sens Actuators B Chem* **2016**, *228*. <https://doi.org/10.1016/j.snb.2015.07.068>.
- (100) Sigg, A. P.; Mariotti, M.; Grütter, A. E.; Lafranca, T.; Leitner, L.; Bonkat, G.; Braissant, O. A Method to Determine the Efficacy of a Commercial Phage Preparation against Uropathogens in Urine and Artificial Urine Determined by Isothermal Microcalorimetry. *Microorganisms* **2022**, *10* (5). <https://doi.org/10.3390/microorganisms10050845>.

- (101) Brooks, T.; Keevil, C. W. *A Simple Artificial Urine for the Growth of Urinary Pathogens*; 1997; Vol. 24.
- (102) Sueksakit, K.; Thongboonkerd, V. Optimization of Artificial Urine Formula for in Vitro Cellular Study Compared with Native Urine. *Int J Med Sci* **2021**, *18* (14), 3271–3279. <https://doi.org/10.7150/IJMS.61720>.
- (103) Motswaledi, M. S.; Kasvosve, I.; Oguntibeju, O. O. The Role of Red Blood Cells in Enhancing or Preventing HIV Infection and Other Diseases. *BioMed Research International*. 2013. <https://doi.org/10.1155/2013/758682>.
- (104) Yun, S. S.; Li, W. Identification of Squalamine in the Plasma Membrane of White Blood Cells in the Sea Lamprey, *Petromyzon Marinus*. *J Lipid Res* **2007**, *48* (12), 2579–2586. <https://doi.org/10.1194/jlr.M700294-JLR200>.
- (105) Kudr, J.; Nguyen, H. V.; Gumulec, J.; Nejd, L.; Blazkova, I.; Ruttkay-Nedecky, B.; Hynek, D.; Kynicky, J.; Adam, V.; Kizek, R. Simultaneous Automatic Electrochemical Detection of Zinc, Cadmium, Copper and Lead Ions in Environmental Samples Using a Thin-Film Mercury Electrode and an Artificial Neural Network. *Sensors (Switzerland)* **2015**, *15* (1), 592–610. <https://doi.org/10.3390/s150100592>.
- (106) Sachdeva, D.; Singh, A.; Agrawal, V. V. Electrochemical Detection of Anti-Anxiety Drug Clonazepam Using Electrophoretically Deposited Gold Nanoparticles. *Mapan - Journal of Metrology Society of India* **2021**, *36* (3), 639–649. <https://doi.org/10.1007/s12647-021-00484-8>.
- (107) Reyes, K. M.; Kuromoto, N. K.; Alves Claro, A. P. R.; Marino, C. E. B. Electrochemical Stability of Binary TiNb for Biomedical Applications. *Mater Res Express* **2017**, *4* (7). <https://doi.org/10.1088/2053-1591/aa6ee4>.

- (108) Gugelmin, B. S.; Santos, L. S.; Ponte, H. D. A.; Marino, C. E. B. Electrochemical Stability and Bioactivity Evaluation of Ti6Al4V Surface Coated with Thin Oxide by EIS for Biomedical Applications. *Materials Research* **2015**, *18* (3), 602–607. <https://doi.org/10.1590/1516-1439.201514>.
- (109) Sivasankaran, U.; Thomas, A.; Jose, A. R.; Kumar, K. G. Poly (Bromophenol Blue)-Gold Nanoparticle Composite: An Efficient Electrochemical Sensing Platform for Uric Acid. *J Electrochem Soc* **2017**, *164* (6), B292–B297. <https://doi.org/10.1149/2.0181707jes>.
- (110) Rahimzadeh, M. R.; Rahimzadeh, M. R.; Kazemi, S.; Moghadamnia, A. A. Cadmium Toxicity and Treatment: An Update. *Caspian Journal of Internal Medicine*. Babol University of Medical Sciences 2017, pp 135–145. <https://doi.org/10.22088/cjim.8.3.135>.
- (111) Ferrero, M. E. Neuron Protection by EDTA May Explain the Successful Outcomes of Toxic Metal Chelation Therapy in Neurodegenerative Diseases. *Biomedicines*. MDPI October 1, 2022. <https://doi.org/10.3390/biomedicines10102476>.
- (112) Jamilaldin Fatemi, S.; Zandevakili, T.; Nejad, F. K.; Iranmanesh, M.; Zarandi, M. F. Determination of Manganese in Rat Blood Samples Based on Ionic Liquid-Liquid Extraction and Chelation Therapy for Evaluation of Manganese Toxicity in Rats. *Analytical Methods in Environmental Chemistry Journal* **2021**, *4* (4), 78–91. <https://doi.org/10.24200/amecj.v4.i04.160>.
- (113) Martell and Smith, Critical Stability Constants.
- (114) Gomez, M.; Domingot, J. L.; Llobet, J. M.; Paternain, J. L. *Effectiveness of Chelation Therapy with Time Acute Vanadium Intoxication*; 1988; Vol. 8.

- (115) Hama Aziz, K. H.; Mustafa, F. S.; Omer, K. M.; Hama, S.; Hamarawf, R. F.; Rahman, K. O. Heavy Metal Pollution in the Aquatic Environment: Efficient and Low-Cost Removal Approaches to Eliminate Their Toxicity: A Review. *RSC Advances*. Royal Society of Chemistry June 12, 2023, pp 17595–17610. <https://doi.org/10.1039/d3ra00723e>.
- (116) He, Y.; Peng, C.; Zhang, Y.; Guo, Z.; Xiao, X.; Kong, L. Comparison of Heavy Metals in Urban Soil and Dust in Cities of China: Characteristics and Health Risks. *International Journal of Environmental Science and Technology* **2023**, *20* (2), 2247–2258. <https://doi.org/10.1007/s13762-022-04051-9>.
- (117) Hoque, M. Md. M.; Sarker, A.; Sarker, Md. E.; Kabir, Md. H.; Ahmed, F. T.; Yeasmin, M.; Islam, Md. S.; Idris, A. M. Heavy Metals in Sediments of an Urban River at the Vicinity of Tannery Industries in Bangladesh: A Preliminary Study for Ecological and Human Health Risk. *Int J Environ Anal Chem* **2021**, *103*, 7909–7927.
- (118) Jabbar, A.; Abbas, A.; Assad, N.; Naeem-Ul-Hassan, M.; Alhazmi, H. A.; Najmi, A.; Zoghebi, K.; Al Bratty, M.; Hanbashi, A.; Amin, H. M. A. A Highly Selective Hg²⁺ Colorimetric Sensor and Antimicrobial Agent Based on Green Synthesized Silver Nanoparticles Using Equisetum Diffusum Extract. *RSC Adv* **2023**, *13* (41), 28666–28675. <https://doi.org/10.1039/d3ra05070j>.
- (119) Gundlach-Graham, A.; Günther, D. Toward Faster and Higher Resolution LA-ICPMS Imaging: On the Co-Evolution of La Cell Design and ICPMS Instrumentation Young Investigators in Analytical and Bioanalytical Science. *Anal Bioanal Chem* **2016**, *408* (11), 2687–2695. <https://doi.org/10.1007/s00216-015-9251-8>.

- (120) Shaban, M. In-Situ SERS Detection of Hg²⁺/Cd²⁺ and Congo Red Adsorption Using Spiral CNTs/Brass Nails. *Nanomaterials* **2022**, *12* (21). <https://doi.org/10.3390/nano12213778>.
- (121) Paredes, E.; Todoli, J. L.; Quéstel, C. R. Limitations of the Exponential Model for the Correction for Mass Discrimination Effects during Isotope Ratio Measurements by MC-ICPMS. Demonstration with Sr at 5-15 ML Min⁻¹ Continuous Liquid Flow Rates. *J Anal At Spectrom* **2013**, *28* (3), 327–333. <https://doi.org/10.1039/c3ja30210e>.
- (122) Craig, G.; Wehrs, H.; Bevan, D. G.; Pfeifer, M.; Lewis, J.; Coath, C. D.; Elliott, T.; Huang, C.; Lloyd, N. S.; Schwieters, J. B. Project Vienna: A Novel Pre-cell Mass Filter for Collision/Reaction Cell MC-ICPMS/MS. *Anal Chem* **2021**, *93* (30), 10519–10527. <https://doi.org/10.1021/acs.analchem.1c01475>.
- (123) Woodhead, J.; Petrus, J. Exploring the Advantages and Limitations of in Situ U-Pb Carbonate Geochronology Using Speleothems. *Geochronology* **2019**, *1* (1), 69–84. <https://doi.org/10.5194/gchron-1-69-2019>.
- (124) Lajin, B.; Feldmann, J.; Goessler, W. Elution with 1,2-Hexanediol Enables Coupling of ICPMS with Reversed-Phase Liquid Chromatography under Standard Conditions. *Anal Chem* **2022**, *94* (24), 8802–8810. <https://doi.org/10.1021/acs.analchem.2c01769>.
- (125) Zhang, X.; Xu, Y.; Li, T.; Li, H.; Yu, Z.; Song, L.; Xu, J. Sequential Speciation Analysis of Heavy Metals on Suspended Particulate Matter in Water Using Electrochemical Mass Spectrometry. *J Anal At Spectrom* **2023**, *38* (3), 716–720. <https://doi.org/10.1039/d2ja00314g>.

- (126) Rosolina, S. M. *Novel Methods and Sensors for the Analysis of Trace Chemicals Novel Methods and Sensors for the Analysis of Trace Chemicals with Potential Environmental Applications with Potential Environmental Applications*. https://trace.tennessee.edu/utk_graddiss.
- (127) Meskher, H.; Ragdi, T.; Thakur, A. K.; Ha, S.; Khelfaoui, I.; Sathyamurthy, R.; Sharshir, S. W.; Pandey, A. K.; Saidur, R.; Singh, P.; Sharifianjazi, F.; Lynch, I. A Review on CNTs-Based Electrochemical Sensors and Biosensors: Unique Properties and Potential Applications. *Critical Reviews in Analytical Chemistry*. Taylor and Francis Ltd. 2023. <https://doi.org/10.1080/10408347.2023.2171277>.
- (128) Bashir, A.; Malik, L. A.; Ahad, S.; Manzoor, T.; Bhat, M. A.; Dar, G. N.; Pandith, A. H. Removal of Heavy Metal Ions from Aqueous System by Ion-Exchange and Biosorption Methods. *Environmental Chemistry Letters*. Springer June 15, 2019, pp 729–754. <https://doi.org/10.1007/s10311-018-00828-y>.
- (129) Mansouri, S. EC3.2 - Miniaturization of Electrochemical Sensors; AMA Service GmbH, 2020; pp 252–253. <https://doi.org/10.5162/imcs2018/ec3.2>.
- (130) Murtada, K.; Moreno, V. Nanomaterials-Based Electrochemical Sensors for the Detection of Aroma Compounds - towards Analytical Approach. *Journal of Electroanalytical Chemistry*. Elsevier B.V. March 15, 2020. <https://doi.org/10.1016/j.jelechem.2020.113988>.
- (131) Ding, R.; Cheong, Y. H.; Ahamed, A.; Lisak, G. Heavy Metals Detection with Paper-Based Electrochemical Sensors. *Anal Chem* **2021**, *93* (4), 1880–1888. <https://doi.org/10.1021/acs.analchem.0c04247>.

- (132) Aihaiti, A.; Li, Z.; Qin, Y.; Meng, F.; Li, X.; Huangfu, Z.; Chen, K.; Zhang, M. Construction of Electrochemical Sensors for Antibiotic Detection Based on Carbon Nanocomposites. *Nanomaterials*. MDPI August 1, 2022. <https://doi.org/10.3390/nano12162789>.
- (133) Manring, N.; Ahmed, M. M. N.; Smeltz, J. L.; Pathirathna, P. Electrodeposition of Dopamine onto Carbon Fiber Microelectrodes to Enhance the Detection of Cu²⁺ via Fast-Scan Cyclic Voltammetry. *Anal Bioanal Chem* **2023**, *415* (18), 4289–4296. <https://doi.org/10.1007/s00216-022-04488-4>.
- (134) Sulthana, S. F.; Iqbal, U. M.; Suseela, S. B.; Anbazhagan, R.; Chinthaginjala, R.; Chitathuru, D.; Ahmad, I.; Kim, T. H. Electrochemical Sensors for Heavy Metal Ion Detection in Aqueous Medium: A Systematic Review. *ACS Omega*. American Chemical Society 2024. <https://doi.org/10.1021/acsomega.4c00933>.
- (135) Bansod, B. K.; Kumar, T.; Thakur, R.; Rana, S.; Singh, I. A Review on Various Electrochemical Techniques for Heavy Metal Ions Detection with Different Sensing Platforms. *Biosensors and Bioelectronics*. Elsevier Ltd August 15, 2017, pp 443–455. <https://doi.org/10.1016/j.bios.2017.03.031>.
- (136) March, G.; Nguyen, T. D.; Piro, B. Modified Electrodes Used for Electrochemical Detection of Metal Ions in Environmental Analysis. *Biosensors*. MDPI 2015, pp 241–275. <https://doi.org/10.3390/bios5020241>.
- (137) Zhao, G.; Wang, H.; Liu, G. Recent Advances in Chemically Modified Electrodes, Microfabricated Devices and Injection Systems for the Electrochemical Detection of Heavy Metals: A Review. *International Journal of Electrochemical Science*. Electrochemical Science Group September 1, 2017, pp 8622–8641. <https://doi.org/10.20964/2017.09.39>.

- (138) Thatikayala, D.; Noori, M. T.; Min, B. Zeolite-Modified Electrodes for Electrochemical Sensing of Heavy Metal Ions – Progress and Future Directions. *Mater Today Chem* **2023**, *29*, 101412. <https://doi.org/10.1016/J.MTCHEM.2023.101412>.
- (139) Shan, Q.; Tian, J.; Ding, Q.; Wu, W. Electrochemical Sensor Based on Metal-Free Materials Composed of Graphene and Graphene Oxide for Sensitive Detection of Cadmium Ions in Water. *Mater Chem Phys* **2022**, *284*. <https://doi.org/10.1016/j.matchemphys.2022.126064>.
- (140) Sacara, A. M.; Pitzalis, F.; Salis, A.; Turdean, G. L.; Muresan, L. M. Glassy Carbon Electrodes Modified with Ordered Mesoporous Silica for the Electrochemical Detection of Cadmium Ions. *ACS Omega* **2019**, *4* (1), 1410–1415. <https://doi.org/10.1021/acsomega.8b03305>.
- (141) Collins, C. J.; Lyons, C.; Strutwolf, J.; Arrigan, D. W. M. Serum-Protein Effects on the Detection of the β -Blocker Propranolol by Ion-Transfer Voltammetry at a Micro-ITIES Array. *Talanta* **2010**, *80* (5), 1993–1998. <https://doi.org/10.1016/j.talanta.2009.10.060>.
- (142) Taylor, G.; Girault, H. H. J. *Preliminary Note ION TRANSFER REACTIONS ACROSS A LIQUID-LIQUID INTERFACE SUPPORTED ON A MICROPIPE 'ITE TIP*; Elsevier Sequoia S.A, 1986; Vol. 208.
- (143) Ishimatsu, R.; Izadyar, A.; Kabagambe, B.; Kim, Y.; Kim, J.; Amemiya, S. Electrochemical Mechanism of Ion-Ionophore Recognition at Plasticized Polymer Membrane/Water Interfaces. *J Am Chem Soc* **2011**, *133* (40), 16300–16308. <https://doi.org/10.1021/ja207297q>.
- (144) Ma, N.; Halley, S.; Ramaiyan, K.; Garzon, F.; Tsui, L. Comparison of Machine Learning Algorithms for Natural Gas Identification with Mixed

- Potential Electrochemical Sensor Arrays. *ECS Sensors Plus* **2023**, 2 (1), 011402. <https://doi.org/10.1149/2754-2726/acbe0c>.
- (145) Sinha, K.; Uddin, Z.; Kawsar, H. I.; Islam, S.; Deen, M. J.; Howlader, M. M. R. Analyzing Chronic Disease Biomarkers Using Electrochemical Sensors and Artificial Neural Networks. *TrAC - Trends in Analytical Chemistry*. Elsevier B.V. January 1, 2023. <https://doi.org/10.1016/j.trac.2022.116861>.
- (146) Halley, S.; Tsui, L.; Garzon, F. Combined Mixed Potential Electrochemical Sensors and Artificial Neural Networks for the Quantification and Identification of Methane in Natural Gas Emissions Monitoring. *J Electrochem Soc* **2021**, 168 (9), 097506. <https://doi.org/10.1149/1945-7111/ac2465>.
- (147) Tsui, L. kun; Benavidez, A.; Palanisamy, P.; Evans, L.; Garzon, F. Automatic Signal Decoding and Sensor Stability of a 3-Electrode Mixed-Potential Sensor for NO_x/NH₃ Quantification. *Electrochim Acta* **2018**, 283, 141–148. <https://doi.org/10.1016/j.electacta.2018.06.133>.
- (148) Stevens, D. M.; Gray, B. L.; Leznoff, D. B.; Furukawa, H.; Khosla, A. 3D Printable Vapochromic Sensing Materials. *J Electrochem Soc* **2020**, 167 (16), 167503. <https://doi.org/10.1149/1945-7111/abc99e>.
- (149) Tsui, L. kun; Benavidez, A.; Palanisamy, P.; Evans, L.; Garzon, F. Quantitative Decoding of the Response of a Ceramic Mixed Potential Sensor Array for Engine Emissions Control and Diagnostics. *Sens Actuators B Chem* **2017**, 249, 673–684. <https://doi.org/10.1016/j.snb.2017.04.060>.
- (150) Wang, X.; Lin, W.; Chen, C.; Kong, L.; Huang, Z.; Kirsanov, D.; Legin, A.; Wan, H.; Wang, P. Neural Networks Based Fluorescence and Electrochemistry Dual-Modal Sensor for Sensitive and Precise Detection of

Cadmium and Lead Simultaneously. *Sens Actuators B Chem* **2022**, 366.

<https://doi.org/10.1016/j.snb.2022.131922>.

- (151) Choi, H.; Shin, H.; Cho, H. U.; Blaha, C. D.; Heien, M. L.; Oh, Y.; Lee, K. H.; Jang, D. P. Neurochemical Concentration Prediction Using Deep Learning vs Principal Component Regression in Fast Scan Cyclic Voltammetry: A Comparison Study. *ACS Chem Neurosci* **2022**, 13 (15), 2288–2297. <https://doi.org/10.1021/acchemneuro.2c00069>.
- (152) Farris, B. R.; Niang-Trost, T.; Branicky, M. S.; Leonard, K. C. Evaluation of Machine Learning Models on Electrochemical CO₂ Reduction Using Human Curated Datasets. *ACS Sustain Chem Eng* **2022**, 10 (33), 10934–10944. <https://doi.org/10.1021/acssuschemeng.2c02941>.
- (153) Zhang, J.; Chen, F.; Zou, R.; Liao, J.; Zhang, Y.; Zhu, Z.; Yan, X.; Jiang, Z.; Tan, F. A CNN-Based Method for Heavy-Metal Ion Detection. *Applied Sciences (Switzerland)* **2023**, 13 (7). <https://doi.org/10.3390/app13074520>.
- (154) Balkourani, G.; Damartzis, T.; Brouzgou, A.; Tsiakaras, P. Cost Effective Synthesis of Graphene Nanomaterials for Non-Enzymatic Electrochemical Sensors for Glucose: A Comprehensive Review. *Sensors*. MDPI January 1, 2022. <https://doi.org/10.3390/s22010355>.
- (155) Lawal, A. T. Recent Developments in Electrochemical Sensors Based on Graphene for Bioanalytical Applications. *Sensing and Bio-Sensing Research*. Elsevier B.V. August 1, 2023. <https://doi.org/10.1016/j.sbsr.2023.100571>.
- (156) Rojas-Romo, C.; Aliaga, M. E.; Arancibia, V.; Gomez, M. Determination of Pb(II) and Cd(II) via Anodic Stripping Voltammetry Using an in-Situ Bismuth Film Electrode. Increasing the Sensitivity of the Method by the

- Presence of Alizarin Red S. *Microchemical Journal* **2020**, *159*.
<https://doi.org/10.1016/j.microc.2020.105373>.
- (157) Ivanišević, I. The Role of Silver Nanoparticles in Electrochemical Sensors for Aquatic Environmental Analysis. *Sensors*. MDPI April 1, 2023.
<https://doi.org/10.3390/s23073692>.
- (158) Bílek, J.; Bílek, O.; Maršolek, P.; Buček, P. Ambient Air Quality Measurement with Low-Cost Optical and Electrochemical Sensors: An Evaluation of Continuous Year-Long Operation. *Environments - MDPI* **2021**, *8* (11). <https://doi.org/10.3390/environments8110114>.
- (159) Elgrishi, N.; Rountree, K. J.; McCarthy, B. D.; Rountree, E. S.; Eisenhart, T. T.; Dempsey, J. L. A Practical Beginner's Guide to Cyclic Voltammetry. *J Chem Educ* **2018**, *95* (2), 197–206.
<https://doi.org/10.1021/acs.jchemed.7b00361>.
- (160) Molinara, M.; Cancelliere, R.; Di Tinno, A.; Ferrigno, L.; Shuba, M.; Kuzhir, P.; Maffucci, A.; Micheli, L. A Deep Learning Approach to Organic Pollutants Classification Using Voltammetry. *Sensors* **2022**, *22* (20).
<https://doi.org/10.3390/s22208032>.
- (161) Dean, S. N.; Shriver-Lake, L. C.; Stenger, D. A.; Erickson, J. S.; Golden, J. P.; Trammell, S. A. Machine Learning Techniques for Chemical Identification Using Cyclic Square Wave Voltammetry. *Sensors (Switzerland)* **2019**, *19* (10). <https://doi.org/10.3390/s19102392>.
- (162) Mistry, A.; Franco, A. A.; Cooper, S. J.; Roberts, S. A.; Viswanathan, V. How Machine Learning Will Revolutionize Electrochemical Sciences. *ACS Energy Letters*. American Chemical Society April 9, 2021, pp 1422–1431.
<https://doi.org/10.1021/acsenerylett.1c00194>.

- (163) Matsushita, G. H. G.; Sugi, A. H.; Costa, Y. M. G.; Gomez-A, A.; Da Cunha, C.; Oliveira, L. S. Phasic Dopamine Release Identification Using Convolutional Neural Network. *Comput Biol Med* **2019**, *114*.
<https://doi.org/10.1016/j.compbiomed.2019.103466>.
- (164) Kennedy, G. F.; Zhang, J.; Bond, A. M. Automatically Identifying Electrode Reaction Mechanisms Using Deep Neural Networks. *Anal Chem* **2019**, *91* (19), 12220–12227. <https://doi.org/10.1021/acs.analchem.9b01891>.
- (165) Puthongkham, P.; Wirojsaengthong, S.; Suea-Ngam, A. Machine Learning and Chemometrics for Electrochemical Sensors: Moving Forward to the Future of Analytical Chemistry. *Analyst* **2021**, *146* (21), 6351–6364.
<https://doi.org/10.1039/d1an01148k>.
- (166) Chen, H.; Kätelhön, E.; Compton, R. G. Machine Learning in Fundamental Electrochemistry: Recent Advances and Future Opportunities. *Current Opinion in Electrochemistry*. Elsevier B.V. April 1, 2023.
<https://doi.org/10.1016/j.coelec.2023.101214>.
- (167) Aguilar-Lira, G. Y.; Hernandez, P.; Álvarez-Romero, G. A.; Gutiérrez, J. M. Simultaneous Quantification of Four Principal NSAIDs through Voltammetry and Artificial Neural Networks Using a Modified Carbon Paste Electrode in Pharmaceutical Samples; MDPI AG, 2021; p 3.
<https://doi.org/10.3390/csac2021-10450>.
- (168) Lokhande, P. E.; Chavan, U. S. Cyclic Voltammetry Behavior Modeling of Fabricated Nanostructured Ni(OH)₂ Electrode Using Artificial Neural Network for Supercapacitor Application. *Proc Inst Mech Eng C J Mech Eng Sci* **2020**, *234* (13), 2563–2568. <https://doi.org/10.1177/0954406220907615>.

- (169) Abu-Ali, H.; Nabok, A.; Smith, T. J. Electrochemical Inhibition Bacterial Sensor Array for Detection of Water Pollutants: Artificial Neural Network (ANN) Approach. *Anal Bioanal Chem* **2019**, *411* (29), 7659–7668. <https://doi.org/10.1007/s00216-019-01853-8>.
- (170) Alimi, A.; Assaker, I. Ben; Mozaryn, J.; Ávila-Brandé, D.; Castillo-Martínez, E.; Chtourou, R. Electrochemical Synthesis of MnO₂/NiO/ZnO Trijunction Coated Stainless Steel Substrate as a Supercapacitor Electrode and Cyclic Voltammetry Behavior Modeling Using Artificial Neural Network. *Int J Energy Res* **2022**. <https://doi.org/10.1002/er.8380>.
- (171) Zhao, G.; Wang, H.; Liu, G. Direct Quantification of Cd²⁺ in the Presence of Cu²⁺ by a Combination of Anodic Stripping Voltammetry Using a Bi-Film-Modified Glassy Carbon Electrode and an Artificial Neural Network. *Sensors (Switzerland)* **2017**, *17* (7). <https://doi.org/10.3390/s17071558>.

Appendix A

Supplementary images for this dissertation

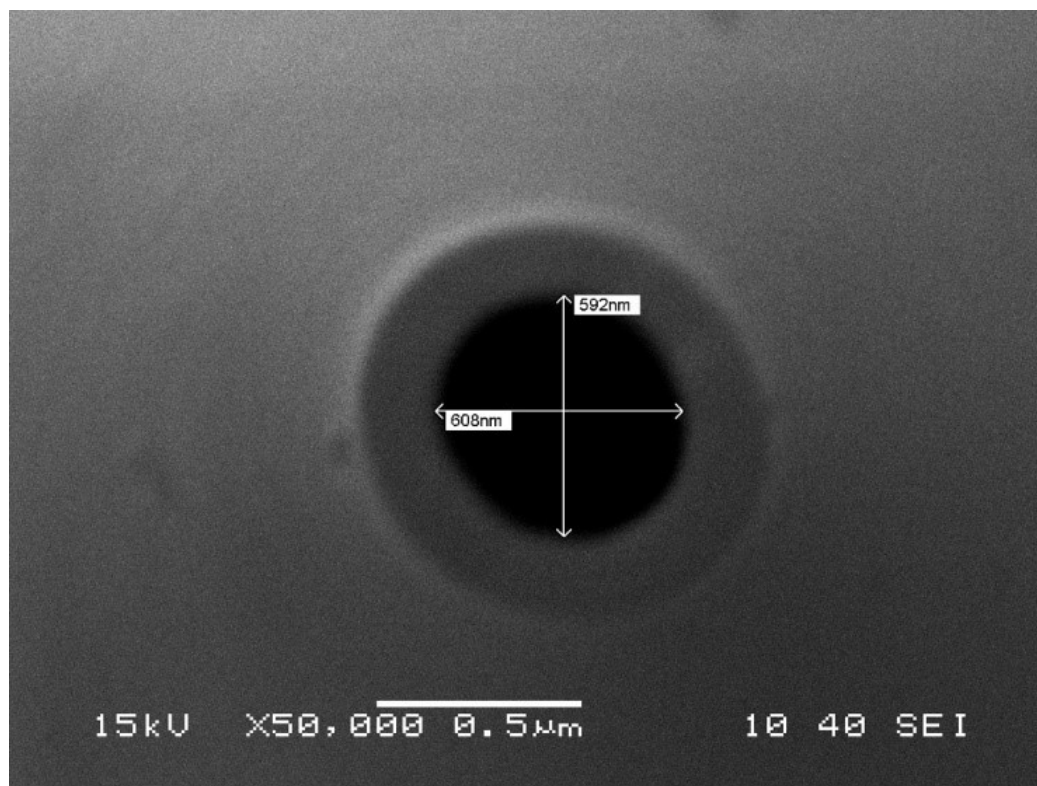


Figure 32 Representative SEM image of the nanopipete.

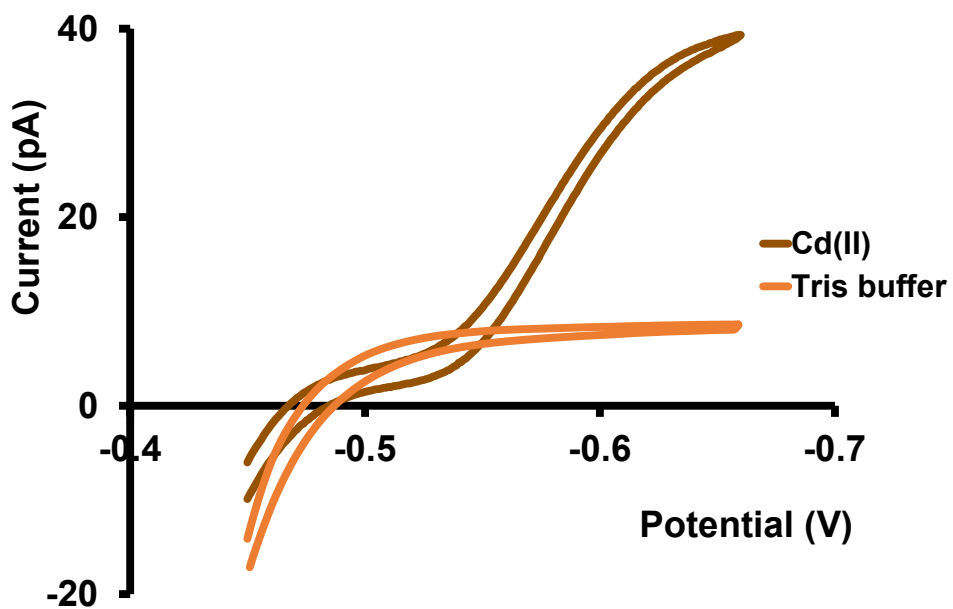


Figure 33 Brown trace is a representative CV of Cd(II) transfer and between water and DCE at 10 mV s^{-1} . Aqueous phase: $400 \text{ } \mu\text{M}$ Cd(II) in tris. Organic phase: 10 mM phen and 0.1 M TDDATFAB. Orange trace represents the background CV.

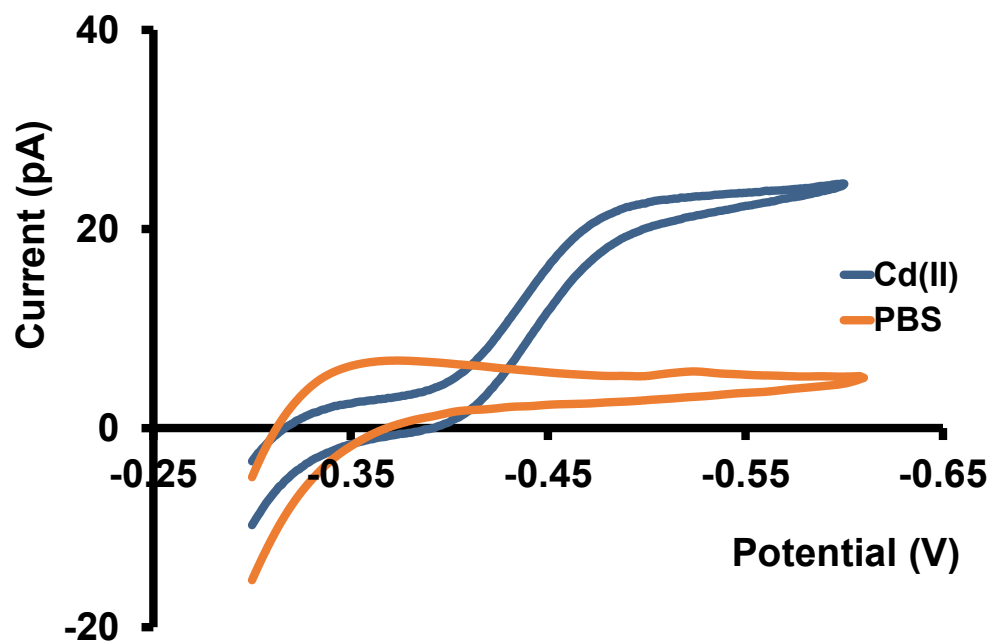


Figure 34 Dark blue trace is a representative CV of Cd(II) transfer and between water and DCE at 10 mV s^{-1} . Aqueous phase: $400 \mu\text{M}$ Cd(II) in PBS. Organic phase: 10 mM phen and 0.1 M TDDATFAB. Orange trace represents the background CV.

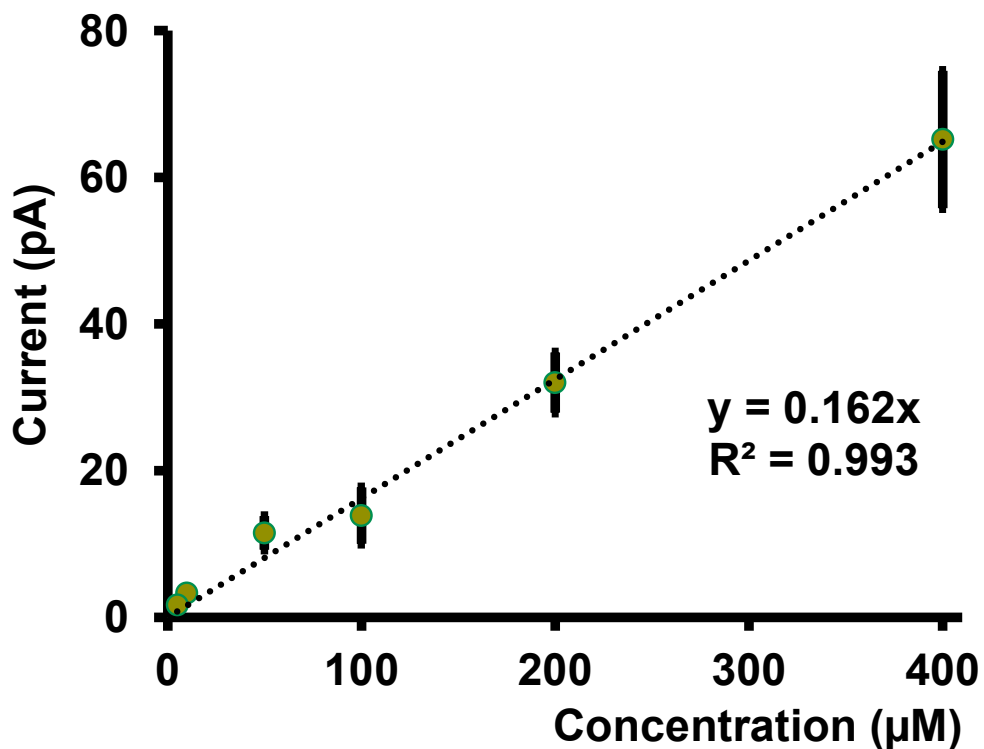


Figure 35 Calibration curve in KCl for Cd(II) transfer. Each data point represents the average current \pm standard error of the mean obtained for 4 nanopipets with at least 3 replicates for each pipet (at minimum 12 replicates in total) Aqueous phase: x μ M Cd(II) in KCl, where $x = 5, 10, 50, 100, 200$ and 400 μ M. Organic phase: 10 mM phen and 0.1 M TDDATFAB.

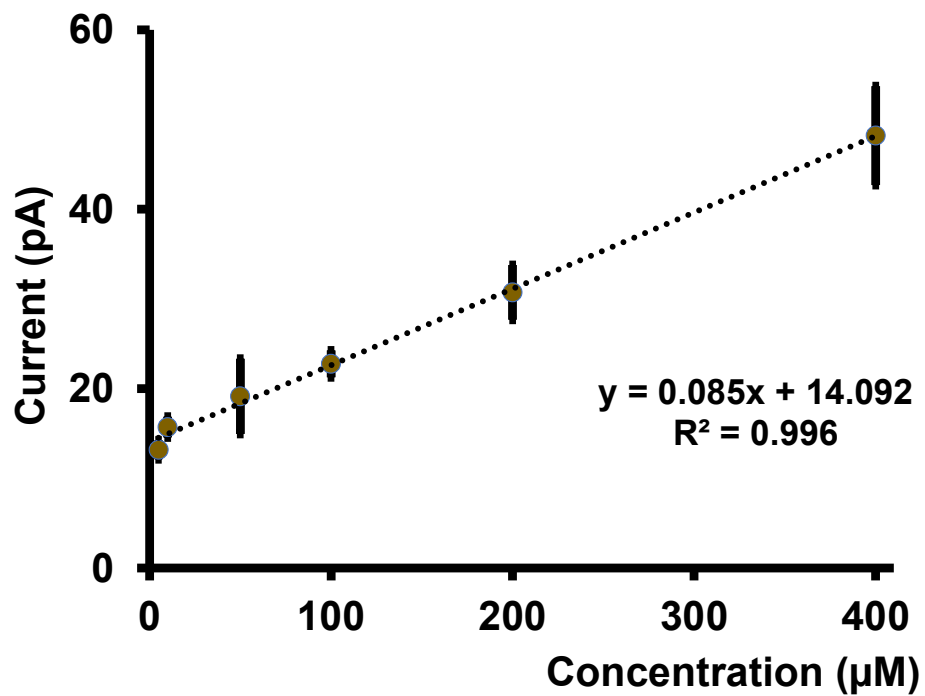


Figure 36 Calibration curve in TRIS buffer for Cd(II) transfer. Each data point represents the average current \pm standard error of the mean obtained for 4 nanopipets with at least 3 replicates for each pipet (at minimum 12 replicates in total) Aqueous phase: x μ M Cd(II) in TRIS buffer, where $x = 5, 10, 50, 100, 200$ and 400 μ M. Organic phase: 10 mM phen and 0.1 M TDDATFAB.

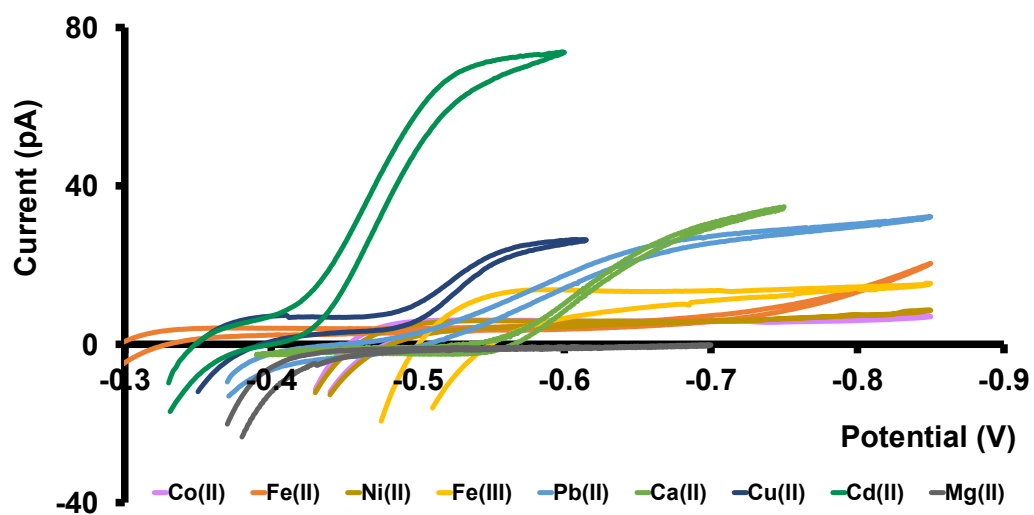


Figure 37 Representative CVs for the transfer of interfering metal ions between water and DCE at 10 mV s^{-1} . Aqueous phase: $400 \text{ } \mu\text{M}$ M(II/III) in KCl. Organic phase: 10 mM phen and 0.1 M TDDATFAB.

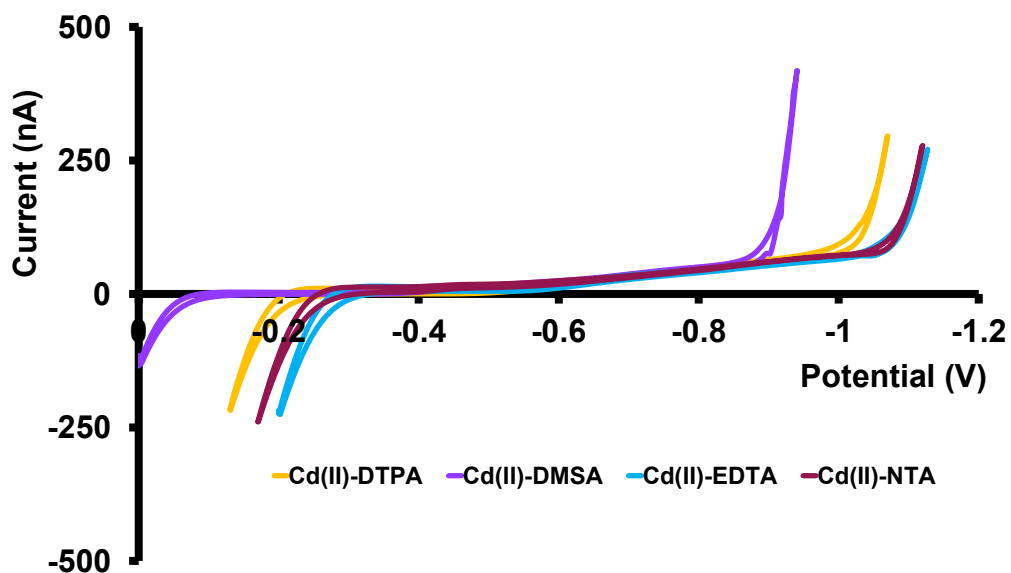


Figure 38 Representative CVs of $[\text{Cd-ligand}]^n$ transfer and between water and DCE at 10 mV.s^{-1} (where $n = -1$ or 0) Aqueous phase: $400 \mu\text{M Cd(II)}$ in ASW. Organic phase: 10 mM phen and 0.1 M TDDATFAB .

Table 6 Experimental parameters used for the standard addition method

Sample no.	Volume of 0.4 mM Cd(II) solution (mL)	Volume of river water sample (mL)	Total volume (mL)	Final conc. of Cd(II) (μM)
1.	1	10	50	8.5
2.	3	10	50	24.5
3.	6	10	50	48.5
4.	9	10	50	72.5
5.	12	10	50	96.5

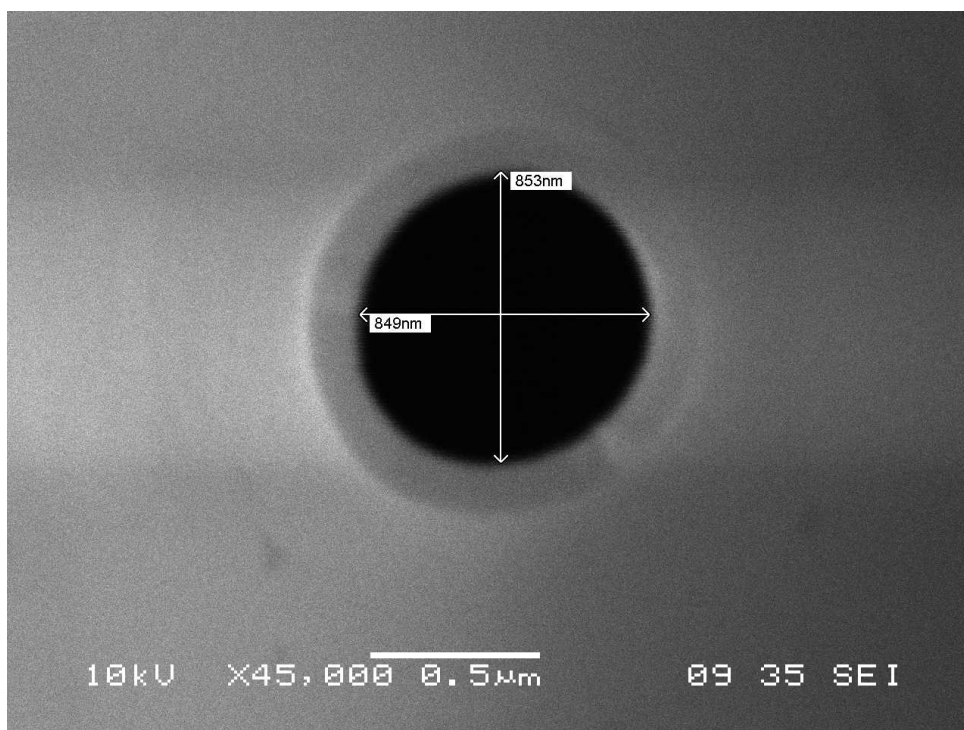


Figure 39 SEM image of nanopipet taken at a magnification of 45000x and spot size of 35.

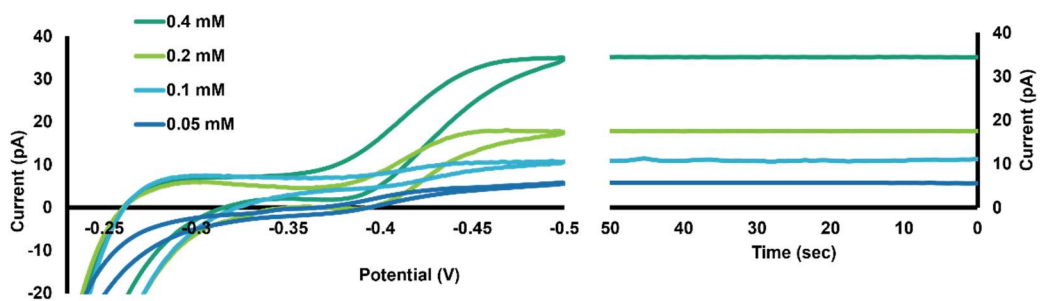


Figure 40 Representative CVs for different concentrations of Cd(II) transfer in MP-AU on the left. Current vs. time ($i-t$) traces for each concentration, on the right. Each $i-t$ curve was obtained for 50 s by applying a constant potential obtained from the plateau region of the CV.

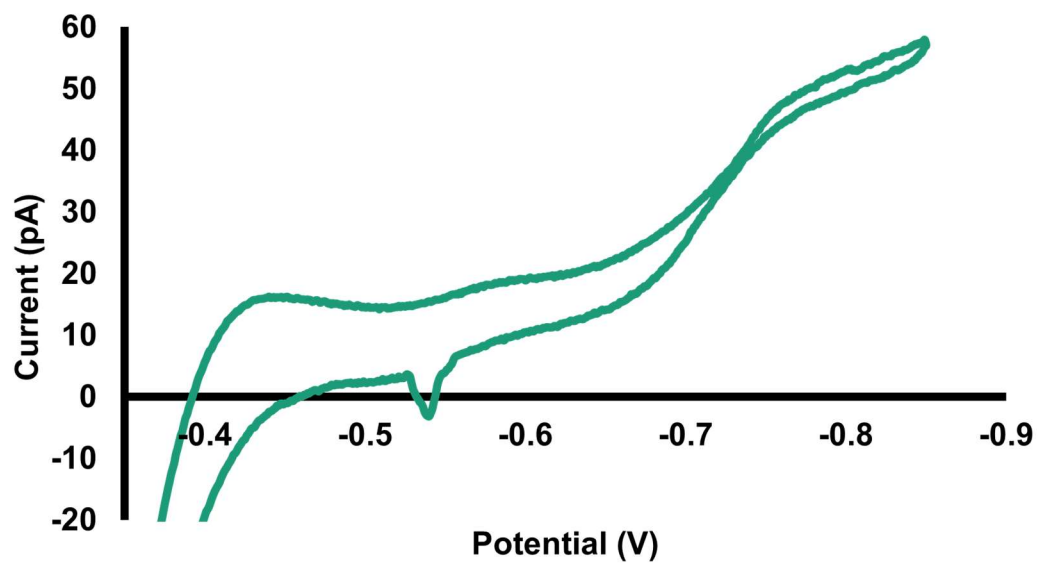


Figure 41 A representative CV of Cd(II) transfer between undiluted AB and DCE at a scan rate of 20 mV/s. Aqueous phase: 0.4 mM Cd(II) in undiluted AB. Organic phase: 10 mM phen and 0.1 M TDDATFAB in DCE.

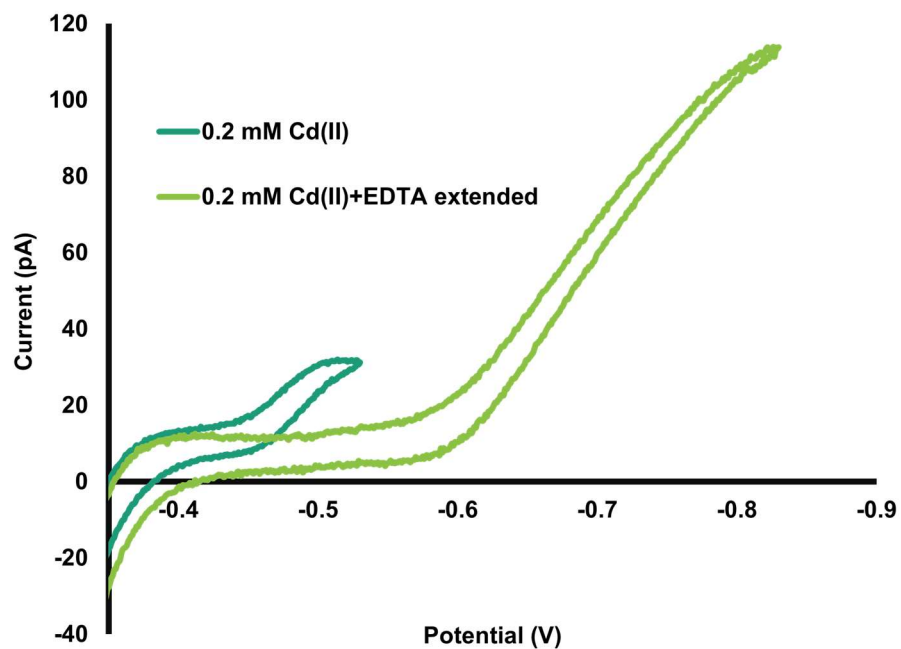


Figure 42 CV (green), and extended CV (light green) of 0.2 mM Cd(II) in AB in the presence of EDTA in the solution with a scan rate of 20 mV/s. Organic phase: Organic phase: 10 mM phen and 0.1 M TDDATFAB in DCE.

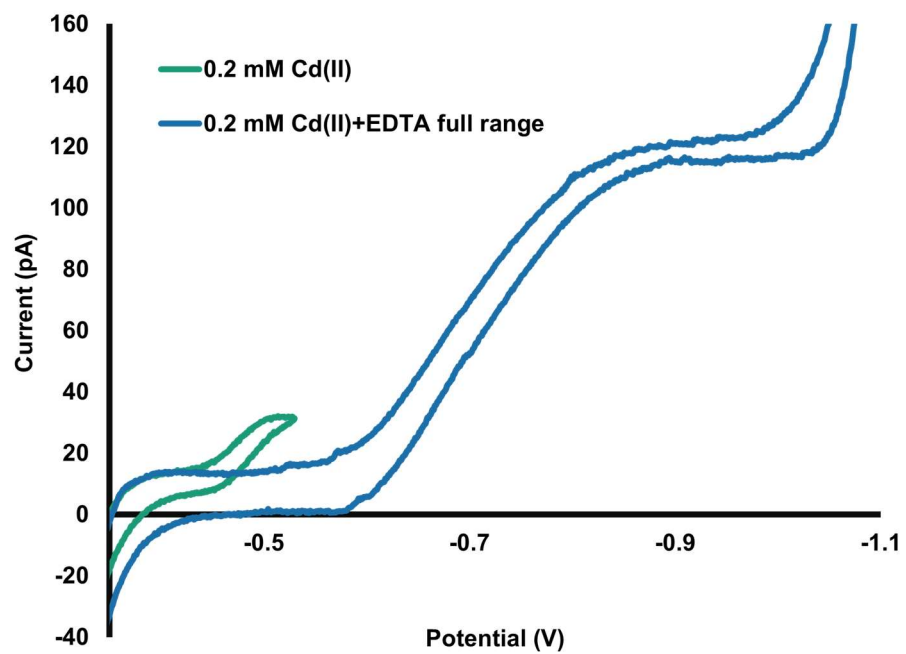


Figure 43 CV (green), and full range CV (blue) of 0.2 mM Cd(II) in AB in the presence of EDTA in the solution with a scan rate of 20 mV/s. Organic phase: Organic phase: 10 mM phen and 0.1 M TDDATFAB in DCE.

Appendix B

Codes used related to chapter 4

MATLAB Code for image generation to train the CNN model

```
% Specify the folder containing your .txt files
```

```
folderPath = 'C:\Users\namuz\OneDrive\Desktop\Cd2+ [Final]\0.05mMcD\Good\Txt'; % Adjust this to your  
folder path
```

```
% List all .txt files in the folder
```

```
txtFiles = dir(fullfile(folderPath, '*.txt'));
```

```
% Initialize an array to store unique identifiers and Y coordinates of the first sharp point
```

```
sharpPointsData = {};
```

```
% Desired image size (32x32)
```

```
desiredSize = [128, 128];
```



```
% Specify the factor by which to adjust the curve thickness

thicknessFactor = 0.3; % Adjust this value as needed

% Loop through each file

for fileIdx = 1:length(txtFiles)

    % Full path to the current .txt file

    filename = fullfile(txtFiles(fileIdx).folder, txtFiles(fileIdx).name);

    % Extract the unique identifier

    pattern = 'P\d+C\d+V\d+'; % Regular expression for the pattern P##V##

    [token, match] = regexp(filename, pattern, 'tokens', 'match');

    if isempty(match) % Skip if pattern not found

        disp(['Pattern not found in ', filename]);

        continue;

    end

end
```

```

uniqueId = match{1}; % Assuming there's at least one match

% Specify the delimiter and read the CV data

delimiter = ','; % Change based on your file's formatting

opts = detectImportOptions(filename, 'Delimiter', delimiter);

data = readmatrix(filename, opts);

% Check if the data has at least two columns

if size(data, 2) < 2

    sharpPointsData{end+1, 1} = uniqueId; % Store unique identifier

    sharpPointsData{end, 2} = NaN; % Store NaN for Y coordinate

    continue;

end

% Adjust the current by multiplying with 10^12

data(:,2) = data(:,2) * 10^12;

```

```
% Assign columns to X and Y

X = data(:,1);

Y = data(:,2);

% Initialize variables to store the first sharp point

first_sharp_X = NaN;

first_sharp_Y = NaN;

% Iterate through the data to find the first sharp point

for i = 2:length(X)

    if abs(X(i)) < abs(X(i-1))

        first_sharp_X = X(i);

        first_sharp_Y = Y(i);

        break; % Exit the loop after finding the first sharp point

    end

end
```

```

end

% Store the unique identifier and corresponding Y coordinate of the first sharp point
sharpPointsData{end+1, 1} = uniqueId; % Store unique identifier

sharpPointsData{end, 2} = first_sharp_Y; % Store Y coordinate

% Plot with original X-axis order

f1 = figure('Visible', 'off'); % Create invisible figure

set(f1, 'Position', [0, 0, desiredSize(1), desiredSize(2)]); % Set figure size to desired size

plot(X, Y, 'k', 'LineWidth', thicknessFactor); % Plot in black with adjusted thickness

xlim([-0.75, -0.2]);

ylim([-20, 60]);

set(gca, 'PlotBoxAspectRatio', [1, 1, 1]); % Set aspect ratio to 1:1

set(gca, 'Visible', 'off'); % Make the axis invisible

% Save the image

```

```
originalImage = frame2im(getframe(gcf)); % Capture the figure as an image

imwrite(originalImage, fullfile(folderPath, [uniqueId, '_original.png']));

close(f1); % Close the figure to free up memory

% Plot with reversed X-axis order

f2 = figure('Visible', 'off'); % Create invisible figure

set(f2, 'Position', [0, 0, desiredSize(1), desiredSize(2)]); % Set figure size to desired size

plot(X, Y, 'k', 'LineWidth', thicknessFactor); % Plot in black with adjusted thickness

set(gca, 'XDir', 'reverse'); % Reverse the X-axis direction

xlim([-0.75, -0.2]); % Adjust the limits to reverse the direction

ylim([-20, 60]);

set(gca, 'PlotBoxAspectRatio', [1, 1, 1]); % Set aspect ratio to 1:1

set(gca, 'Visible', 'off'); % Make the axis invisible

% Save the image
```

```
reversedImage = frame2im(getframe(gcf)); % Capture the figure as an image

imwrite(reversedImage, fullfile(folderPath, [uniqueId, '_reversed.png']));

close(f2); % Close the figure to free up memory

end

% Convert the array to a table for better readability

sharpPointsTable = cell2table(sharpPointsData, 'VariableNames', {'UniqueIdentifier', 'Current'});

% Display the table

disp(sharpPointsTable);
```

MATLAB Code for data generation and preprocessing to train the ANN model

```
% Specify the folder containing your .txt files
```

```
folderPath = 'C:\Users\namuz\OneDrive\Desktop\retxt'; % Adjust this to your folder path
```

```
% List all .txt files in the folder
```

```
txtFiles = dir(fullfile(folderPath, '*.txt'));
```

```
% Initialize a cell array to store the table data
```

```
tableData = cell(length(txtFiles), 7);
```

```
% Loop through each file
```

```
for fileIdx = 1:length(txtFiles)
```

```
    % Full path to the current .txt file
```

```
    filename = fullfile(txtFiles(fileIdx).folder, txtFiles(fileIdx).name);
```

```
    % Extract the unique identifier
```

```

pattern = 'P\d+C\d+V\d+'; % Regular expression for the pattern P##V##

[token, match] = regexp(filename, pattern, 'tokens', 'match');

if isempty(match) % Skip if pattern not found

    disp(['Pattern not found in ', filename]);

    continue;

end

uniqueId = match{1};

% Specify the delimiter and read the CV data

delimiter = ','; % Change based on your file's formatting

opts = detectImportOptions(filename, 'Delimiter', delimiter);

data = readmatrix(filename, opts);

% Check if the data has at least two columns

if size(data, 2) < 2

```



```

        disp(['Data in ', filename, ' does not have two columns. Skipping.']);

        continue;

end

% Adjust the current by multiplying with 10^12

data(:,2) = data(:,2) * 10^12;

% Assign columns to X and Y

X = data(:,1);

Y = data(:,2);

% Identify the direction change point in X

dX = diff(X);

changePointIdx = find(dX(1:end-1) .* dX(2:end) < 0, 1, 'first') + 1;

if isempty(changePointIdx)

    disp(['No change in direction detected in ', filename, '. Skipping.']);

```

```
        continue;

end

% Extract the sharp point values

sharpPointX = X(changePointIdx);

sharpPointY = Y(changePointIdx);

% Separate into forward and backward scans

X_forward = X(1:changePointIdx);

Y_forward = Y(1:changePointIdx);

X_backward = X(changePointIdx:end);

Y_backward = Y(changePointIdx:end);

% Now plot using X_forward and Y_forward

%figure;

%plot(X_backward, Y_backward, 'g-', 'LineWidth', 2); % Plot backward scan in green
```

```
%hold on;

%plot(X_forward, Y_forward, 'b-', 'LineWidth', 2); % Plot forward scan in blue

%xlabel('Potential (V)');

%ylabel('Current (pA)');

%title(['Current vs. Potential for ', uniqueId]);

%grid on;

%xlabel('X-Axis');

%ylabel('Y-Axis');

%legend('Data', 'First Sharp Point');

%xlim([-0.65, -0.2]);

%ylim([-20, 70]);

% Calculate the derivative of Y in the forward scan

dy_forward = diff(Y_forward);
```

```

% Set a threshold for derivative values close to zero for plateau detection

derivative_threshold = 8e-2;

% Set a threshold for the x-axis distance between plateau points and sharp point

X_threshold = 0.1;

% Find the indices where the derivative in the forward scan is close to zero

% and the x-values are above the x-threshold

plateau_indices_forward = find(abs(dy_forward) < derivative_threshold & abs(X_forward(1:end-1) -
sharpPointX) >= X_threshold);

% Extract the coordinates of the last plateau value in the forward scan

if ~isempty(plateau_indices_forward)

    lastPlateauX = X_forward(plateau_indices_forward(end));

    lastPlateauY = Y_forward(plateau_indices_forward(end));

```

```

else

    lastPlateauX = NaN;

    lastPlateauY = NaN;

end

% Calculate the derivative of Y in the reverse scan

dy_backward = diff(Y_backward);

% Find the indices where the derivative in the reverse scan is close to zero

% and the x-values are above the x-threshold

plateau_indices_backward = find(abs(dy_backward) < derivative_threshold & abs(X_backward(2:end) -
sharpPointX) >= X_threshold);

% Extract the coordinates of the last plateau value in the reverse scan

if ~isempty(plateau_indices_backward)

    lastPlateauX_backward = X_backward(plateau_indices_backward(1) + 1);

```

```
        lastPlateauY_backward = Y_backward(plateau_indices_backward(1) + 1);  
  
    else  
  
        lastPlateauX_backward = NaN;  
  
        lastPlateauY_backward = NaN;  
  
    end  
  
    % Store the data in the table  
  
    tableData{fileIdx, 1} = uniqueId;  
  
    tableData{fileIdx, 2} = sharpPointX;  
  
    tableData{fileIdx, 3} = sharpPointY;  
  
    tableData{fileIdx, 4} = lastPlateauX;  
  
    tableData{fileIdx, 5} = lastPlateauY;  
  
    tableData{fileIdx, 6} = lastPlateauX_backward;  
  
    tableData{fileIdx, 7} = lastPlateauY_backward;
```

```

% Save the sharp point and last plateau point values in a new text file

newFileName = ['shrBK', uniqueId, '.txt'];

newFilePath = fullfile(folderPath, newFileName);

fileID = fopen(newFilePath, 'w');

fprintf(fileID, '%.6f,%.6f\n', sharpPointX, sharpPointY);

fprintf(fileID, '%.6f,%.6f\n', lastPlateauX, lastPlateauY);

fprintf(fileID, '%.6f,%.6f\n', lastPlateauX_backward, lastPlateauY_backward);

fclose(fileID);

% Identify the plateau region in terms of X values in the forward scan

if ~isempty(plateau_indices_forward)

    plateau_X_forward = X_forward(plateau_indices_forward);

    % Visualize the detected plateau region in the forward scan

```

```

        %plot(plateau_X_forward, Y_forward(plateau_indices_forward), 'ro', 'MarkerSize', 8); % Mark
plateau points

    else

        disp(['No plateau found in forward scan of ', filename]);

    end

    % Identify the plateau region in terms of X values in the reverse scan

    if ~isempty(plateau_indices_backward)

        plateau_X_backward = X_backward(plateau_indices_backward + 1);

        % Visualize the detected plateau region in the reverse scan

        %plot(plateau_X_backward, Y_backward(plateau_indices_backward + 1), 'mo', 'MarkerSize', 8); %
Mark plateau points

        %legend('Backward Scan', 'Forward Scan', 'Plateau Region (Forward)', 'Sharp Point', 'Plateau
Region (Reverse)');

    else

```



```

        disp(['No plateau found in reverse scan of ', filename]);

        %legend('Backward Scan', 'Forward Scan', 'Plateau Region (Forward)', 'Sharp Point');

    end

    % Plot the sharp point

    %plot(sharpPointX, sharpPointY, 'ko', 'MarkerSize', 10, 'LineWidth', 2);

    %hold off;

end

% Create a table with the collected data

varNames = {'File Name', 'Sharp Point X', 'Sharp Point Y', 'Last Plateau X (Forward)', 'Last Plateau Y
(Forward)', 'Last Plateau X (Reverse)', 'Last Plateau Y (Reverse)'};

resultTable = cell2table(tableData, 'VariableNames', varNames);

% Display the table

disp(resultTable);

```

Python Codes for CNN model

```
import os

import tempfile

from datetime import datetime

import numpy as np

import cv2

import tensorflow

from keras.callbacks import ModelCheckpoint

from sklearn.model_selection import train_test_split

from sklearn.preprocessing import LabelEncoder

from keras.models import Sequential

from keras.layers import Conv2D, MaxPooling2D, Flatten, Dense
```

```
from tensorflow.keras.callbacks import EarlyStopping, LearningRateScheduler

from tensorflow.keras.optimizers import Adam, SGD

from tensorflow.keras.utils import to_categorical

from tqdm import tqdm

from matplotlib import pyplot as plt

# Function to load images and labels from the dataset folder

def load_dataset(dataset_path):

    images = []

    labels = []

    # Get the list of concentration folders

    concentration_folders = [folder for folder in os.listdir(dataset_path) if
os.path.isdir(os.path.join(dataset_path, folder))]
```

```
for concentration_folder in tqdm(concentration_folders, desc="Loading Concentrations"):

    concentration_path = os.path.join(dataset_path, concentration_folder)

    # Get the list of quality folders (good, not good)

    quality_folders = [folder for folder in os.listdir(concentration_path) if
os.path.isdir(os.path.join(concentration_path, folder))]

    for quality_folder in quality_folders:

        quality_path = os.path.join(concentration_path, quality_folder)

        # Check if the PNG folder exists

        png_folder = os.path.join(quality_path, "PNG")

        if os.path.exists(png_folder):

            # Get the list of PNG files

            png_files = [file for file in os.listdir(png_folder) if file.endswith('.png')]

            for png_file in png_files:
```

```
    png_path = os.path.join(png_folder, png_file)

    # Read the image

    image = cv2.imread(png_path)

    # # Resize the image to fit the CNN model architecture

    image = cv2.resize(image, (128, 128))

    # Append the image and label to the lists

    images.append(image)

    labels.append(quality_folder)

    return np.array(images), np.array(labels)

# Load dataset

dataset_path = 'C:\Cu2+ (-incomplete)' # Change to your dataset folder path

images, labels = load_dataset(dataset_path)

print(labels)
```

```
# Preprocess images and labels

images = images.astype('float32') / 255.0

label_encoder = LabelEncoder()

labels = label_encoder.fit_transform(labels)

labels = to_categorical(labels)

# Split dataset into training and testing sets

train_images, test_images, train_labels, test_labels = train_test_split(images, labels, test_size=0.2,
random_state=42, shuffle=True)

train_images, val_images, train_labels, val_labels = train_test_split(train_images, train_labels,
test_size=0.125, random_state=42, shuffle=True) # 0.125 x 0.8 = 0.1

# Define LeNet model architecture

model = Sequential()

model.add(Conv2D(6, kernel_size=(5, 5), strides=(1, 1), activation='relu', input_shape=(128,128,3)))
```

```
model.add(MaxPooling2D(pool_size=(2, 2), strides=(2, 2)))

model.add(Conv2D(16, kernel_size=(5, 5), strides=(1, 1), activation='relu'))

model.add(MaxPooling2D(pool_size=(2, 2), strides=(2, 2)))

model.add(Flatten())

model.add(Dense(120, activation='relu'))

model.add(Dense(84, activation='relu'))

model.add(Dense(len(label_encoder.classes_), activation='softmax'))

# Define early stopping callback

early_stopping = EarlyStopping(monitor='val_accuracy', patience=10, restore_best_weights=True)

# Define learning rate scheduler

def lr_scheduler(epoch, learning_rate):

    if epoch % 5 == 0 and epoch > 0:

        learning_rate = learning_rate * 0.7
```

```
        return learning_rate

lr_scheduler_callback = LearningRateScheduler(lr_scheduler)

# Define model checkpoint callback

checkpoint_callback = ModelCheckpoint(filepath='model_checkpoint.h5', monitor='val_accuracy',
save_best_only=True, verbose=1)

# Compile the model

optimizer = Adam(learning_rate=0.0003)

model.compile(loss='binary_crossentropy', optimizer=optimizer, metrics=['accuracy'])

log_dir = r"C:\GitHub Projects\Runs\run"+ datetime.now().strftime("%Y%m%d-%H%M%S")

model_checkpoint_callback = tensorflow.keras.callbacks.ModelCheckpoint(

    filepath=log_dir)

# Train the model

print("Training LeNet model...")
```



```
history = model.fit(train_images, train_labels, batch_size=32, epochs=100,
validation_data=(val_images, val_labels), callbacks=[early_stopping, lr_scheduler_callback,
checkpoint_callback,model_checkpoint_callback], verbose=1)

#Evaluation

plt.style.use('seaborn')

plt.figure(figsize=(6,6))

plt.plot(history.history['loss'], color='b', label="training loss")

plt.plot(history.history['val_loss'], color='r', label="validation loss")

plt.legend()

plt.show()

plt.figure()

plt.figure(figsize=(6,6))

plt.plot(history.history['accuracy'], color='b', label="training accuracy")
```

```

plt.plot(history.history['val_accuracy'], color='r',label="validation accuracy")

plt.legend()

plt.show()

# Load the best model checkpoint

model.load_weights('model_checkpoint.h5')

# Function to visualize predictions on a subset of images

def visualize_predictions(images, true_labels, predicted_labels, num_samples=20):

    fig, axes = plt.subplots(nrows=num_samples, ncols=2, figsize=(10, 20))

    for i in range(num_samples):

        axes[i, 0].imshow(images[i])

        axes[i, 0].set_title(f"True:
{label_encoder.inverse_transform([np.argmax(true_labels[i])])[0]}")

        axes[i, 0].axis('off')

```

```
axes[i, 1].imshow(images[i])

axes[i, 1].set_title(f"Predicted:
{label_encoder.inverse_transform([np.argmax(predicted_labels[i])])[0]}")

axes[i, 1].axis('off')

plt.tight_layout()

plt.show()

# Evaluate the model on the test set

print("Evaluating the model on the test set...")

test_loss, test_accuracy = model.evaluate(test_images, test_labels)

print(f'Test Loss: {test_loss}')

print(f'Test Accuracy: {test_accuracy}')

# Make predictions on the test set

test_predictions = model.predict(test_images)
```

```
# Visualize predictions on a subset of test images  
  
visualize_predictions(test_images, test_labels, test_predictions)
```

Python Codes for ANN model

```
import os

import cv2

import numpy as np

import pandas as pd

from keras.callbacks import EarlyStopping, LearningRateScheduler

from matplotlib import pyplot as plt

from sklearn.model_selection import train_test_split

from sklearn.preprocessing import LabelEncoder

from keras.models import Sequential

from keras.layers import Dense

from tqdm import tqdm
```

```
from tensorflow.keras.optimizers import Adam, SGD

# Function to load data from text files

def load_dataset(dataset_path):

    data = []

    labels = []

    # Get the list of concentration folders

    concentration_folders = [folder for folder in os.listdir(dataset_path) if
os.path.isdir(os.path.join(dataset_path, folder))]

    for concentration_folder in tqdm(concentration_folders, desc="Loading Concentrations"):

        concentration_path = os.path.join(dataset_path, concentration_folder)

        print(concentration_folder)

        # Get the list of quality folders (good, not good)
```

```
quality_folders = [folder for folder in os.listdir(concentration_path) if
os.path.isdir(os.path.join(concentration_path, folder))]

#

for quality_folder in quality_folders:

    if(quality_folder == 'Good'):

        quality_path = os.path.join(concentration_path, quality_folder)

        print(quality_folder)

    # Check if the PNG folder exists

    txt_folder = os.path.join(quality_path, "txt")

    if os.path.exists(txt_folder):

        # Get the list of PNG files

        txt_files = [file for file in os.listdir(txt_folder) if file.endswith('.txt')]

        #print(txt_files)
```

```
for txt_file in txt_files:

    txt_path = os.path.join(txt_folder, txt_file)

    with open(txt_path, 'r') as f:

        lines = f.readlines()

        x_coords = []

        y_coords = []

        for line in lines:

            # Split each line by comma

            parts = line.strip().split(',')

            # Convert parts to floating-point numbers

            x = float(parts[0])

            y = float(parts[1])
```



```
        # Append x and y coordinates to lists

        # x_coords.append(x)

        y_coords.append(y)

    # Append x and y coordinates as a tuple to data

    data.append(y_coords)

    # Append the label (concentration_folder) to labels

    labels.append(float(concentration_folder.split('mM')[0]))

return np.array(data), np.array(labels)

# Load dataset

dataset_path = 'C:\Trim_CdTxtfiles' # Change to your dataset folder path

data, labels = load_dataset(dataset_path)

# Determine the maximum length of x and y coordinate lists

max_length = max(len(y_coords) for y_coords in data)
```

```
min_length = min(len(y_coords) for y_coords in data)

print(min_length,max_length)

# Pad or truncate x and y coordinate lists to max_length

#padded_data = []

#for y_coords in data:

#    padded_y_coords = np.pad(y_coords, (0, max_length - len(y_coords)), mode='empty')

#    padded_data.append(padded_y_coords)

# Convert padded_data to NumPy array

#reshaped_data = np.array(padded_data)

print(data, labels)

# Split the reshaped data into training and testing sets

train_data, test_data, train_labels, test_labels = train_test_split(data, labels, test_size=0.2,
random_state=42)
```

```
# Define the ANN model architecture

model = Sequential([

    Dense(128, activation='relu', input_shape=(240,)),

    Dense(64, activation='relu'),

    Dense(32, activation='relu'),

    Dense(1, activation='linear')

])

early_stopping = EarlyStopping(monitor='mae', patience=5, restore_best_weights=True)

# Define learning rate scheduler

def lr_scheduler(epoch, learning_rate):

    if epoch % 5 == 0 and epoch > 0:

        learning_rate = learning_rate * 0.5

    return learning_rate
```

```
lr_scheduler_callback = LearningRateScheduler(lr_scheduler)

optimizer = Adam(learning_rate=0.001)

model.compile(loss='mse', optimizer=optimizer, metrics=['mae']) # Use appropriate loss and optimizer
for regression

# Train the model

history = model.fit(train_data, train_labels, epochs=100, batch_size=32, validation_split=0.2,
callbacks=[early_stopping, lr_scheduler_callback], verbose=1)

plt.style.use('seaborn')

plt.figure(figsize=(6,6))

plt.plot(history.history['loss'], color='b', label="training loss")

plt.plot(history.history['val_loss'], color='r', label="validation loss")

plt.legend()

plt.show()
```

```
plt.figure()

plt.figure(figsize=(6,6))

plt.plot(history.history['mae'], color='b', label="Mean absolute error")

plt.plot(history.history['val_mae'], color='r',label="Validation Mean absolute error")

plt.legend()

plt.show()

# Evaluate the model on the test set

test_loss, test_mae = model.evaluate(test_data, test_labels)

print(f'Test Loss: {test_loss}')

print(f'Test MAE: {test_mae}')

# Make predictions

predictions = model.predict(test_data)

predictions_df = pd.DataFrame(np.ravel(predictions),columns=["Predictions"])
```

```
comparison_df = pd.concat([pd.DataFrame(test_labels,columns=["Real Values"]), predictions_df],axis=1)

print(comparison_df)

# # Visualize predictions against actual concentrations

# # Add visualization code here
```

Appendix C

Experimental operating parameters related to electrochemical experiments

Table 7 Silanization setup operating parameters

S.No	Date	Pressure (atm)	Temperature (F)	% Humidity	Vacuum Prep Time (min)	Silanization Time (min)
1	12/31/2020	0.0164	68	49	10	60
2	1/1/2021	0.0165	70	45	10	50
3	1/2/2021	0.0167	70	45	10	40
4	1/6/2021	0.0167	70	42	8	40
5	1/8/2021	0.0169	70	44	9	40
6	1/11/2021	0.0165	70	45	9	45
7	1/12/2021	0.0165	72	64	7	30
8	1/13/2021	0.0036	70	46	10	30
9	1/14/2021	0.0165	70	41	11	40
10	1/14/2021	0.0165	72	36	9	50
11	1/19/2021	0.0166	70	33	8	45
12	2/19/2021	0.0166	70	47	10	35
13	2/24/2021	0.0176	70	46	8	40
14	3/3/2021	0.0193	70	48	11	50
15	3/5/2021	0.0204	68	48	9	60

16	3/10/2021	0.0190	70	47	12	60
17	3/11/2021	0.0190	70	48	13	40
18	3/12/2021	0.0193	68	48	15	40
19	3/13/2021	0.0188	70	49	10	45
20	3/15/2021	0.0193	70	49	15	50
21	3/16/2021	0.0193	68	48	10	40
22	3/17/2021	0.0195	70	48	15	60
23	3/18/2021	0.0195	68	50	15	60
24	3/22/2021	0.0172	70	49	15	45
25	3/23/2021	0.0172	68	49	13	50
26	3/23/2021	0.0170	68	49	14	45
27	3/24/2021	0.0171	68	50	12	40
28	3/25/2021	0.0170	68	49	15	60
29	3/29/2021	0.0172	68	51	15	60
30	3/29/2021	0.0170	68	50	15	50
31	3/30/2021	0.0170	68	50	14	40
32	4/1/2021	0.0172	68	50	12	50

Table 8 P-2000 Laser Puller operating parameters

Starting Material	B100-58	B100-58
Line	1	1
Heat	490	480
Filament	4	4
Velocity	25	26
Delay	140	140
Pull	0	0
Loop	1	1
Internal Diameter	~600 nm	~850 nm

Construction of Electrode Holders

The electrochemical experiments were performed using working electrodes that were fabricated from borosilicate glass capillaries with an outer diameter of 1.0 mm. The working electrodes should be held in position with great stability and precision to ensure that accurate measurements are made during the electrochemical experiments. To achieve this, custom-built 3D-printed electrode holders were produced. The 3D model was created using Creo software (PTC, Inc.) and was printed using polylactic acid filament. The holder was then threaded with appropriate screws with a rubber washer to ensure comfortable handling of the electrodes. Three distinct models were created for different purposes: a single-electrode holder, a dual-electrode holder and a multi-electrode holder (9 electrodes). Many trials were performed to achieve the final product, which was used to perform all the electrochemical experiments for this dissertation.

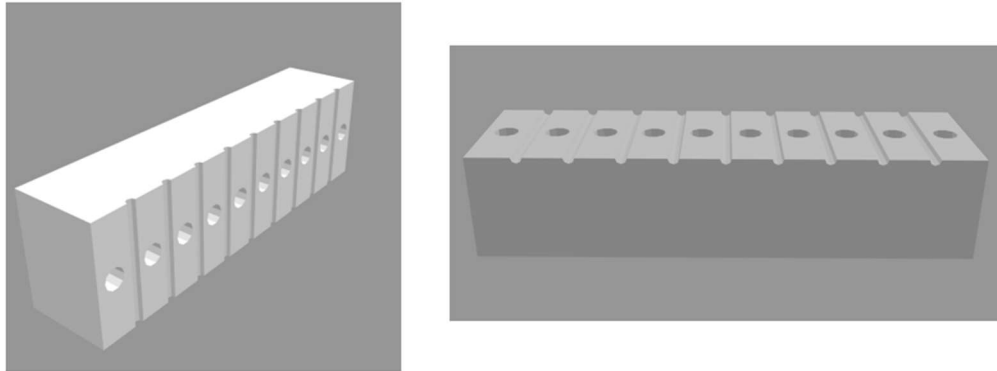


Figure 44 3D model of multi-electrode holder.

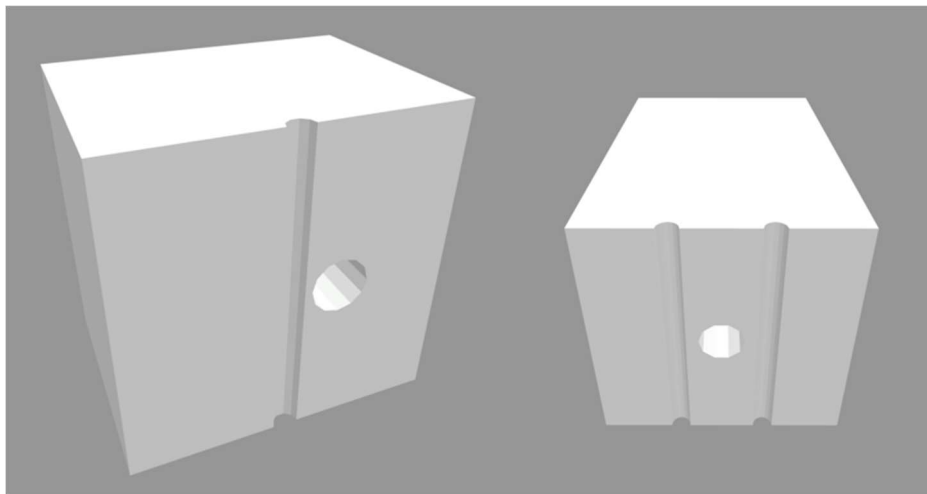


Figure 45 3D model of single and dual electrode holder.

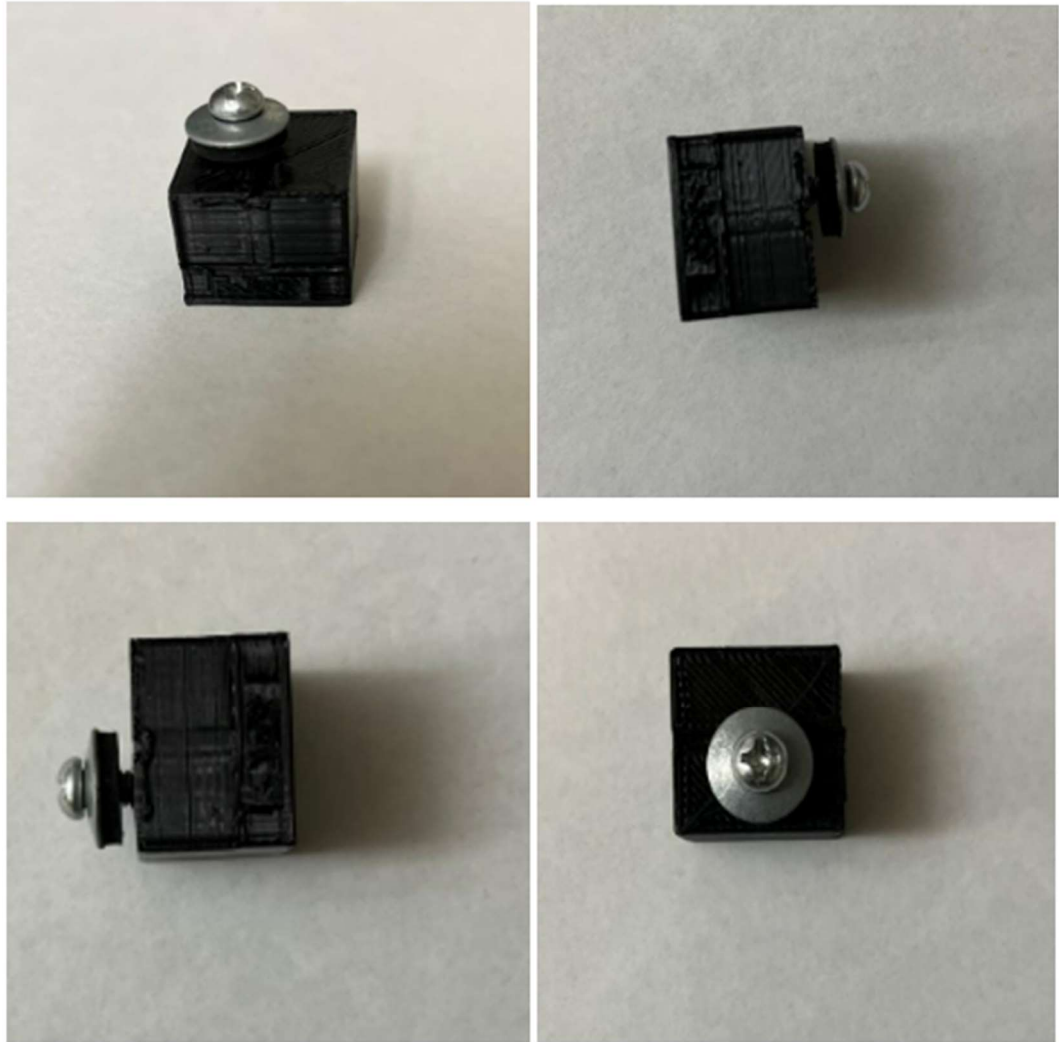


Figure 46 Images of the single electrode holder with rubber holding mechanism



Figure 47 Image of multi-electrode holder.

Construction of Faraday Cage

To perform the electrochemical experiments with great accuracy, the system must be insulated from any external electrical noise. A Faraday cage is used to achieve this electrical insulation, ensuring that the signal-to-noise ratio remains high. A Faraday cage was constructed from scratch, and all the electrochemical experiments for this dissertation were performed in it. Materials were purchased from a hardware shop, and the parts were drilled with screws to fix them in place. A hinge mechanism was employed to ensure ease of access when opening and closing the door. A locking mechanism was used to ensure the door remained still when closed.



Figure 48 Images of the constructed Faraday cage.

The top left shows a general picture, top right shows the screws drilled to hold the structure, bottom left shows the locking hook mechanism, bottom right shows the hinge mechanism used to open the door.

Appendix D

Internship at X-BATT

The focus of the internship was to develop a novel anode material configuration for high-performance batteries ideal for small utility devices (portable potentiostats).

The development of such batteries will enable efficient miniaturization of potentiostats which can be deployed for on-field applications. Many duties were carried out during the internship ranging from making design of experiments, optimizing unit operation such as vacuum oven and wet ball mill, conducting feasibility study and techno-economic analysis of several processes, performing mass and energy balance and electrochemical analysis of anode material.

Some of the relevant duties include:

- Preparation of anode material for coin cells
- Assemble the coin cells in a glove box
- Put the coin cells for testing
- Analyze the testing results

Preparing the anode material for the coin cells

Synthesis of Active Material

Graphite and biobased materials are sieved, dried, and mixed with a resin system, DVB, and Cat-TX. The mixture is processed in a Flak Tek mixer and cured in an oven under argon flow at specific temperatures and times.

Processing of Cured Active Material

The cured material is removed from the petri dishes, broken into small pieces, and blended in a coffee processing apparatus until the desired particle size is achieved. The processed material is then stored in labeled bags.

Pyro in Tube Furnace

The furnace is prepared, and the processed material is weighed and placed in cleaned and labeled ceramic crucibles. The pyro process is carried out for approximately 24 hours, and the material is weighed again after cooling.

Milling and Sieving

The pyro-treated material is milled overnight in a dry alumina milling container with milling media. The milled material is then sieved under 32 μm until 1.5 g is obtained and dried overnight in a vacuum oven.

Assembling the coin cells inside a glove box

Slurry Mixing

The active material is dried, and the slurry composition is determined using a template. C65, AM, NMP, and binder are mixed in a thinky mixer, and the Hegman particle size is checked and recorded.

Electrode Preparation

The coating table is cleaned with ethanol/isopropyl. A copper sheet is placed on the coating table (shiny side down) and wiped with ethanol. The active material is scooped onto the copper, and a doctor blade set to 200 μm is placed. The material is coated at speed 4. The convection oven is preheated to 70 °C. The electrode is baked for 20 minutes or until thoroughly dried. It is then placed in the top vacuum oven overnight at 120 °C. The horizontal plates are heated up to 200 °C, ensuring they are pressed together for even heating. A ½ inch strip is trimmed from the top and bottom of the electrode.

Half-Cell Battery Assembly

Ideally, the glove box settings should have $\text{H}_2\text{O} < 1$ ppm, and the pressure should be 6-8 mbar. The stage is cleaned with ethanol if needed. The electrode is punched out using the bottom half. The electrode is layered with weighing paper and quickly punched along the straight edge to avoid fraying. The electrode discs are weighed, and the weight is recorded to the nearest 0.1 microns on the cell container. The

coating is brushed off the Li chip, keeping containers closed as much as possible to avoid oxidation. The brushed Li chips are pressed to the spacer with flat sides touching. The anode is centered in the cell bottom. 185 μL of LiPF_6 is pipetted, and a few drops are applied to the center of the anode until it is covered. The separator is placed on top of the anode, and the remaining LiPF_6 solution is pipetted on top of the separator. The Li chip and 1 mm spacer are layered on top of the separator, with the Li chip side touching the separator. The spring with the larger cone opening is placed on the spacer and gently pressed with forceps. The cell lid is placed on top using plastic forceps and pushed down, ensuring that the spring is not displaced in this step. The cell is crimped by putting it in the center of the crimper bed, setting the crimper to 8.00, and pressing start. The cell is removed from the crimper with a Kimwipe, and the excess electrolyte solution is dried outside. The cells are put into a transparent battery storage case and put into the antechamber. The glovebox gloves may be cleaned with propanol after use.

Electrochemical Testing

Take the assembled coin cell and make sure it is properly connected to the battery testing system in the open circuit voltage (OCV) mode. Let the cell rest in this mode for about one hour to allow it to stabilize before starting the test. Based on the active material used in the working electrode, define the appropriate voltage window for testing the cell. This voltage range should be selected to avoid any unwanted side reactions or degradation of the electrode materials. To evaluate the

performance of the coin cell, calculate its theoretical capacity using the weight of the active material in the electrode. This will serve as a reference to compare against the actual measured capacity during testing. Set up the battery tester to perform repeated charge and discharge cycles on the coin cell at the required C-rate (current). The C-rate determines how fast the cell is charged or discharged relative to its capacity. For example, a 1C rate means the cell is fully charged or discharged in one hour.

Analysis of Electrochemical Results

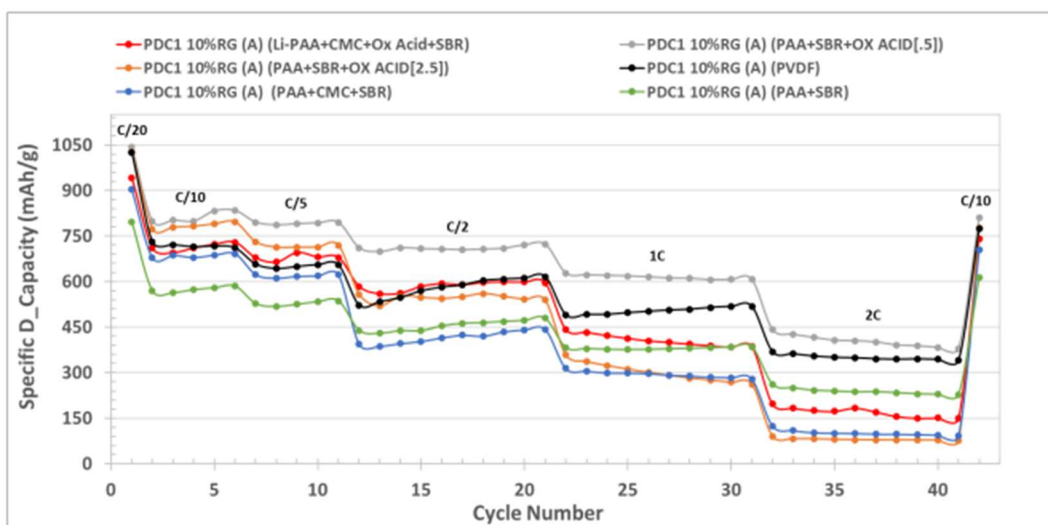


Figure 49 Example of half coin cell rate progression study with a potential window of 0.005 – 3.0V.

Figure 49 shows the half-coin cell rate progression for a specific half-cell configuration. From the plot the specific discharge capacity is examined across multiple cycles at various C-rates. It also gives us capacity retention over time and

illustrates the cell's rate capability, showing how performance changes as charge/discharge rates increase. Coulombic efficiency can often be inferred from the data. The overall trend of the capacity curves provides insights into the long-term cycling stability of the material. After high-rate cycling, the cell's ability to recover capacity when returned to lower C-rates is assessed, indicating the reversibility of electrochemical processes and structural stability. Different binder formulations or additives, as seen in the legend of this diagram, are often compared on the same plot to evaluate their relative effectiveness. The initial capacity, usually at a low C-rate, is examined to assess the material's theoretical versus practical capacity utilization. By systematically analyzing these aspects, we can gain comprehensive insights into the electrochemical behavior of the anode material, guiding further optimization efforts and assessing its suitability for specific battery applications.

Appendix E

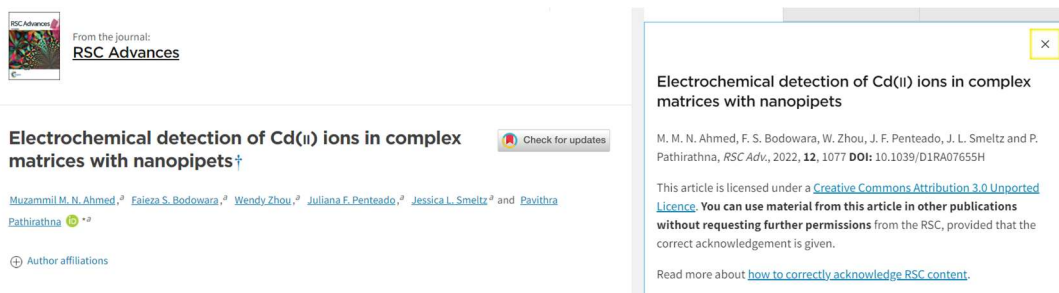
This dissertation was complimented with the following awards:

1. **Outstanding Graduate Student Award**, from the Department of chemistry and Chemical Engineering, April 2024
2. **Outstanding Graduate Student in a Research Institution** (given annually to only one from all research institution under Orlando Section), from the **American Chemical Society**, Orlando Section, December 2022
3. **Outstanding Graduate Student Oral Presentation**, from the 86th Annual Meeting Florida Academia of Science, March 2022
4. **Outstanding Graduate Student Oral Presentation**, from the 85th Annual Meeting Florida Academia of Science, March 2021
5. **Best Oral Presenter**, from the 19th Raymond N. Castle Conference, April 2021

Appendix F

Copyright from publisher


The copyright for the material used in chapter 2 is shown below.





The screenshot shows the RSC Advances article page for the paper "Electrochemical detection of Cd(II) ions in complex matrices with nanopipets". The article is by M. M. N. Ahmed, F. S. Bodowara, W. Zhou, J. F. Pentead, J. L. Smeltz, and P. Pathirathna, published in *RSC Adv.*, 2022, 12, 1077. The DOI is 10.1039/D1RA07655H. The article is licensed under a Creative Commons Attribution 3.0 Unported Licence. The authors listed are Muzammil M. N. Ahmed, Faieza S. Bodowara, Wendy Zhou, Juliana F. Pentead, Jessica L. Smeltz, and Pavithra Pathirathna. There is a "Check for updates" button and an "Author affiliations" link.

From the journal:
RSC Advances

Electrochemical detection of Cd(II) ions in complex matrices with nanopipets †

[Muzammil M. N. Ahmed](#), [Faieza S. Bodowara](#), [Wendy Zhou](#), [Juliana F. Pentead](#), [Jessica L. Smeltz](#) and [Pavithra Pathirathna](#)  [✉]

 Check for updates

 Author affiliations

Electrochemical detection of Cd(II) ions in complex matrices with nanopipets

M. M. N. Ahmed, F. S. Bodowara, W. Zhou, J. F. Pentead, J. L. Smeltz and P. Pathirathna, *RSC Adv.*, 2022, **12**, 1077 DOI: 10.1039/D1RA07655H

This article is licensed under a [Creative Commons Attribution 3.0 Unported Licence](#). You can use material from this article in other publications without requesting further permissions from the RSC, provided that the correct acknowledgement is given.

Read more about [how to correctly acknowledge RSC content](#).